

AN ABSTRACT OF THE THESIS OF

Kevan William Fox Gahan for the degree of Master of Science in Mechanical Engineering presented on May 29, 2020.

Title: Fatigue Testing and Analysis of Polymer and Composite Materials Used in Heavy-Duty Trucks.

Abstract approved:

John P. Parmigiani

As structural durability analysis is increasingly trusted during the design processes of the automotive industry, more complete and sophisticated modeling of material behavior under both static and dynamic loading conditions is paramount. This is especially true regarding the application of heavy-duty trucks, where modern designs contain large parts such as body panels, splash shields and hoods that are made of polymers or polymer-composite materials rather than metal as found in small passenger vehicles or historical truck designs. While the use of these more advanced materials provides a significant reduction in the total weight of a truck, there is a severe lack of research-backed knowledge regarding their mechanical behavior when subjected to static and dynamic loads. Data that is necessary input information for achieving accurate analysis results for truck models containing such materials is often replaced by generic properties, or taken from third-party testing reports that can be easily misinterpreted. Thus, there are multiple opportunities for improvement in this area of work. The research presented in this thesis is focused on obtaining the above-mentioned

data for three materials that are commonly used on large trucks: polydicyclopentadiene (pDCPD), 40% wt. chopped-glass-fiber-reinforced polypropylene (40% GF-PP) and 35-40% wt. vinyl ester Sheet-Molding Compound (SMC), though the results for SMC are not presented in this thesis. This is done by adapting practices from several standard testing procedures for both monotonic and strain-controlled uniaxial fully-reversed fatigue testing. The validity of applying the strain-based fatigue approach to these types of materials is then questioned and studied. In addition, a procedure is suggested for obtaining a stress-life fatigue definition from strain-controlled fatigue test data, and the results are compared to the stress-life definition obtained from load-controlled fatigue testing of the same material. Lastly, the finalized material property information is applied to improve the durability simulations of a pre-existing model of a truck part; the significant increase in calculated damage due to the integration of the new data is discussed. The conclusions of this research can thus be divided into two categories. The primary outcome is the procurement of new, more accurate material data that will be directly used to improve design and analysis processes for heavy-duty trucks. The secondary outcome is the investigation and improvement of test methods that can be used to evaluate the monotonic and fatigue characteristics of polymers and polymer-composite materials. Specifically, if the strain-life fatigue definition is perused for a polymer or polymer-composite material, it is suggested that this data should only be applied to analysis simulations if there exists a *fatigue transition point* on the strain-life curve. Otherwise, the simpler stress-life definition will suffice.

©Copyright by Kevan William Fox Gahan

May 29, 2020

All Rights Reserved

Fatigue Testing and Analysis of Polymer and Composite Materials Used in Heavy-Duty Trucks

by

Kevan William Fox Gahan

A THESIS

submitted to

Oregon State University

in partial fulfillment of
the requirements for the
degree of

Master of Science

Presented May 29, 2020
Commencement June 2020

Master of Science thesis of Kevan William Fox Gahan presented on May 29, 2020.

APPROVED:

Major Professor, representing Mechanical Engineering

Head of the School of Mechanical, Industrial, and Manufacturing Engineering

Dean of the Graduate School

I understand that my thesis will become part of the permanent collection of Oregon State University libraries. My signature below authorizes release of my thesis to any reader upon request.

Kevan William Fox Gahan, Author

ACKNOWLEDGEMENTS

I would like to express my most sincere appreciation to Dr. John Parmigiani for the continuous technical support and feedback throughout the course of this project and my career as a graduate student as a whole. His Prototype Development Lab is a special place that provides students with opportunities that are not available anywhere else. I feel more prepared for a career as an engineer than I ever thought I would before this experience.

Also thank you to Alan, Paul, Tim, Tony, Brandon and the entire Structural & Dynamic Analysis team at Daimler Trucks North America. The skills I learned from my time at DTNA could not be replaced by any class and I appreciate the team providing me with this opportunity and helping me out along the way.

I would also like to acknowledge the other (past and present) graduate students of the Prototype Development Lab, listed in no particular order here, who have provided endless technical support within the lab and great memorable times outside of the lab: Kevin Carpenter, Patrick Sellars, David (Mom's Spaghetti) Plechaty, Satish Solanki, Carter Marr, Jacob Porter, Arthur Wells, and Kyle McGann.

Special thanks to Amanda for the persistent mental support, and for always being there for me through the highs and lows.

Lastly, I would not be where I am today if I did not have support from my amazing family: Mom, Dad, Curran and Cailin. Thank you for everything you do for me.

CONTRIBUTION OF AUTHORS

Dr. John Parmigiani provided technical feedback and support throughout chapters 1-7.

Nicole LeRoux and Thomas Hope assisted with completing fatigue tests, the results of which are presented in chapter 4.

TABLE OF CONTENTS

Page

1	Introduction.....	1
2	Literature Review.....	9
2.1	History of Fatigue Theory	9
2.2	Fatigue of Polymers.....	13
2.3	Manufacturing and Fatigue of Short-Fiber-Composites.....	14
2.4	Application of Fatigue Data to Digital Simulations	16
2.5	Summary.....	17
3	Methods and Procedures	19
3.1	Testing Equipment.....	19
3.1.1	Hydraulic System	19
3.1.2	Data Acquisition.....	23
3.1.3	Software	25
3.1.4	Machined Fixtures.....	26
3.2	Material Selection and Sample Preparation.....	29
3.2.1	Selection of Materials.....	29
3.2.2	Preparation of Testing Samples.....	30
3.3	Testing Methods	34
3.3.1	Monotonic Testing	35
3.3.2	Strain-Controlled Fatigue Testing.....	36
3.3.3	Load-Controlled Fatigue Testing	39
3.4	Data Analysis and Post-Processing	41
3.4.1	Mathematical Relationships – Monotonic	41

TABLE OF CONTENTS (Continued)		<u>Page</u>
3.4.2	Mathematical Relationships – Strain-Life Fatigue.....	44
3.4.3	Mathematical Relationships – Stress-Life Fatigue.....	50
3.5	Automation of Test Data Post-Processing.....	51
4	Results for DTNA Material Database.....	57
4.1	Monotonic Results.....	57
4.1.1	pDCPD Monotonic Results.....	57
4.1.2	40% GF-PP Monotonic Results (In-Flow).....	60
4.1.3	40% GF-PP Monotonic Results (Cross-Flow).....	63
4.1.4	40% GF-PP Monotonic Results – comparison.....	66
4.2	Strain-Controlled Fatigue Results	67
4.2.1	pDCPD Strain-Controlled Fatigue Results	67
4.2.2	40% GF-PP Strain-Controlled Fatigue Results (In-Flow)	75
4.2.3	40% GF-PP Strain-Controlled Fatigue Results (Cross-Flow)	82
4.2.4	40% GF-PP Strain Controlled Fatigue Results – Comparison.....	88
5	Additional Considerations	92
5.1	pDCPD Strain-Softening Behavior	92
5.1.1	Plastic Deformation in Metals – a brief summary.....	93
5.1.2	Atomic Structure of Polymers.....	97
5.1.3	Polymerization and Molding Process for pDCPD	99
5.1.4	Plastic Deformation of Polymers	101
5.1.5	Summary	102
5.2	Comparison of Strain-Controlled and Load-Controlled Testing.....	103

TABLE OF CONTENTS (Continued)		<u>Page</u>
5.2.1	pDCPD Load-Controlled Fatigue Results.....	104
5.2.2	pDCPD Strain-control and Load-control Stress-life Comparison...	107
6	Discussion.....	109
6.1	Applying the Strain-Life Fatigue Method to Plastics.....	109
6.1.1	Overlap of the Strain-Life and Stress-Life Derivations	110
6.1.2	Plastic-Elastic Strain-Life Intersection Point	110
6.1.3	Summary	112
6.2	Comparisons to Pre-Existing Material Data.....	113
6.2.1	Corrections Applied to Stress-Life Data	115
6.3	Updated Simulation Results	117
6.3.1	IMAGE Results Using Old Data.....	118
6.3.2	IMAGE Results Using New Data – Stress-Life.....	118
6.3.3	IMAGE Results Using New Data – Strain-Life.....	119
7	Conclusion	121
	Bibliography	125
	APPENDICES	129
	Appendix A: Project Cost Breakdown.....	130
	Appendix B: Monotonic Testing Procedure/Checklist.....	131
	Appendix C: Fatigue Testing Procedure/Checklist.....	132
	Appendix D: Individual Monotonic Stress vs. Strain Plots	136
	PDCPD Monotonic Stress vs. Strain	136
	40% GF-PP Monotonic (In-Flow) Stress vs. Strain.....	138

TABLE OF CONTENTS (Continued)

Page

40% GF-PP Monotonic (Cross-Flow) Stress vs. Strain..... 139

LIST OF FIGURES

<u>Figure</u>	<u>Page</u>
Figure 1: MTS 810 Hydraulic Load Frame at OSU	20
Figure 2: Modified MTS Hydraulic Power Unit.....	22
Figure 3: Instron "dynacell" +/-25kN Dynamic Load Cell.....	23
Figure 4: Axial (left) and Transverse (right) Extensometers during a Tensile Test ...	24
Figure 5: Instron 8800 FastTrack Controller before (left) and after (right) the added input channel.....	25
Figure 6: Anti-Buckling Fixture for Fatigue Tests with Sample Installed [38].....	27
Figure 7: Anti-Spin Fixtures, Showing Axial Extensometer Installed [38].	28
Figure 8: Anti-Spin Fixture for Upper Hydraulic Wedge Grip [38].....	29
Figure 9: ASTM D638 Standard Test Specimen Dimensions. Adapted from [2].	31
Figure 10: Long ASTM D638 Type 1 Geometry for pDCPD (units: mm)	32
Figure 11: pDCPD 4" × 12" Plaque with Four Test Coupons Cut	32
Figure 12: Shorter D638 Type 1 Coupon Geometry (for 40% GF-PP).....	33
Figure 13: Cross-Flow (left) and In-Flow (right) 40% GF-PP Coupons [38].	34
Figure 14: Excel Spreadsheet for Fatigue Test Bookkeeping.....	39
Figure 15: Excerpt from a Fatigue Test Tracking .csv File	44
Figure 16: Example Strain-Life Log-Log Plot.....	49
Figure 17: Test Data Post-Processing GUI.....	52
Figure 18: "Monotonic_Results" Folder Contents	53
Figure 19: GUI Monotonic analysis output: Stress-strain curve (top) and material parameters (bottom).....	54
Figure 20: Example Fatigue Parameters Output from the GUI.	55
Figure 21: pDCPD Monotonic Engineering Stress vs. Strain (overlaid).....	59

LIST OF FIGURES (Continued)

<u>Figure</u>	<u>Page</u>
Figure 22: 40% GF-PP (In-Flow) Monotonic Engineering Stress vs. Strain (overlaid)	62
Figure 23: 40% GF-PP (Cross-Flow) Monotonic Engineering Stress vs. Strain (overlaid)	65
Figure 24: pDCPD Fatigue Parameters (strain-controlled results).....	70
Figure 25: pDCPD Plastic Strain-Life.....	71
Figure 26: pDCPD Elastic Strain-Life.....	71
Figure 27: pDCPD Total Strain Amplitude vs. Reversals.....	72
Figure 28: log-log Strain-Life with Elastic and Plastic lines.....	73
Figure 29: pDCPD Cyclic Stress-Strain Curve.....	74
Figure 30: pDCPD Strain-Controlled Stress-Life.....	75
Figure 31: 40% GF-PP in-Flow Fatigue Parameters (strain-controlled results).....	77
Figure 32: 40% GF-PP in-Flow Plastic Strain-Life.....	78
Figure 33: 40% GF-PP in-Flow Elastic Strain-Life.....	78
Figure 34: 40% GF-PP in-Flow Total Strain Amplitude vs. Reversals.....	79
Figure 35: 40% GF-PP in-Flow log-log Strain-Life with Elastic and Plastic Lines...	80
Figure 36: 40% GF-PP in-Flow Cyclic Stress-Strain Curve	81
Figure 37: 40% GF-PP in-Flow Strain-Controlled Stress-Life.....	81
Figure 38: 40% GF-PP cross-Flow Fatigue Parameters (strain-controlled results)....	84
Figure 39: 40% GF-PP cross-Flow Plastic Strain-Life.....	85
Figure 40: 40% GF-PP cross-Flow Elastic Strain-Life.....	85
Figure 41: 40% GF-PP cross-Flow Total Strain Amplitude vs. Reversals.....	86
Figure 42: 40% GF-PP cross-Flow log-log Strain-Life with Elastic and Plastic Lines	86

LIST OF FIGURES (Continued)

<u>Figure</u>	<u>Page</u>
Figure 43: 40% GF-PP cross-Flow Cyclic Stress-Strain Curve	87
Figure 44: 40% GF-PP (cross-flow) Strain-Controlled Stress-Life.....	88
Figure 45: 40% GF-PP Stress-Life Comparison (in-flow and cross-flow).....	90
Figure 46: 40% GF-PP Strain-Life Comparison (in-flow and cross-flow).....	90
Figure 47: pDCPD Monotonic Tests (annotated)	93
Figure 48: Crystal Structure of Metals – FCC (left), BCC (center) and HCP (right) (adapted from [5]).....	94
Figure 49: Edge Dislocation (adapted from [5]).....	95
Figure 50: Shear Stress τ' Induced on Crystallographic Plane p' from Applied Normal Stress σ (adapted from [5]).	95
Figure 51: Edge Dislocation Motion on Slip Plane (adapted from [5]).....	96
Figure 52: Stress-Strain Curve for an Arbitrary Steel Type	97
Figure 53: Polymer Structures: Linear (top left), branched (top right), and cross-linked (bottom). (adapted from [5]).....	99
Figure 54: pDCPD Reaction Injection Molding Process (adapted from [44])	100
Figure 55: Strain Softening Followed by Strain Hardening (adapted from [5]).....	102
Figure 56: pDCPD Load-Controlled Stress-Life Parameters	106
Figure 57: pDCPD Load-Controlled Stress-Life	106
Figure 58: pDCPD Stress-Life Comparison (Load-Control and Strain-Control).....	107
Figure 59: Strain-Life Transition Point – Expected (left) vs. Results (right)	111
Figure 60: New Data vs. Old Data Stress-Life Comparison.....	115
Figure 61: Stress-Life Curve with Corrections Applied.....	116
Figure 62: Truck Hood with pDCPD Part Shown	117
Figure 63: IMAGE Results using Old pDCPD Stress-Life Properties	118

LIST OF FIGURES (Continued)

<u>Figure</u>	<u>Page</u>
Figure 64: IMAGE Results Using New pDCPD Stress-Life Properties.....	119
Figure 65: IMAGE Results Using New pDCPD Strain-Life Properties.....	120

LIST OF TABLES

<u>Table</u>	<u>Page</u>
Table 1: Example Strain Amplitudes Based on Monotonic Failure Elongation.....	37
Table 2: PDCPD Monotonic Test Results and Properties	58
Table 3: pDCPD Strain Amplitude Input Values	60
Table 4: 40% GF-PP (In-Flow) Monotonic Test Results and Properties	61
Table 5: 40% GF-PP In-Flow Strain Amplitude Input Values	63
Table 6: 40% GF-PP (Cross-Flow) Monotonic Test Results and Properties.....	64
Table 7: 40% GF-PP Cross-Flow Strain Amplitude Input Values	66
Table 8: 40% GF-PP In-Flow and Cross-Flow Monotonic Comparison.....	67
Table 9: pDCPD Strain-Controlled Fatigue Tests	68
Table 10: 40% GF-PP (In-Flow) Strain-Controlled Fatigue Tests	76
Table 11: 40% GF-PP (Cross-Flow) Strain-Controlled Fatigue Tests	83
Table 12: 40% GF-PP Strain-Controlled Fatigue Results Comparison.....	89
Table 13: pDCPD Load-Amplitude Input Values	104
Table 14: pDCPD Load-Controlled Fatigue Tests.....	105
Table 15: pDCPD Load-control vs. Strain-control Stress-Life Comparison.....	107
Table 16: Comparison of pDCPD Properties – old vs. new	114

DEDICATION

The following thesis is dedicated to my parents, Kim and Greg Gahan, because their support has greatly contributed to my success in completing this work.

Thank you for everything!

Fatigue Testing and Analysis of Polymer and Composite Materials Used in Heavy-Duty Trucks.

Chapter 1

1 Introduction

The use of plastic and composite materials in the heavy-duty truck industry for non-critical parts such as exterior body panels, hoods, dashboards and splash shields is becoming increasingly common. Incorporating these types of materials in designs provides a significant advantage over a traditional metal construction due to the weight reduction and subsequent improved fuel economy that can be achieved. While these parts may not be subject to the most substantial structural loads that are experienced by a vehicle during its intended use, they must be able to withstand various cyclic loading conditions that exist in a wide range of frequency and amplitude for the entire duration of a vehicle's operation. While the formation of a crack or other failure in one of these non-critical parts may not be immediately catastrophic to the performance of a truck, it could point to more detrimental failures within the structure, and potentially make the quality of the truck appear sub-par. Furthermore, the process to replace such a part can be expensive and time-consuming, leading to a decrease in profit and productivity for the customer.

A desire to accurately identify the locations of possible failure points in plastic truck parts before conducting physical testing on full-scale prototype trucks has prompted engineers to re-evaluate the digital simulation procedures used to validate

designs at Daimler Trucks North America (DTNA), a heavy-duty truck manufacturer that is based in Portland, Oregon and owned by Daimler AG. A new process is being developed at DTNA that incorporates the results of both multibody simulation (MBS) and finite element analysis (FEA) to perform a fatigue calculation that determines the damage accumulated by the structure throughout a defined load profile. More specifically, the MBS is first conducted by “driving” a digital truck model (described by several rigid bodies connected with springs and dampers) over a digital representation of the DTNA test track in Madras, Oregon. From this simulation, information is collected to describe the relationship between the rigid bodies in terms of interaction forces that can be applied to an FEA model in subsequent simulations. The MBS provides a significant improvement over using FEA alone due to its ability to incorporate non-linearity in connection points such as tires and bushings, providing realistic force inputs. The FEA is then implemented for two reasons: first, a modal stress analysis of the model determines the possible modes of deformation – called “Eigen modes” – based on the geometry of the structure, and second, a transient analysis applies the forces from the MBS to find the participation of each deformation mode in response to the loading. The fatigue calculation then uses the information from the modal stress and transient FEA to apply a predetermined “duty cycle” (or load history) to the structure, producing a metric for the cumulative damage that every part will experience. From this, analysis engineers are able to identify failure points before parts are sent into production, and designers are able to make revisions as needed. This process is called IMAGE: Integrated Multibody Fatigue.

The simulations included in IMAGE – both FEA and MBS – rely on accurate input data of three forms: geometry, loading conditions, and material data. Geometry is given in the form of digital 3D computer-aided design (CAD) models of parts created by the design engineers, and loading conditions are determined by the intended use of a specific vehicle – some trucks stay on the highway while others are used for vocational purposes, requiring a different set of test track conditions in their duty cycle. The material data can be more challenging, however, due to variability caused by testing equipment, analysis methods or environmental effects. This form of input data is also one of the most important for running simulations because it provides a connection to the physical world from which a digital simulation model can build, rather than being purely mathematical.

Steel and other alloys that have been used in vehicle designs throughout history are well defined in terms of their mechanical properties related to both static and fatigue loading response, and there is a large amount of literature to back up the existing data. Conversely, far less research has been dedicated to defining these properties (specifically strain-life fatigue) for plastic and composite materials or incorporating these materials into digital simulation tools. This body of research intends to fill this gap, further defining the properties of three plastic and composites that are commonly included in modern truck designs: polydicyclopentadiene (pDCPD), 40% wt. chopped-glass-fiber-reinforced polypropylene (40% GF-PP) and 35-40% wt. vinyl ester Sheet-Molding Compound (SMC), though the results for SMC are not presented in this thesis. The validity of applying standardized fatigue testing methods to these types of materials is also studied. The major deliverables of the research described in this

document are the addition of derived material parameters to the material database used by DTNA, and a detailed examination of the response of these materials to various testing conditions.

The behavior of materials in response to loading and deformation is an important and heavily studied topic within the engineering community, providing base knowledge from which all design and analysis builds. The most common loading scenario used for research is monotonic loading, where a material sample is deformed at a constant rate until a failure occurs. This is commonly referred to as a “tension test” and the results are conveniently displayed on a graph of stress vs. strain, where stress is expressed in pressure units (force per unit cross-section area), and strain is expressed as a unit-less quantity of percentage elongation [1]. Monotonic tests are the basis of material characterization because they provide underlying properties such as ultimate tensile strength, yield strength, percent elongation, Poisson’s ratio, and tensile modulus – all of which can be obtained from the stress-strain curve for any given test excluding the Poisson’s ratio, which is calculated during post-processing of test data. Due to the widespread familiarity with this form of testing, there exists a standard testing procedure for monotonic testing of plastic materials: ASTM D638, “Standard Test Method for Tensile Properties of Plastics”. This method calls for an extension rate of 5 millimeters per minute and provides guidance as to what properties can be calculated from test data as well as how to do so in a way that is applicable to plastic materials [2]. Standard method D638 will also be used to perform monotonic testing on the composite materials being studied here, using samples cut at various orientations with respect to the direction of reinforcement fibers.

To define the full behavior of a material in a way that is useful for the dynamic simulations that will be conducted at DTNA, a material's response to fatigue loading must also be studied in conjunction with the monotonic load case. However, fatigue testing provides a set of challenges beyond those presented by simple monotonic tensile tests. First, the equipment used to conduct fatigue testing is much more advanced, usually consisting of a servo-hydraulic load frame with a hydraulic pump to produce power, rather than a screw-driven load frame that is not capable of performing fast, cyclic motion. Function generators, load cells and strain gauges are required to collect and produce data at extreme rates, using a closed-loop system to control tests using displacement, load, or strain as the control variable [3]. Most often, fatigue tests are conducted in load-control mode, using the load cell to produce a waveform that applies a set load amplitude to the material during every cycle. Load controlled testing produces the stress-life fatigue relation, where the controlled load is converted to stress, and results are expressed in terms of stress amplitude vs. the number of loading cycles necessary to cause material failure. The stress-life fatigue approach is characterized by the Basquin equation, providing a mathematical representation of a materials response to load-controlled (or stress-controlled) fatigue loading [4]. The Basquin equation is a power-law relationship between the stress amplitude and the cycles-to-failure. It is important to note that, in some cases during this study, the Basquin equation will be represented in terms of stress-range, which is simply double the stress amplitude.

The stress-life fatigue relationship is applicable to high-cycle region of a material's fatigue response, where the applied load is small enough for the deformation to remain elastic (non-permanent stretching of atomic bonds [5]) and the material can

withstand more than 10^5 loading cycles [6]. Not all loading scenarios fit the high-cycle condition, however. It is often the case that when a cyclic load is applied to a material, it is sufficient to cause the deformation to exceed the elastic region, allowing the material to deform plastically (atomic movement within the material's crystal structure [5]) during every cycle. This is most commonly the case near stress concentrations in a part such as notches and sharp corners, where that area deforms plastically while the rest of the part's material remains in the elastic region.

The larger plastic deformation is more easily described by the strain (or deformation) that occurs, rather than the stress that is applied to the material. For this, the strain-life fatigue approach is applied – proving to be widely applicable in both the low-cycle, high-stress and the high-cycle, low-stress fatigue regions [7]. Because this strain-based fatigue approach provides a relationship between the applied strain amplitude and the cycles-to-failure, tests must be conducted in strain-control mode such that the strain amplitude is the independent variable of the relation. Two standard procedures exist that outline several common methods for conducting this form of testing: ASTM E606 “Standard Practice for Strain-Controlled Fatigue Testing”, and SAE J1099 “Technical Report on Low Cycle Fatigue Properties of Ferrous and Non-Ferrous Materials” [8,9]. As the names suggest, the intended application of these documents is for the testing of metals and other crystalline materials. However, portions of the standard methods that are presented can still be followed as a general outline for testing plastics and composites. Some methods from ASTM E739 “Standard Practice for Statistical Analysis of Linear or Linearized Stress-Life (S-N) and Strain-

Life (ϵ -N) Data” will also be followed to perform data analysis and curve-fitting operations [10].

Strain-life fatigue is derived on the idea that the total measured and controlled strain during a fatigue test can be mathematically divided into two parts: elastic strain and plastic strain. The elastic strain is determined by using Hooke’s Law to solve for strain from stress, and the plastic strain is the remaining value after the calculated elastic strain is subtracted from the total measured strain. The plastic strain can be expressed in terms of the Coffin-Manson relationship, which is a power-law relationship of similar form to the stress-life Basquin equation [11]. The total strain-life relationship is defined by adding the Coffin-Manson relationship to a modified Basquin relationship where stress is converted to strain using Hooke’s Law (it is important to note that this conversion of the Basquin equation is only performed in the case of strain-controlled testing and strain-life analysis). This goes to show that the strain-life method accounts for both low-cycle and high-cycle fatigue, and includes the Basquin relationship, therefore accounting for both strain and stress-oriented fatigue behavior – an idea that will be expanded on in sections 3.4 and 5.2 of this document. This versatility in the application of the strain-life method (to both high-cycle and low-cycle fatigue) can result in more accurate and applicable results.

For the application of gaining material data for the DTNA analysis process, there will be a goal of obtaining a full definition of the monotonic and fatigue properties, both stress-life and strain-life, for plastics and composites in a way that is valid and applicable for these types of material. However, in the interest of efficiency, it is not feasible to perform separate load-controlled and strain-controlled testing

programs on every material that engineers want to define. Ideally, a single strain-controlled testing program will allow engineers to retrieve all applicable fatigue parameters for a material without wasting time on unnecessary testing. Portions of this research will serve to prove or disprove this proposal by exploring the applicability of the strain-controlled strain-life method to plastic and composite materials. Furthermore, stress-life results from both load-controlled and strain-controlled fatigue testing will be compared, and the differences between the two methods will be discussed. Before-and-after IMAGE simulation results will also be presented to provide a visualization of the direct impacts of the research topics that are considered and material data that is collected during this work. It is hoped that this will lay the groundwork for the structural analysis of plastic materials at DTNA from which a robust database and workflow can build, providing both monetary and time-oriented savings.

Chapter 2

2 Literature Review

The purpose of this research is to fill a gap in existing literature regarding either the application of fatigue methods (specifically strain-life) to plastic and composite materials, or the integration of these materials into digital simulation models. Consequently, most of the existing literature covering similar topics is applied to metals, or uses a stress-life definition for polymers and polymer composites. In order to gain background on prior work that has been completed in this field, the contents of this literature review are divided into four subsections. The first subsection discusses the vast history of fatigue theory in general; the second subsection covers existing literature regarding fatigue of polymer materials; the third subsection discusses the fatigue and manufacturing effects of short-fiber-composite materials; finally, the fourth subsection will briefly discuss examples of digital fatigue analysis applications.

2.1 History of Fatigue Theory

Material fatigue is an area of study that has gathered significant interest throughout the technological development of society, mostly due to the potential for catastrophic consequences caused by the phenomenon. While this specific material behavior is seemingly well-documented and heavily accounted for during most product development, there are infinite fatigue-related topics left to study despite the significant advancements already made. The history of fatigue analysis starts 183 years ago in 1837 with Wilhelm Albert, a mine worker who noticed in-service failures of metal

conveyor chains within the Clausthal mines where he worked [12]. Albert is credited with collecting the first fatigue data, as he created a machine to test these chains for fatigue failure. He is also credited with inventing the metal wire rope to be used in place of expensive imported hemp rope [12].

The term “fatigue”, however, was not associated with this material behavior until 1854, when Frederick Braithwaite published a document warning of the dangers presented by mysterious and seemingly random failures of metal structures [13]. He specifically mentions an incident at a brewery in London, where a fermentation tank burst open due to fatigue failure after the tank had been filled and emptied multiple times. This is believed to be the London Beer Flood of 1814, which killed 8 people [14]. Braithwaite also mentions many instances where fatigue failure occurred in machinery such as railroad axels, specifically mentioning a publication by William Rankine (famous for his work in the field of thermal-fluid science) in 1843 [13]. In this publication, Rankine discusses several unexpected failures of railway axels, and proposes that they occurred due to slow “deterioration” of the metal over time [15].

Following up Rankine’s work and Braithwaite’s coining of the term “fatigue”, there was a period of several years where numerous instances of fatigue failure in railway axles occurred, sparking interest in the topic of repeated-loading behavior of metallic materials [12]. This motivated the work of August Wöhler, who is widely known as the “founding father” of material fatigue research [16]. Wöhler is credited with the development of the first reliable equipment that was used to measure the deflections and loads experienced by railway axels during use, creating test stands to simulate fatigue loading scenarios, and for the initial advancements in fatigue theory

regarding stress-ratio and endurance limit [16,17]. The work of Wöhler is quite impressive in the sense that it provided significant groundwork from which all fatigue theory could build.

Following up on Wöhler's discoveries and measurements, the next account of fatigue data is not recorded until the 1930's, and it was during that same time that Wöhler's collected data (originally presented as tabulated values) was plotted and presented for the first time as the SN or stress-life curve – then called the “Wöhler curve” – in 1936 [12]. The work of O.H. Basquin in 1910 also suggested that these curves could be mathematically represented by an exponential relationship between cyclic stress amplitude and stress-cycles-to-failure, linearized when plotted on log-log axes [18]. This is the “Basquin equation” that is used to this day to represent the stress-life fatigue definition in the finite-life region, Where C and b in Equation (1) are the stress-life coefficient and slope, respectively:

$$\sigma_a = CN^b \quad (1)$$

In the following years, progress was made to further expand beyond the study of fatigue in metals using the stress-life definition, with the work of S.M. Cadwell in 1940. Cadwell was the first to publish major research regarding the fatigue of rubbers, where the number of oscillations-to-failure was recorded with respect to varied levels of combined shear and tensile deformation of rubber samples [19]. The literature did not provide distinct theories behind the recorded results and explained that at the time of publication, such theories would be conjecture. Also in this time-frame was the development of Miner's rule in 1945 by M.A. Miner. Miner suggested that the damage accumulated in a material due to fatigue can be represented as a summation of the ratio of the cycles-to-failure at a certain stress S_i to the number of times the stress S_i has been

applied to the material, for a number (i) of different stress levels. When this summation reaches a pre-determined value (usually 1.0 for design and analysis work), it is indicative of a failure or crack within the material [20]. Miner's Rule has become a very well-used and expanded-upon idea that plays a role in most design and structural analysis work to this day.

The advancement in fatigue theory that is most applicable to this thesis is the work of S.S. Manson and L.F. Coffin in 1953-1954, within which the term "Low Cycle Fatigue" was first coined, accurately defining the low-cycle region of a material's fatigue life [21,22]. The low cycle fatigue definition accounts for plastic strain (permanent deformation) and elastic strain separately – considering any large deformation occurring near stress concentrations in a part, while the rest of the part may appear to only experience elastic deformation [23]. This provides a large improvement over the stress-life method as it is much more accurate in representing the total cyclic deformation (and subsequent fatigue damage) that is occurring within a material. Low cycle fatigue is mathematically defined by the Coffin-Manson Equation, similar in form to the Basquin equation (Equation (1)) except it is in terms of plastic strain amplitude and reversals (2 reversals per cycle), rather than cyclic stress amplitude and cycles. The Coffin-Manson equation is presented as Equation (12) in section 3.4.2 of this document.

The Coffin-Manson relation is paramount in defining the strain-life fatigue method, where it is combined with the Basquin relationship to create the Coffin-Manson-Basquin Equation (Equation (24)), commonly called the strain-life equation [23]. Being that strain-life and stress-life fatigue are the basis of this work, the fatigue

history outline will conclude here. While further advancements have been made in more recent history – including the work of Matsuishi and Endo in 1968 to expand on Miner’s rule to create a damage-counting algorithm [24] – these other historical topics will not be discussed in detail.

2.2 Fatigue of Polymers

The study of fatigue and general mechanics in polymers is a fairly new topic that provides unique challenges [25]. These materials have increased sensitivity to environmental effects such as strain-rate and temperature, and often exhibit behavior under cyclic load that may not be well understood. This section of the literature review will provide examples of prior work discussing these topics.

Opp et al. [26] performed an investigation regarding the application of the low-cycle fatigue methods derived by Coffin and Manson to six structural plastic materials. The study included fatigue testing at a large range of frequency in an effort to fully record the dynamic characteristics of these materials, and then compared multiple low-cycle fatigue models including the strain model, energy model, empirical model, and combined energy model. The results of the study suggest two polymer fatigue failure mechanisms: “melt failure” at large strain levels, and crack-propagation at low strain levels. It is also stated that significant work is yet to be done to simplify the polymer fatigue models.

Hertzberg, Manson and Skibo studied the sensitivity of polymeric materials to varying frequency used for fatigue testing [27]. A frequency range of 0.1 Hz to 100 Hz was considered, using various waveform shapes. It was concluded that the sensitivity

to frequency is highest in materials that are prone to crazing; a phenomenon where significant surface-cracking appears when the material is subjected to load.

Lesser [28] performed load-controlled fatigue testing of polyacetal and nylon at 2 Hz using ASTM D638 Type 1 coupon geometry. The goal of the study was to monitor the hysteretic behavior of the materials and document any changes in the mechanical behavior over time (throughout a fatigue test). This was completed using a stress-life fatigue definition and considering both dynamic and viscoelastic properties of the materials. The results of the study suggest that stress hardening, stress softening, and thermal softening can all occur due to variations in dynamic material properties.

Mortazavian and Fatemi [29] also conducted load-controlled testing on two polymer materials, as well as two other short-glass-fiber reinforced polymer materials of varied fiber-orientation. The conclusion was made that mold-flow direction has a negligible effect on the fatigue properties of unreinforced materials, and the opposite is true for the reinforced materials that were tested. The study also showed that mean-stress has a large effect on fatigue life for both types of material.

2.3 Manufacturing and Fatigue of Short-Fiber-Composites

The studies mentioned in section 2.2 are regarding non-reinforced polymeric materials. This section will provide examples of research about the fatigue of short-fiber composites – most of which involve SMC materials. Short-glass-fiber composites provide additional challenges as they are specifically affected by the density of reinforcement, often expressed as a weight percent (wt %), as well as the presence of fiber ends within the material – increasing sensitivity to stress concentrations [30]. It is

often the case that the manufacturing methods will also greatly affect material properties due to fiber orientation affects.

Olsson et al. [31] studied the effects of molding parameters on the flow-properties during the molding process of 15-35 wt% sheet-molding-compound or SMC. It was found that high vacuum, low ram velocity, and low mold temperature facilitated a uniform flow, creating a part with minimal voids and varying fiber density throughout. Pan et al. [32] carried out a similar study regarding the mechanical properties of polydicyclopentadiene (pDCPD) graphite nano-sheet composites, based on a reaction injection-molding (RIM) manufacturing method and a coupling agent called TEG. After testing and analysis, it was found that the TEG agent worked to reinforce the pDCPD matrix, and provided slightly stronger mechanical properties with some interesting forms of wear showing.

Much of the research regarding the fatigue of short-fiber composites is regarding SMC materials. P.K. Mallick studied the fatigue characteristics of 50-65 wt% glass-fiber reinforced SMC, using both a polyester and a vinyl ester matrix [33]. The research involved 3-point bending fatigue tests at various elevated temperatures, followed by static 3-point bending tests of the failed fatigue samples (fatigue failure defined as 15-20% drop in dynamic modulus). It was found that vinyl ester SMC has superior fatigue performance and retains more static strength than polyester specimens, which showed a larger amount of surface micro-cracking. This work also discusses the fact that short-fiber composites with random fiber orientation are much more matrix-dependent than unidirectional composites.

Fleckenstein et al. [34] conducted fatigue testing of un-notched, flat SMC samples with 1.0 inch-long fibers of 0 and 90-degree orientation, varying between 20, 30 and 50 wt% fiber density. Testing was conducted in load-control using both a 0-tensile ($R = 0$) and a fully-reversed ($R = -1$) stress ratio (supports were used to prevent buckling during the fully-reversed tests), and the frequency was kept low enough to prevent any self-heating of the material. The results were displayed using the stress-life (SN) definition with a single slope “k”. The work states that the idea of an endurance limit or two-sloped stress-life curve is not applicable to polymer-composites – though this concept is also questioned even for metals [35]. The results of the testing performed by Fleckenstein et al. [34] showed that the 0-degree (parallel to load) fiber orientation experienced the best fatigue resistance, whereas the 90-degree orientation induced more strain in the matrix. It was also found that fiber orientation does not affect the slope of the SN curve, whereas the fiber content does – lower content (wt%) flattens the SN slope.

2.4 Application of Fatigue Data to Digital Simulations

While the study of fatigue in plastic and composite materials is new, the application of these materials within digital analysis simulation models seems even less common. This section will briefly provide some examples of studies involving fatigue simulations of polymers or composite materials.

Malo et al. [36] studies two models of SN fatigue in composites: one using pseudo-grain modeling to compute SN response at any fiber orientation state, and another based on damage evolution in the composite’s matrix phase. These models were tested on a polymer-composite automotive part – results were compared between

FEA/fatigue solver results derived from the models and fatigue testing that was completed at low frequency (3 Hz) to prevent heating. It is suggested from this work that the strain-life method is not used for plastic materials as it could cause complications. The author states that the stress-based fatigue approach best suits these materials, but goes on to state that distinct conclusions about the correct fatigue testing methods for polymers have yet to be made.

In another study by Bi and Mueller [37], the process of using FEA models to predict fatigue failure during product development is considered. Mathematical modeling including the use of Miner's Rule [20] is suggested as a way to account for a lack of literature regarding the damage-modeling of composite materials under dynamic loading. As with most other studies mentioned in this literature review, the fatigue data that is included in this work is stress-based, and the application of a strain-based approach is not mentioned.

2.5 Summary

Within this literature review, a brief overview of the history of fatigue analysis was provided, followed by several examples of studies involving the fatigue of both polymers and short-fiber polymer-composites, and finally examples of the application of digital fatigue simulations. From this, it can be seen that very little prior work has applied the strain-life fatigue method to a non-metal material. Furthermore, the previously mentioned work of Malo et al., Opp et al. and Winkler [25,26,36] specifically suggests that strain-based fatigue could be problematic for plastic materials, but do not discuss in detail the reason why or give data-backed examples other than stating that hysteretic heating and creep-effects can hamper the analysis. This gap in

existing work provides an area of focus for this thesis. By performing strain-controlled fatigue testing and using a strain-based fatigue definition for a polymer and short-fiber-composite material, not only will necessary data be provided to DTNA, but it can also be determined whether the strain-life fatigue method can successfully be applied to these materials. While other works have briefly mentioned concerns regarding this approach, this topic has not been the focus of any study. This thesis intends to mitigate obscurity related to this topic.

Chapter 3

3 Methods and Procedures

In order to provide the desired data for the materials specified by DTNA, a combination of several standard testing procedures is followed, including some modifications to account for the necessary testing conditions. Monotonic testing follows ASTM D638, and fatigue testing follows ASTM E606, SAE J1099 and ASTM E739. This chapter will describe the equipment and mathematical procedures used for performing the testing and the post-processing of collected test data.

3.1 Testing Equipment

All of the testing for this project was completed at Oregon State University (OSU), using equipment that is owned by OSU. Although the equipment is shared between several research labs, it was reserved for this testing throughout the span of the project, allowing for undisturbed and continuous testing.

3.1.1 Hydraulic System

Fatigue testing requires more complicated equipment than monotonic testing. Specifically, a closed-loop servo-hydraulic load frame is essential for completing fast, cyclic waveforms with accuracy – a function that screw-driven load frames are not usually capable of performing. At OSU, hydraulic systems are hard to come by, and those that are available tend to be quite old, requiring maintenance in order to be brought back into ideal condition. The system chosen for this project, shown in Figure 1, is an MTS 810 Model 318.25B, 250 kN hydraulically actuated load frame.



Figure 1: MTS 810 Hydraulic Load Frame at OSU

This load frame is powered by an MTS 510.10C hydraulic power unit (HPU) that can produce a hydraulic flowrate of 10.1 gallons per minute (gpm). This HPU, shown in Figure 2, has been heavily modified from its original form as the facility in which the system is located (Dearborn Hall, OSU) does not allow a circulating, self-cooling water system to be connected to the HPU's heat exchanger – the feature that is

responsible for regulating the temperature of the hydraulic oil. The water-cooled heat exchanger that comes stock with the HPU was therefore originally not used, and an air-cooling heat exchanger was installed. At the beginning of this project, it was determined that the air-cooling system had become clogged throughout the several years since this hydraulic system was used regularly, preventing a sufficient flow of oil through the heat exchanger. The pump would then quickly overheat after just hours of running, which is not conducive for running fatigue tests that can last several days per test. To solve this issue prior to running any tests, the air-cooled heat exchanger was replaced with the new air-cooled heat exchanger, labeled in Figure 2 below. A (single pass) flow of cold water through the original water-cooled heat exchanger was also added to aid in system temperature regulation. The water from this additional water-cooled heat exchanger empties to a nearby drain.

It should be noted that when this hydraulic system was originally installed at OSU, it was used by a research group who performed high-cycle, high frequency fatigue-crack-growth experiments on metals. Due to the nature of this type of testing and the high stiffness of the materials being tested, these tests typically involved a very low amplitude waveform that did not challenge the capabilities of the hydraulic system. The plastic material being tested for this research, however, are a lot less stiff and therefore require a much larger displacement to induce fatigue effects. These more aggressive waveforms present a greater challenge to this hydraulic equipment and are the main cause for the maintenance issues described above.

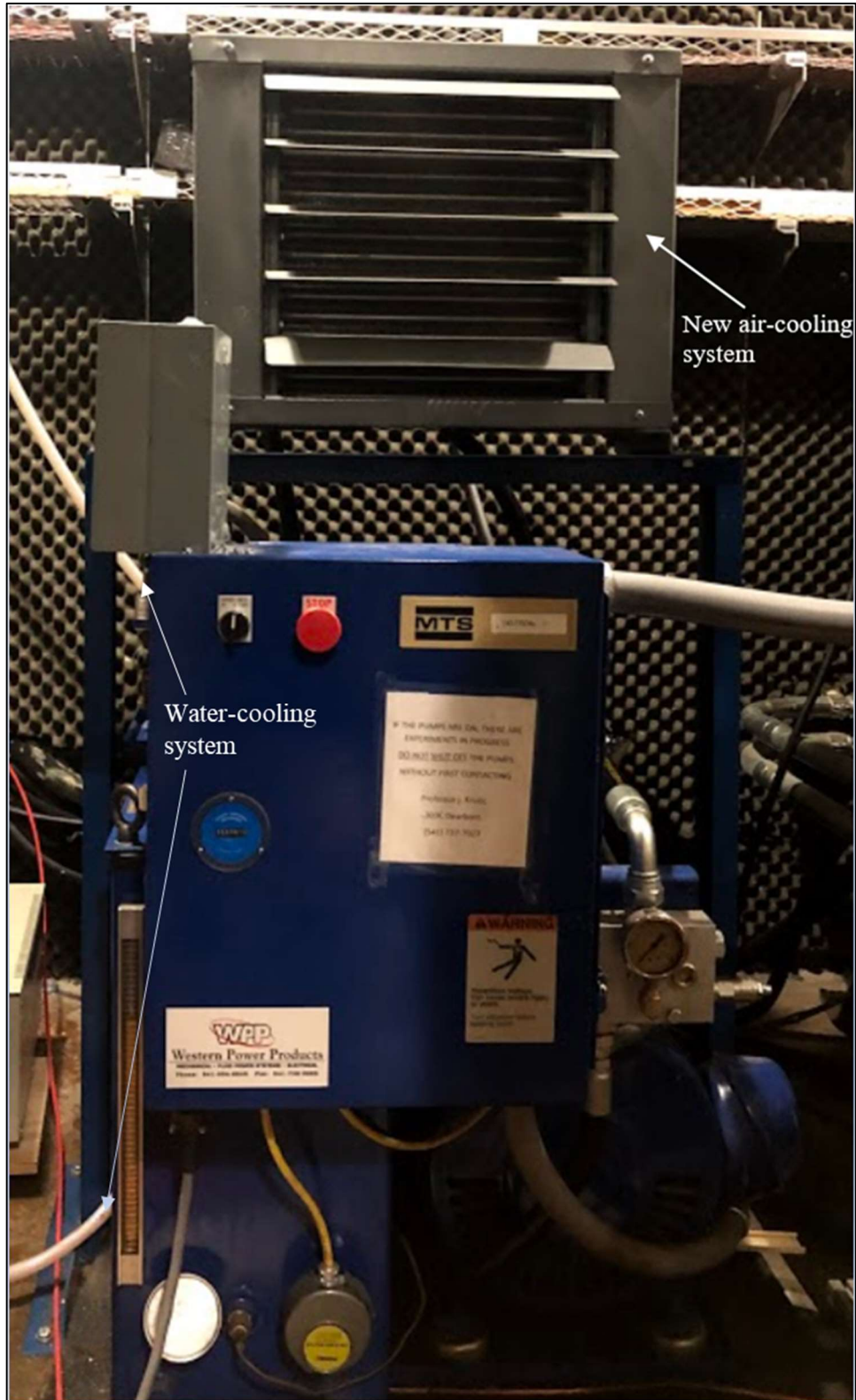


Figure 2: Modified MTS Hydraulic Power Unit

3.1.2 Data Acquisition

There are four necessary channels of live data that must be available from this testing: load (kN), position (mm), axial strain (%), and transverse strain (%). This section discusses the hardware and software that is incorporated to manage this data acquisition.

The MTS load frame described above contains a stroke indicator, which outputs data regarding the actuator's position (mm) relative to a set starting point. The position data is not used to calculate strain, but it is necessary for setting safety limit switches as well as monitoring deformation rate during monotonic tests. In addition, the load frame is retrofitted with an Instron dynacell +/-25kN dynamic load cell that is used to collect load data throughout all tests (Figure 3). The standard MTS load cell that comes with the MTS 810 load frame is not used because it does not interface well with the Instron software and components that are used.



Figure 3: Instron "dynacell" +/-25kN Dynamic Load Cell

The testing system does not have a built-in method for measuring strain data during tests. For this purpose, two extensometers were selected that fit the budget of the project and provide the most accurate strain measurement possible (Figure 4). The first extensometer is the Epsilon axial 3542-050M-025-ST with a gauge-length of 50mm, and a measurement range of +25%/-10% strain. The second extensometer, which is only to be used during monotonic testing, is the Epsilon transverse 3575-250M-ST extensometer, with a measurement range of +/-2.5 mm. These two extensometers are ideal when paired together as the axial unit can produce static and dynamic readings of axial strain – in units of percentage or mm/mm– during both monotonic and fatigue testing, and the transverse extensometer can be used during monotonic tests to accurately measure the change in cross-section as a sample is deformed, using units of mm or percentage. The transverse data is necessary for calculation of Poisson’s ratio, as well as obtaining the instantaneous cross-sectional area of a tensile test sample.



Figure 4: Axial (left) and Transverse (right) Extensometers during a Tensile Test

The hydraulic system is connected to an Instron 8800 FastTrack controller that has auxiliary input channels as shown in Figure 5. This is the input location for the extensometers described above. Because there are two extensometers, two input channels are necessary for simultaneous data acquisition. Being that the controller had previously only one channel, one additional input was installed prior to testing.

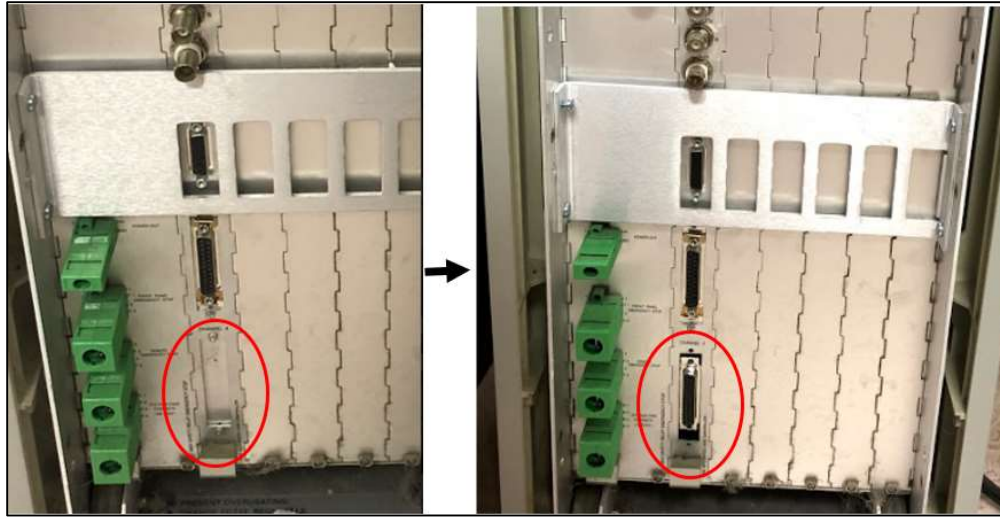


Figure 5: Instron 8800 FastTrack Controller before (left) and after (right) the added input channel.

3.1.3 Software

The load frame is controlled with the Instron Wavematrix and Console software packages. Wavematrix allows for easy test method set up, and Console is an interface for controlling channel parameters and arming/disarming limit switches. The monotonic test method sequence includes a position hold for 3 seconds, followed by a constant position-controlled ramp segment set to a rate of 5mm/minute until a significant drop in load indicates specimen failure. This test method collects data at 100 Hz for Time (s), Position (mm), Load (kN), Transverse Strain (%), and Axial Strain (%). The fatigue test method includes a 3-second strain-controlled hold period, followed by a strain-controlled triangular waveform of a user-set frequency and strain

amplitude (%). The waveform for this test method is fully-reversed, meaning that the specimen will be subject to a +/- strain amplitude, going from tension into compression by the same percentage axial strain during every cycle. A maximum frequency of 10 Hz is used. This test method is also set to stop when the maximum (tensile) load drops significantly, indicating specimen failure. The Time (s), Cycle Count, max/min Position (mm), max/min Load (kN), and max/min Axial Strain (%) channels are collected for every cycle.

All data is analyzed using a combination of Microsoft Excel, MATLAB, and Python. Excel is used for bookkeeping purposes, containing test logs and tables containing information about every type of test. MATLAB was used for the post-processing and analysis of test data before this process was replaced with a Python program.

3.1.4 Machined Fixtures

Following ASTM E606, the cyclic waveforms used for the fatigue tests are fully reversed (as stated above), meaning there is both a tensile and a compressive portion of each loading cycle [8]. Because the plastic materials being tested are relatively easy to bend as compared to metal, an anti-buckling fixture must be used to assure that there is no induced bending stress due to buckling when the sample is compressed. The anti-buckling fixture is shown in Figure 6 below, labeled “A”.

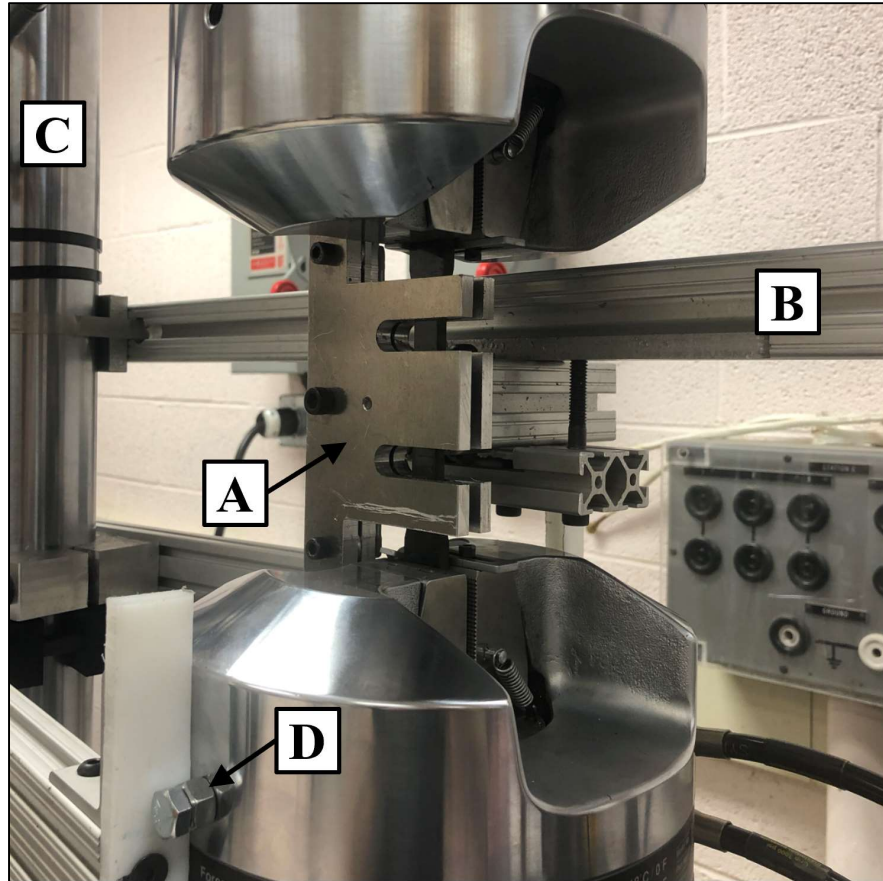


Figure 6: Anti-Buckling Fixture for Fatigue Tests with Sample Installed [38].

This anti-buckling fixture is made from two sandwiched pieces of aluminum, machined such that there is a slot slightly wider than the thickness of the test sample that is axially aligned with the closed position of the hydraulic grips. There are also two notches cut out of the fixture within the gauge length of the sample for the axial extensometer to clip onto the material during a test. The fixture is held in place by aluminum T-slot (labeled “B” in Figure 6) that is tied to the vertical columns of the load frame (labeled “C” in Figure 6). The anti-buckling fixture with the axial extensometer installed can be seen in Figure 7.

The hydraulic grips on the MTS 810 load frame are able to spin freely about the axis of loading. This would not be an issue when testing metals and other stiff

materials, but due to the relatively low stiffness of the plastics being tested here, there could potentially be an induced torsional load due to the twisting of a sample if the two grips become misaligned throughout a cyclic test. To mitigate this, there are two sections of aluminum T-slot that attach to one of the load frame's vertical columns with sets of machined half-moon-shaped clamps that match the diameter of the column. These T-slot bars extend to the actuated hydraulic grip and have plastic attachments on the end to decrease frictional heating as it contacts the head of a bolt protruding from the grip assembly (as shown in Figure 6, labeled "D"). Figure 7 shows that there are two of these anti-spin fixtures contacting the bottom grip (labeled "1" and "2"): one on each side such that the grip cannot spin in either direction.

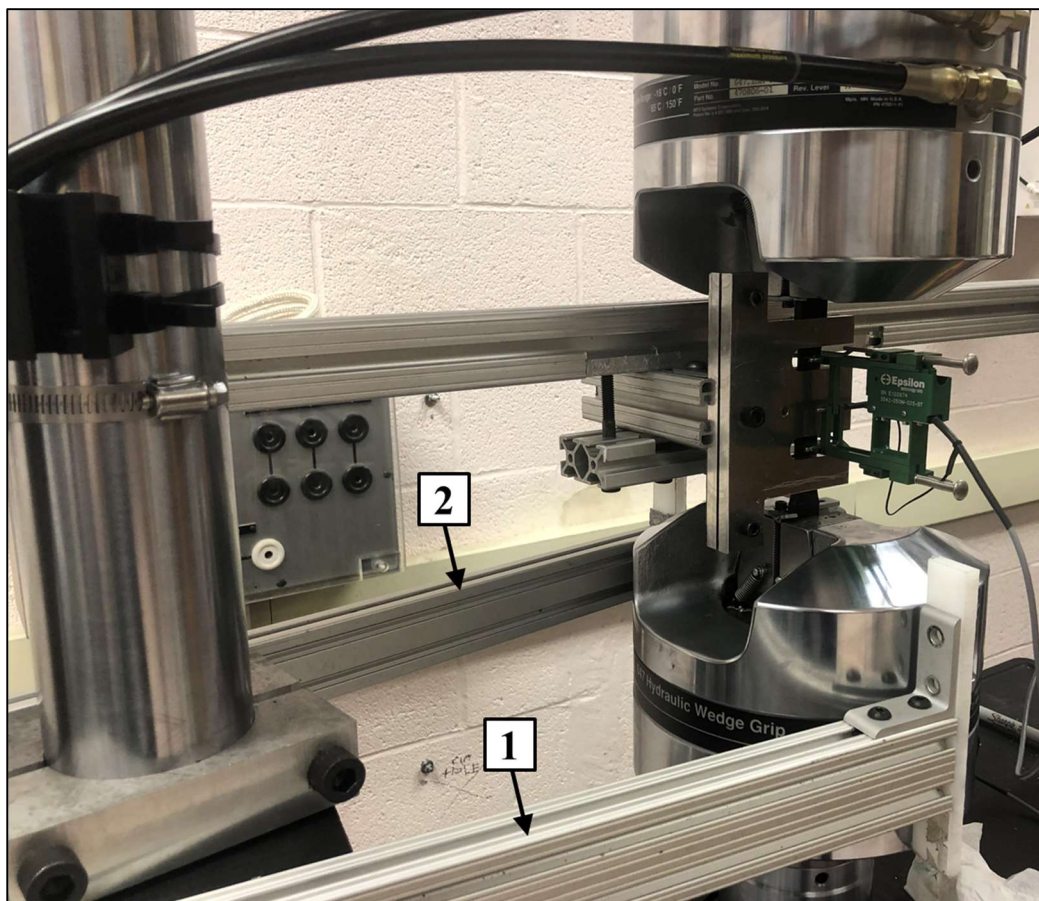


Figure 7: Anti-Spin Fixtures, Showing Axial Extensometer Installed [38].

The upper grip, mounted directly below the load cell, is also free to spin as the actuator cycles during a fatigue test. To mitigate its movement, another section of T-slot material is used with cutouts that line up with bolt heads protruding from the top of the upper grip assembly (see Figure 8). The ends of the T-slot section contact the two vertical columns of the load-frame to prevent rotation in either direction. Because the load cell is attached directly above the grip, the weight of this anti-spin fixture must be balanced out of the load-cell reading.



Figure 8: Anti-Spin Fixture for Upper Hydraulic Wedge Grip [38].

3.2 Material Selection and Sample Preparation

3.2.1 Selection of Materials

The materials studied during this research are identified based on the lack of material parameters that are available to engineers at DTNA. As previously stated, various design, digital simulation and analysis techniques rely on accurate material information to achieve usable results. For the polymers and composite materials being studied here, it was found that their properties were either estimated or based on data

from the material supplier that can be easily misinterpreted and unsubstantiated. It was determined that fully defining at least three of these materials would significantly improve the design and analysis process, providing an excellent base from which the DTNA material property database can expand. The selected materials are polydicyclopentadiene (pDCPD), 40%wt. glass-fiber-reinforced polypropylene (40% GF-PP), and sheet-molding compound (SMC). It was agreed that testing for pDCPD and 40% GF-PP could take place at OSU, and testing for SMC would be completed by test engineers at DTNA. For that reason, the results for SMC will not be presented in this thesis, and the research will instead focus on pDCPD and 40% GF-PP.

Including both pDCPD and 40% GF-PP in this study provides a representation of the variety of materials that the research aims to discuss. pDCPD is an isotropic, cross-linked thermoset polymer that is used for hoods and exterior body panels. The 40% GF-PP material is an injection-molded chopped-glass-fiber reinforced composite with a thermoplastic polypropylene matrix – classified as a fiberglass reinforced plastic (FRP). 40% GF-PP is used for splash shields and other non-critical exterior parts. These two types of materials are very commonly used in new truck designs within the heavy-duty truck industry as a whole.

3.2.2 Preparation of Testing Samples

Following ASTM D638, the D638 Type 1 material coupon geometry is used as it is most applicable to the plastic materials that are being tested. This geometry (shown in Figure 9 below) calls for a gauge section width (W) of 13 mm, and a fillet radius (R) of 76 mm leading to a 19 mm wide grip section (W_o) [2]. In Figure 9, these dimensions

are given symbolically because they may differ based on the thickness of the material being tested.

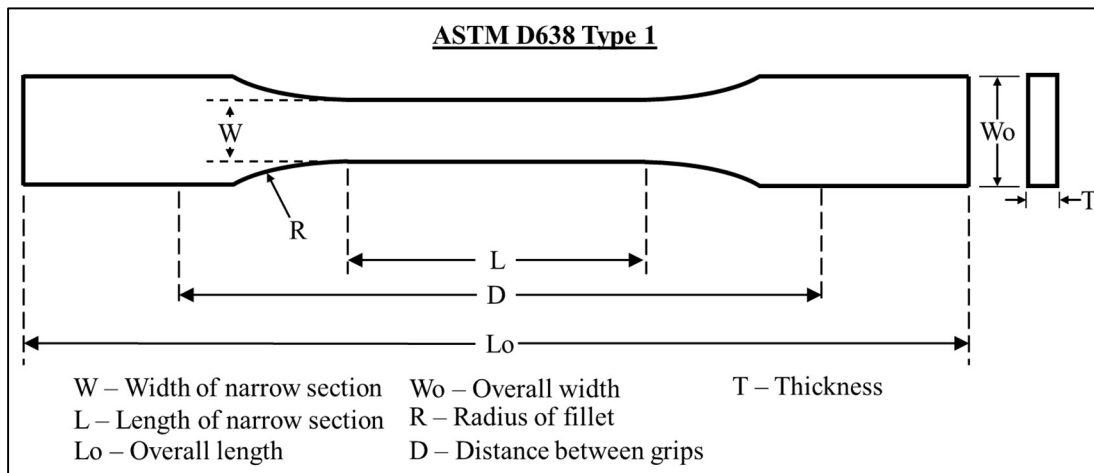


Figure 9: ASTM D638 Standard Test Specimen Dimensions. Adapted from [2].

The materials are received in the form of flat plaques of various dimensions, depending on what the material supplier has available. Therefore, some of the dimensions called out in Figure 9 are slightly modified for each material based on the geometry of the plaques that are received. However, only the lengths of the gauge section and grip section are changed, shortening or adding length to the specimen as a whole without changing its mechanical properties.

pDCPD is available from Paramont Mfg. LLC in the form of 4" × 12" panels that are 5 mm thick, having been cut from a flat section of a truck's hood top-panel. Two batches of 30 panels each were received for testing, molded on September 17, 2018 and April 15, 2019, respectively. Because pDCPD is an isotropic polymer, there is no need to have samples cut at varied orientations on the plaque. Therefore, it is possible to get four samples from each 4" × 12" panel as shown in Figure 11. Due to the plaque geometry, the total length of the pDCPD coupons (samples) are increased to 248 mm by making the grip section 50 mm long and the gauge length 110 mm long,

rather than 25 mm and 50 mm, respectively, as called for by D638. The updated dimensions are shown in Figure 10.

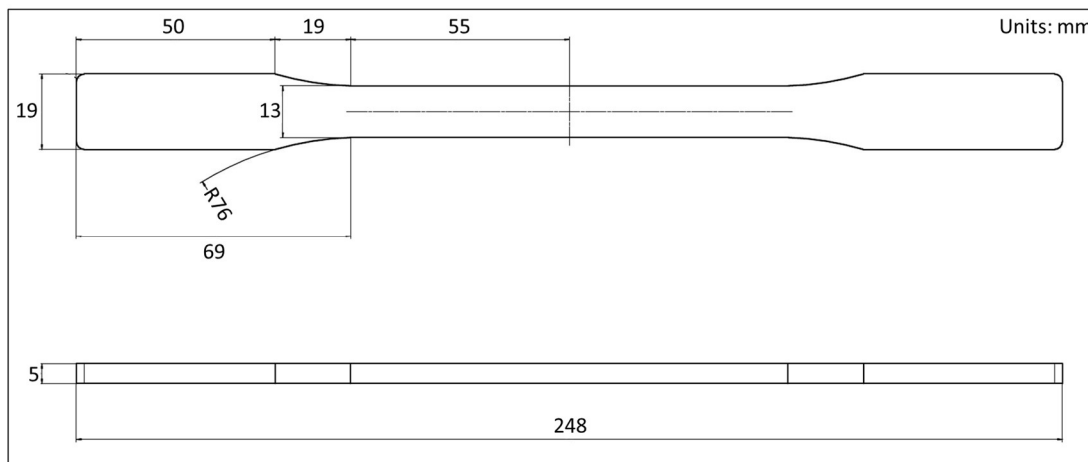


Figure 10: Long ASTM D638 Type 1 Geometry for pDCPD

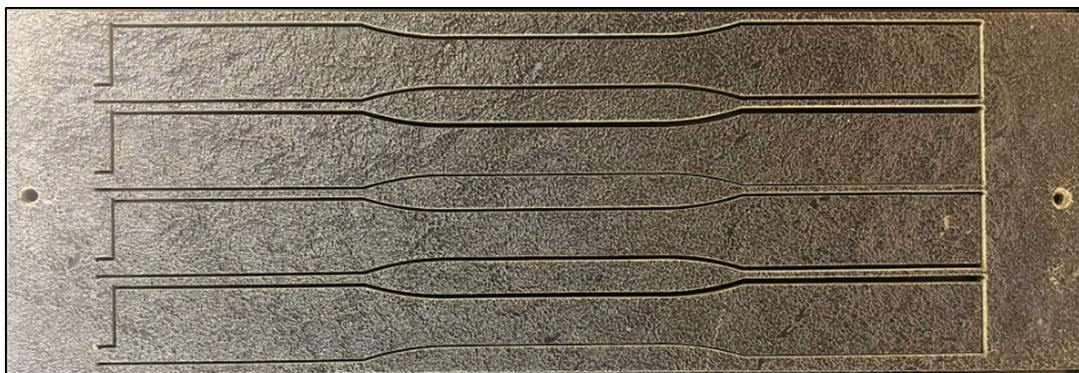


Figure 11: pDCPD 4" × 12" Plaque with Four Test Coupons Cut

The increased length of the pDCPD coupon geometry is preferable over shorter material coupons, as it provides more room for an extensometer to be attached and more contact area between the sample and the hydraulic grips of the load frame to prevent any unaccounted-for slipping. Increasing the length to this extent is not possible for the 40% GF-PP material, however, because it is shipped from Asahi Kasei in the form of square 8 inch × 8 inch, 3mm thick injection-molded plaques. These plaques are made using a single-gated mold, meaning that the material enters from one edge and

flows in a single direction until the mold is full. This induces an orientation of the glass reinforcement fibers, where the majority of the fibers will be aligned with the direction of flow within the mold. Consequently, this material is not isotropic and samples must be cut in multiple directions with respect to the reinforcement fibers to account for this.

The material coupons for 40% GF-PP have only been elongated slightly from the ASTM D638 standard dimensions. As shown in Figure 12 below, the gauge length is 55 mm, with a 47 mm grip section and a total length of 197 mm, keeping within the 8-inch length restriction set by the size of the plaques.

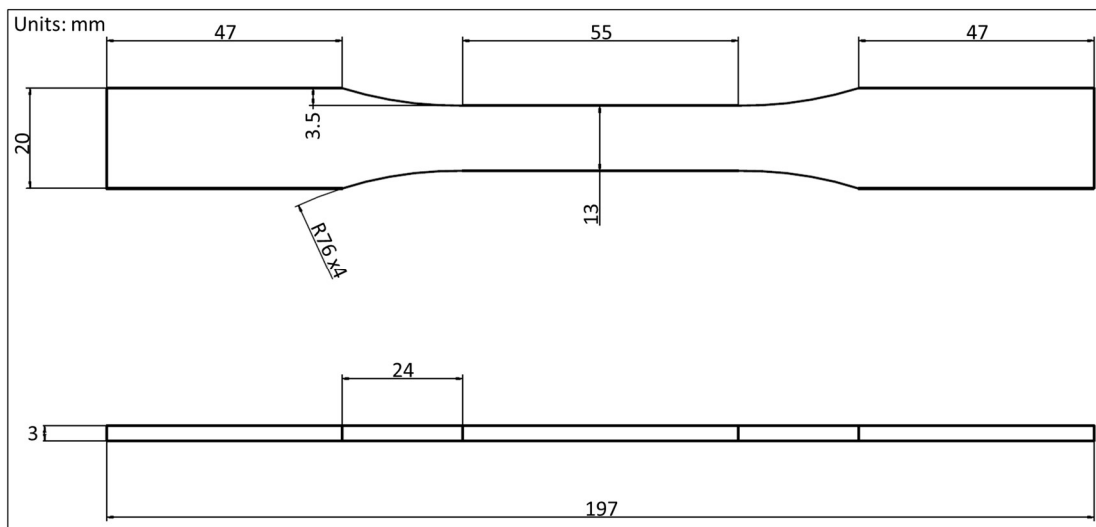


Figure 12: Shorter D638 Type 1 Coupon Geometry (for 40% GF-PP)

The number of coupons generated from the 40% GF-PP plaques depends on the desired fiber orientation, as shown in Figure 13. When cross-flow coupons are cut (fiber direction is perpendicular to the length of the coupon), the first 1/3 of the plaque closest to the mold opening must be discarded. This is because the fibers are not truly aligned to their flow direction as they first enter the mold, and therefore a coupon cut from that region cannot confidently be classified as “cross-flow”. When in-flow coupons are cut (fiber direction is parallel to the length of the coupon), then the entire plaque can be

used because, in this orientation, the mold-flow is consistent throughout the length of the plaque. Each 8 inch \times 8 inch 40% GF-PP plaque yields seven in-flow coupons, or five cross-flow coupons. In Figure 13, the arrows drawn on the plaques indicate the direction of mold-flow.



Figure 13: Cross-Flow (left) and In-Flow (right) 40% GF-PP Coupons [38].

A waterjet is used to cut both the pDCPD and the 40% GF-PP coupons from their respective plaques. This method of cutting is chosen because it significantly decreases the amount of internal damage added to the material during the manufacturing process. This is ideal compared to more standard machining methods because unwanted defects in the material will inevitably affect test results if they are not accounted for. The waterjet cutting was completed by both Viper Northwest, Inc. in Albany, Oregon and King Machine Products, Inc. in Corvallis, Oregon.

3.3 Testing Methods

This section will outline the methods by which testing is completed for the monotonic, strain-controlled fatigue, and load-controlled fatigue tests. Monotonic

tensile testing follows the guidelines of ASTM D638 [2], whereas the fatigue testing roughly follows ASTM E606, SAE J1099, and ASTM E739 [8, 9, 10].

3.3.1 Monotonic Testing

Before fatigue tests can be performed on any material, monotonic tensile testing must be completed to determine the material's tensile properties. These properties include the tensile modulus, Poisson's ratio, failure elongation (% strain), yield stress, ultimate strength and several others. The results of these tests – mainly the average failure elongation – are used to plan the input parameters for the subsequent strain-controlled or stress-controlled fatigue testing.

After a sample has been selected for a monotonic test, the width and thickness of the sample's gauge section must be measured to the nearest 100th millimeter. The sample is then loaded into the grips of the hydraulic tensile tester, and both the axial and transverse extensometers are installed on the gauge section. After the strain and load channels have been balanced such that they read value of 0.00% and 0.00 kN respectively, the test is started and the load frame deforms the sample at a rate of 5 millimeters per minute while recording live data of position (mm), load (kN), axial strain (%) and transverse strain (%). A sharp and sudden drop in the measured load will indicate the system that a failure has occurred, and the computer will signal for the test to stop while saving a .csv file that contains all of the data for the channels previously listed. The saved data is then formatted and input to post-processing scripts that perform the mathematical operations outlined in section 3.4.1 and 3.5 below. According to ASTM D638, at least five samples should be tested for monotonic properties, and the results of these tests are averaged.

3.3.2 Strain-Controlled Fatigue Testing

The input parameters for strain-controlled fatigue testing (strain amplitude and frequency) are determined using the value of failure elongation from the monotonic results. The ideal outcome from the fatigue-testing program, as it is described in this study, is to have 20-50 data points (fatigue tests) in a range of strain amplitude that results in a subsequent range of cycles-to-failure between 2 cycles and 2 million cycles. Any test that runs beyond 2 million cycles is considered a “runout test”, and the results are not included in data analysis operations, according to ASTM E606 [8]. In order to determine which strain amplitude values result in the desired range of cycle-count, the monotonic failure elongation is used as a reference. This value (the average percentage of elongation in the material when monotonic failure occurs) is multiplied by 0.7, 0.6, 0.5, 0.4, and so on, down to 0.05, resulting in values of strain (%) that can be input as the strain amplitude for a fatigue test.

The strain amplitude values determined from the monotonic failure elongation – an example of which is shown below in Table 1 – provide a starting point from which a material’s relationship of strain amplitude vs. cycles-to-failure can begin to form. Most often, a material can withstand the strain amplitude from to the 0.7 multiplier for less than 10 cycles, and that from the 0.05 multiplier for over 2 million cycles – this gives a general idea of how the material will behave and assists in the planning of subsequent fatigue tests.

Table 1: Example Strain Amplitudes Based on Monotonic Failure Elongation

Axial Strain at Failure (Monotonic) = 5.0%	
Multiplier (Relative to Failure Elongation)	Strain Amplitude (%)
0.7	3.5
0.6	3
0.5	2.5
0.4	2
0.3	1.5
0.27	1.35
0.25	1.25
0.2	1
0.17	0.85
0.15	0.75
0.12	0.6
0.1	0.5
0.09	0.45
0.075	0.375
0.05	0.25

The frequency (rate of cycling) at which fatigue tests are conducted is determined, in part, by the capabilities of the hydraulic tensile tester system, and varies between 1 and 10 Hz (where 1 Hz = 1 cycle per second). The flow capabilities of the hydraulic system – the HPU pump and the load frame servo-valve – limit how quickly and accurately the actuator can move to meet the required strain amplitude and frequency for a fatigue test. If the test frequency is set too high and the machine cannot move fast enough to meet the target displacement during every cycle, the waveform is “saturated”. MTS supplies a plot of performance data for the 810 hydraulic load frame model that is being used for this testing. This curve defines the maximum displacement that is possible at every frequency to prevent the waveform from becoming saturated.

The performance curve shows the expected trend of a decrease in frequency as the required displacement is increased [39].

Once values are determined for the strain amplitude and frequency inputs, the strain-controlled fatigue tests can begin. For every test, a sample is selected and the width and thickness of the gauge section are measured to the nearest 100th millimeter. The sample is then placed within the anti-buckling fixture and secured with the hydraulic grips, aligning it up or down such that the gauge section is centered within the fixture. The axial extensometer can then be installed and secured to the sample with rubber bands to prevent any slippage during the fast and occasionally violent fatigue cycling. Before starting the test, the position must be adjusted such that the load cell is reading as close to 0.00 kN as possible, the axial strain (extensometer) channel must be balanced to read 0.00% strain, and the specific test parameters (strain amplitude and frequency) must be input to the computer. When the test start command is selected, the load frame deforms the sample in a cyclic fashion – applying both tension and compression according to the strain amplitude and frequency that are demanded. Because the testing is performed in strain-control, the system uses a closed-loop control system to monitor the axial extensometer reading hundreds of times every second. It will do this until a drop in tensile load indicates that the specimen has failed, and the test is stopped by the computer.

The computer saves two .csv files: one that contains the continuous data for the time (s), cycle-count, position (mm), load (kN) and axial strain (%) channels, and another that saves the maximum and minimum value for each of those channels during every cycle. The saved data can then be formatted and input to post-processing scripts

that perform the mathematical operations outlined in section 3.4.2 and 3.5 below. Microsoft Excel is implemented for bookkeeping purposes throughout all of the testing, as shown in Figure 14 below – information highlighted in red indicates that a problem occurred during the test and the data should not be used.

Test #	Test Start Date	Test End Date	Target Strain Level (Relative to Mono. Failure)	Target Strain Amplitude (%)	Actual Strain Amplitude (%) (average Value)	Waveform	Duration (hours)	Frequency (Hz)	Room Temp C	Sample #	Flow Dir.	Gauge W (mm)	Gauge T (mm)	Cycles at Test End	Cycles to Failure	Half-Life Cycle #	
C-D-30-1	2/26/2019	2/26/2019	0.3	3.7881	3.813097	Sine			3	21	4-2	N/A	13.122	5.22	10	10	5
C-D-30-2	2/26/2019	2/26/2019	0.3	3.7881	3.799294	Sine			1	21	7-4	N/A	13.19	5.14	9	9	5
C-D-20-1	2/26/2019	2/26/2019	0.2	2.5254	2.53343	Sine			3	21	9-4	N/A	13.184	5.06	80	80	40
C-D-20-2	2/26/2019	2/26/2019	0.2	2.5254	2.52663	Sine			1	21	12-4	N/A	13.19	5.21	209	209	100
C-D-20-3	2/26/2019	2/26/2019	0.2	2.5254	2.52249	Sine			3	21	15-4	N/A	13.12	5.05	213	213	100
C-D-05-1	2/26/2019	2/28/2019	0.05	0.63135	0.607931	Sine	48		10	21	11-1	N/A	13.134	5.1	1649190	2000000	1000000
C-D-10-1	3/1/2019	3/1/2019	0.1	1.2627	1.201072	Sine	-12		10	20	4-4	N/A	13.17	5.208	55000	N/A	
C-D-10-2	3/1/2019	3/1/2019	0.1	1.2627	1.240718	Sine	-12		5	20	9-1	N/A	13.078	5.06	112080	67510	33700
C-D-10-3	3/1/2019	3/2/2019	0.1	1.2627	1.23539	Sine	-12		5	20	19-2	N/A	13.108	5.134	105922	71010	35500
C-D-10-4	3/2/2019	3/3/2019	0.1	1.2627	1.250475	Sine	6.86		3	20.5	16-2	N/A	13.1	5.04	471300	74030	37000
C-D-15-1	3/4/2019	3/4/2019	0.15	1.89405	1.902569	Sine	0.039		5	20	20-2	N/A	13.11	5.03	702	667	300
C-D-15-2	3/4/2019	3/4/2019	0.15	1.89405	1.887845	Sine	0.0096		5	20	8-4	N/A	13.19	5.825	173	165	80
C-D-15-3	3/4/2019	3/4/2019	0.15	1.89405	1.899521	Sine	0.0158		3	20.5	17-1	N/A	13.13	5.188	166	165	80
C-D-15-4	3/4/2019	3/4/2019	0.15	1.89405	1.897102	Sine	0.01		3	21	12-4	N/A	13.13	5.188	163	163	80

Figure 14: Excel Spreadsheet for Fatigue Test Bookkeeping

3.3.3 Load-Controlled Fatigue Testing

The load-controlled fatigue testing procedure is very similar to that of strain-controlled fatigue testing, except that the closed-loop control system is reading the load channel rather than the axial strain channel to control the amount of deformation that it applies to the material sample. It is often the case that load-controlled tests provide more conservative stress-life fatigue results than those from strain-controlled tests. Samples tested in load-control often fail sooner because the system continues to apply the same amount of force to the sample even as a crack begins to form. This means that the same amount of force is applied to a continuously shrinking cross-section, quickly increasing the stress that is experienced within the material. When testing in strain control, the load that is necessary to deform the sample to the desired strain value will decrease as a crack forms, allowing the test to (generally) last for more cycles than the equivalent load-controlled test.

A load-controlled test has two input parameters: force amplitude and frequency. Similar to the strain-control method, these test inputs are determined by using multipliers of the type presented in Table 1, though the values are relative to the ultimate tensile strength (UTS) determined from monotonic testing, rather than the failure elongation. The load-amplitude will be converted to a stress-amplitude during post-processing using the measured sample cross-section. Because the MTS performance-curve [39] is in terms of displacement rather than load, the test frequency must be determined through trial and error. After several tests, it will be clear which load amplitude can be conducted at which frequency to avoid a saturated waveform.

Once the limits are determined regarding the load amplitude and frequency inputs, the load-controlled fatigue tests can begin. For every test, a sample is chosen and the width and thickness of the sample's gauge section are measured to the nearest 100th millimeter. The sample is then placed into the anti-buckling fixture and secured with the hydraulic grips, aligning it up or down such that the gauge section is centered within the fixture. The axial extensometer can then be installed – for consistency with the other testing, the axial extensometer will be used during load-controlled tests, even though the axial strain channel will not be used for test control or data analysis. Before starting the test, the position must be adjusted such that the load cell is reading as close to 0.00 kN as possible, the axial strain (extensometer) channel must be balanced to read 0.00% strain, and the test parameters (load amplitude and frequency) must be input to the computer. When the test start command is selected, the load frame loads the sample in a cyclic fashion, going into both tension and compression equally by the specified load amplitude (kN), at the specified frequency (Hz). It will do this until a drop in

tensile load indicates that the specimen has failed, and the test is stopped by the computer. Similar to the strain-controlled fatigue testing, the computer will save .csv files containing all applicable data for every channel, and Microsoft Excel is implemented for book keeping purposes.

3.4 Data Analysis and Post-Processing

The data collected by performing the testing methods described in section 3.3 must be analyzed and reduced into useful material parameters that can be kept in a database. This section will describe the mathematical relationships that are implemented to do so.

3.4.1 Mathematical Relationships – Monotonic

During a monotonic tensile test, the axial extensometer outputs data in terms of percentage strain by automatically multiplying 100 by the mm change in material length divided by the set 50 mm gauge length of the extensometer. The elongation at failure is taken as the direct reading from this extensometer when the material coupon breaks. Calculations involving strain are performed in terms of m/m rather than percentage to avoid unit errors – this is referred to as “Engineering Strain”. To convert percentage strain to m/m, the raw percentage strain data from the extensometer can be divided by 100 as shown in Equation (2), where $\varepsilon_{extensometer}$ is the direct data reading from the extensometer, and ε_{engr} is engineering strain.

$$\varepsilon_{axial} = \frac{\varepsilon_{extensometer}}{100} = \varepsilon_{engr} \quad (2)$$

The transverse extensometer also outputs data in terms of percentage strain, where it multiplies 100 by the change in length in the transverse direction (width), divided by the set gauge length of the extensometer. In this case, the gauge length of

the extensometer has to be changed to the measured width of the sample before every test because this value may vary slightly between samples. Calculations will also be performed using transverse strain units of m/m to avoid unit errors, as shown in Equation (3) where $\varepsilon_{transvers\ extensometer}$ is the direct reading from the extensometer and $\varepsilon_{transverse}$ is the transverse strain used for subsequent calculations.

$$\varepsilon_{transverse} = \frac{\varepsilon_{transvers\ extensometer}}{100} \quad (3)$$

Load data comes direct from the load cell in terms of kilonewtons (kN) and is converted to N by multiplying by 1000. Engineering stress is then calculated from this by dividing the load (N) by the original measured gauge section width multiplied by the original measured gauge section thickness, as in Equation (4), to get units of pascals (N/m²).

$$\sigma_{engr} = \frac{Load * 1000}{T * W} \quad (4)$$

Where σ_{engr} is the engineering stress, and T and W and the samples thickness and width. From Equations (2), (3) and (4), there is enough information to make plots of engineering stress vs. engineering strain, true stress vs. true strain, and to calculate values for elastic tensile modulus (E) and Poisson's ratio (ν). The true fracture strength and true fracture ductility are taken as the true stress and true strain when the sample breaks. True stress (σ_{true}) and true strain (ε_{true}) are defined in Equations (5) and (6):

$$\sigma_{true} = \sigma_{engr}(1 + \varepsilon_{engr}) \quad (5)$$

$$\varepsilon_{true} = \ln(1 + \varepsilon_{engr}) \quad (6)$$

Tensile modulus and Poisson's ratio are calculated using engineering stress and engineering strain. The tensile modulus is taken as the slope of the engineering stress vs. engineering strain curve in the region between 0.00125 m/m and 0.0025 m/m strain,

as in Equation (7), and will be expressed in gigapascals (GPa). Poisson's ratio is the ratio of the change in transverse strain to the change in axial strain within the region of 0.0005 m/m to 0.0025 m/m, as in Equation (8).

$$E = \frac{\Delta\sigma_{engr}}{\Delta\varepsilon_{engr}} \Big|_{\substack{\varepsilon = 0.0025 \\ \varepsilon = 0.00125}} \quad (7)$$

$$\nu = \frac{\Delta\varepsilon_{transverse}}{\Delta\varepsilon_{engr}} \Big|_{\substack{\varepsilon = 0.0025 \\ \varepsilon = 0.0005}} \quad (8)$$

For most plastic materials, the yield point is the maximum of the engineering stress-strain curve, or the first point where an increase in engineering strain causes no increase in engineering stress [2]. For the purposes of this project, this criteria is used for yield, but the 0.2% offset yield criteria is also included because it is highly unfavorable for plastic truck parts to deform to the yield point as defined for plastic materials. The 0.2% offset yield point is found by drawing a straight line with a slope of E that begins at $\varepsilon_{engr} = 0.002$ m/m, and recording the engineering stress and engineering strain at the point where this line intersects the engineering stress vs. strain curve.

Lastly, the percent reduction in area (%RA) is calculated by assuming that the strain occurring in the transverse (width) direction is also occurring in the thickness direction – causing a corresponding change in width and thickness. Therefore, %RA can be calculated directly from transverse strain data as in Equation (9) where W_0 and T_0 are the original measured width and thickness of the sample.

$$\%RA = \frac{(W_0 * T_0) - (W_{final} * T_{final})}{W_0 * T_0} \quad (9)$$

3.4.2 Mathematical Relationships – Strain-Life Fatigue

After several strain-controlled fatigue tests have been completed at various strain amplitude multiplier levels (as shown in Table 1), the mathematical analysis of the data can begin according to standardized strain-life fatigue theory. One of the .csv files that is saved by the system after the completion of every test is called a “tracking file” – this file contains continuous data from the position (mm), load (kN), axial strain (%) and displacement (mm) channels acquired at a rate of 1000 Hz during the test. An excerpt from a tracking file is shown in Figure 15.

	A	B	C	D	E	F
1	Total Time (s)	Total Cycles	Position(8800 (0,1):Position) (mm)	Load(8800 (0,1):Load) (kN)	Strain(8800 (0,1):Axial Strain) (%)	Displacement(8800 (0,1):Position) (mm)
2	2.177	1	35.68419733	0.008570938	-0.000606361	35.68419733
3	2.178	1	35.68459743	0.007036212	-0.000837026	35.68459743
4	2.179	1	35.68464884	0.007076538	-0.00090145	35.68464884
5	2.18	1	35.6843985	0.00705407	-0.000788271	35.6843985
6	2.181	1	35.68397605	0.006016484	-0.000750902	35.68397605
7	2.182	1	35.68387994	0.006266451	-0.00082138	35.68387994
8	2.183	1	35.68434709	0.007597962	-0.000837655	35.68434709
9	2.184	1	35.68492376	0.007258006	-0.000752928	35.68492376
10	2.185	1	35.6846019	0.005922071	-0.000723777	35.6846019
11	2.186	1	35.6837123	0.005879393	-0.000785361	35.6837123
12	2.187	1	35.68374359	0.00653211	-0.000648922	35.68374359
13	2.188	1	35.6844365	0.006409478	-0.000382867	35.6844365
14	2.189	1	35.68451696	0.006275997	-0.000462565	35.68451696
15	2.19	1	35.68394923	0.006732531	-0.000728038	35.68394923
16	2.191	1	35.68382182	0.006876304	-0.000735698	35.68382182
17	2.192	1	35.68419733	0.006061909	-0.000557769	35.68419733
18	2.193	1	35.68451473	0.006251805	-0.000246079	35.68451473
19	2.194	1	35.68447002	0.008177478	0.00014354	35.68447002
20	2.195	1	35.68447226	0.009198976	0.000472576	35.68447226
21	2.196	1	35.68470248	0.008282661	0.000672764	35.68470248

Figure 15: Excerpt from a Fatigue Test Tracking .csv File

Within this file, the data that was collected from these channels during the half-life cycle – any cycle that occurs at roughly half of the number of cycles-to-failure for any given test – should be extracted and used for analysis. This is following ASTM E606, which says that using data from the half-life simplifies the analysis by assuming that cycle represents the stabilized material behavior at the respective strain level [8]. When the half-life cycle data is extracted for every test, the analysis begins by converting load to stress, and converting both stress and strain to true stress and true strain following equations (2), (4), (5) and (6). Then, the subsequent maximum and

minimum values should be determined for true stress, true strain and position during the half-life cycle. The transverse strain channel is not included during fatigue tests because the transverse extensometer cannot be installed while the sample is within the anti-buckling fixture.

Next, true strain can be broken into its elastic strain (ε_e) and plastic strain (ε_p) parts following the relationship defined by Equation (10). In this context, *plastic* carries the same meaning as *inelastic* or *non-elastic*.

$$\Delta\varepsilon_{true} = \Delta\varepsilon_e + \Delta\varepsilon_p \quad (10)$$

In Equation (10), the character Δ represents the range (maximum – minimum) of the associated variable. Following Hooke's law, the elastic strain range is determined by dividing the true stress range by the tensile modulus value determined from monotonic testing. The plastic strain range is then calculated using Equation (10) by subtracting the elastic strain range from the total strain range. The elastic, plastic and total strain ranges are then divided by 2 in order to determine the elastic, plastic, and total strain amplitudes (amplitude = $\frac{range}{2}$), as shown in Equation (11), where E is the tensile modulus.

$$\frac{\Delta\varepsilon_p}{2} = \frac{\Delta\varepsilon_{true}}{2} - \frac{\Delta\sigma_{true}}{2E} \quad (11)$$

The standard strain-life practices suggest that the total strain-life is the sum of the elastic strain-life and the plastic strain-life, which can be determined separately. The elastic and plastic strain-life relationships are both defined by a power-law function of similar form. The plastic strain-life relationship is Equation (12) and the elastic

strain-life is Equation (13), where ε'_f and c are the fatigue ductility coefficient and exponent, and σ'_f and b are the fatigue strength coefficient and exponent.

$$\frac{\Delta\varepsilon_p}{2} = \varepsilon'_f(2N_f)^c \quad (12)$$

$$\frac{\Delta\sigma}{2} = \sigma'_f(2N_f)^b \quad (13)$$

In the plastic strain-life equation, the dependent variable is the plastic strain amplitude determined in Equation (11), and the independent variable is the reversals-to-failure ($2N_f$), where N_f is the cycles-to-failure, and there are two reversals of direction per cycle. The two material parameters representing the plastic strain-life are the fatigue ductility coefficient (ε'_f), and the fatigue ductility exponent (c). If the plastic strain amplitude is plotted over reversals-to-failure on a log-log scale, the data should form a straight, downward-sloping line – where c is the slope of the line, and ε'_f is the plastic strain amplitude at the point where $2N_f = 1$. The plastic strain-life relationship is mostly applicable to the low-cycle region, because significant inelastic strains usually only occur at high strain amplitudes that result in a low cycle count.

The elastic strain-life is defined in terms of the true stress amplitude, as shown in Equation (13), and will be converted to elastic strain later via Hooke's law of first-order linear elastic behavior. This relationship is a function of true stress amplitude vs. reversals to failure ($2N_f$), where again, N_f is the cycles-to-failure and there are two reversals of direction per cycle. The two material parameters representing the elastic strain-life are the fatigue strength coefficient (σ'_f) defined in terms of megapascals (MPa), and the fatigue strength exponent (b). If the true stress amplitude is plotted over reversals-to-failure on a log-log scale, the data should result in a straight, downward-

sloping line – where b is the slope of the line, and σ'_f is the true stress amplitude at the point where $2N_f = 1$.

To determine the values of the four strain-life material parameters (ϵ'_f , c , σ'_f , and b), the data-fitting and statistical methods from ASTM E739 are followed. The calculated data for plastic strain amplitude vs. reversals to failure and true stress amplitude vs. reversals to failure are fitted using separate but identical operations, presented simultaneously here. The process begins by defining variables x and y , where x is the log (base 10) of plastic strain amplitude (for the plastic strain-life operation) or the log (base 10) of the true stress amplitude (for the elastic strain-life operation), and y is the log (base 10) of cycles-to-failure for both operations.

$$\text{Plastic strain-life:} \quad x = \log_{10}\left(\frac{\Delta\epsilon_p}{2}\right) \text{ and } y = \log_{10}(N_f) \quad (14)$$

$$\text{Elastic strain-life:} \quad x = \log_{10}\left(\frac{\Delta\sigma}{2}\right) \text{ and } y = \log_{10}(N_f) \quad (15)$$

It is important to note that the x and y variables are each the culmination of data (for plastic strain amplitude, true stress amplitude, and cycles-to-failure), each containing a value for every strain-controlled fatigue test that was conducted excluding any non-failure (runout) tests. From this, the variables \bar{x} and \bar{y} are defined in both operations as the average of x and y , respectively.

$$\bar{x} = \text{average}(x) \text{ and } \bar{y} = \text{average}(y) \quad (16)$$

Two “estimator” values, \hat{A} and \hat{B} , are then defined, stemming from a linear model of the form $Y = A + BX$. The calculations for these estimators are shown

below in Equations (17) and (18), where k is the number of data points (the number of non-runout tests included in the fitting operations).

$$\hat{B} = \frac{\sum_{i=1}^k (x_i - \bar{x})(y_i - \bar{y})}{\sum_{i=1}^k (x_i - \bar{x})^2} \quad (17)$$

$$\hat{A} = \bar{y} - \hat{B}\bar{x} \quad (18)$$

The strain-life fatigue parameters are then determined from these estimators according to the relationships presented in Equations (19) and (20). Note that the plastic strain-life and elastic strain-life fitting operations each have unique values for \hat{A} and \hat{B} , but the two operations are combined in Equations (19) and (20) for convenience.

$$b \text{ (or } c) = 1/\hat{B} \quad (19)$$

$$\sigma_f' \text{ (or } \varepsilon_f') = 10^{\left(\frac{\hat{A}}{-\hat{B}}\right)} * \left(\frac{1}{2}\right)^{b \text{ (or } c)} \quad (20)$$

Finally, the standard error of the fitting operations can be calculated in order to quantify the inherent error within the results. First, the value \hat{y}_i is determined for each data point in the respective fitting operation.

$$\hat{y}_i = \hat{A} + \hat{B}x_i \quad (21)$$

The \hat{y}_i values are then used in calculating the variance of the data set ($\hat{\sigma}^2$), where again, k is the number of data points (the number of non-runout tests included in the fitting operations).

$$\hat{\sigma}^2 = \frac{\sum_{i=1}^k (y_i - \hat{y}_i)^2}{k - 2} \quad (22)$$

The standard error (SE) can then be calculated using the variance, as follows.

The value of the standard error should be a positive value, less than 1.

$$SE = \frac{\sqrt{\hat{\sigma}^2}}{k} \quad (23)$$

Once the elastic and plastic strain-life material parameters have been determined with their respective standard errors, the total strain-life relationship can be defined as the sum of the elastic and plastic strain-life relationships, as shown in Equation (24). It is important to note that the elastic portion has been converted from true stress to elastic strain by dividing the fatigue strength coefficient (σ_f') by the monotonic tensile modulus (E).

$$\frac{\Delta\varepsilon}{2} = \left(\frac{\sigma_f'}{E}\right)(2N_f)^b + \varepsilon_f'(2N_f)^c \quad (24)$$

As shown below in Figure 16, this relationship can be plotted using a log-log scale of true strain amplitude vs. reversals-to-failure, including the elastic strain-life and plastic strain-life curves also plotted separately. The slope of the plastic strain-life curve will be steeper than that of the elastic strain-life, and the point at which these lines intersect is called the *fatigue transition point*.

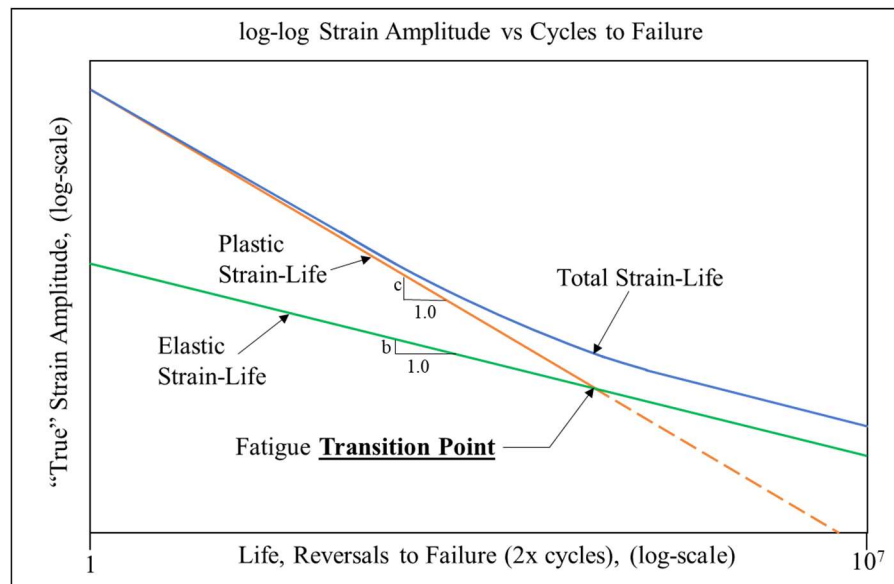


Figure 16: Example Strain-Life Log-Log Plot

The final relationship that should be considered to define the full strain-life fatigue behavior for a material is the cyclic stress-strain curve. This can be compared to the monotonic stress-strain curve, as it is a plot of stress vs. strain. However, in the cyclic case, the stress amplitude and strain amplitude are considered. The fitting methods used for the elastic and plastic strain-life parameters are also used for the cyclic stress-strain curve – defined by the cyclic strength coefficient (K') in MPa, and the cyclic strain-hardening exponent (n'). A standard error is also calculated for the cyclic stress-strain curve and included with the fatigue results. The cyclic stress-strain parameters (K' and n') can also be solved for using Equations (25) and (26).

$$n' = \frac{b}{c} \quad (25)$$

$$K' = \frac{\sigma_f'}{\varepsilon_f'^{n'}} \quad (26)$$

3.4.3 Mathematical Relationships – Stress-Life Fatigue

The stress-life fatigue relationship is quantified following a similar procedure to that of the strain-life fatigue analysis. The testing system will collect data from the load channel whether the test is controlled through strain or load, and therefore the ability to obtain the stress-life fatigue parameters is independent of the control mode – a concept that is fundamental to the comparison of the two methods that this thesis provides.

The stress-life fatigue relationship is represented by a power-law function of similar form to that of the elastic and plastic strain-life relationships. However, the dependent variable for stress-life is in terms of the true stress range rather than the true stress amplitude and the independent variable is cycles-to-failure rather than reversals.

This is shown in Equation (27) below, where $\Delta\sigma$ is the true stress range, N_f is the cycles-to-failure, $SRI1$ is the stress-range intercept, and $b1$ is the stress-life slope.

$$\Delta\sigma = SRI1(N_f)^{b1} \quad (27)$$

If the true stress range is plotted against cycles-to-failure on a log-log scale, the data should form a downward sloping straight line. In the stress-life relationship shown in Equation (27), $b1$ is the slope of this line, and $SRI1$ is the value of the stress range at the point where $N_f = 1$. This form of the Basquin equation (stress-life relationship) differs from most literature that defines stress-life in terms of stress amplitude vs. reversals to failure, and uses the fatigue strength coefficient σ'_f rather than the stress range intercept [11]. This difference is made so that the data collected for the DTNA material database is compatible with the information that is accepted by nCode, the fatigue analysis software that is used by the DTNA analysis team [40].

The stress-life material parameters – $b1$ and $SRI1$ – are determined, along with the standard error, using the same fitting methods presented in the previous section regarding the strain-life method. Equations (14) through (23) are applicable, using the log (base 10) of true stress range for the variable x , and the log (base 10) of the cycles-to-failure for the variable y .

3.5 Automation of Test Data Post-Processing

In an effort to both save time during the data analysis process and to standardize the material analysis procedures for others to use, a graphical-user-interface (GUI) was developed that can automatically perform all of the mathematical operations outlined in section 3.4 on an entire data set for any material that is being tested. The GUI saves the desired results in an accessible format that can be presented and easily understood

by all who are concerned. A screenshot of this GUI is shown below in Figure 17 – it is created in Python.

The program contains two main functions – the monotonic analysis and the fatigue analysis. First, the monotonic analysis function processes monotonic data and outputs the calculated material parameters for an entire set of tensile tests using equations (2) through (9). Secondly, the fatigue analysis function sets up the half-life max/min values for a set of fatigue tests using equations (10) through (13), and performs the strain-life and stress-life curve fitting operations on the half-life fatigue data using equations (14) through (27).

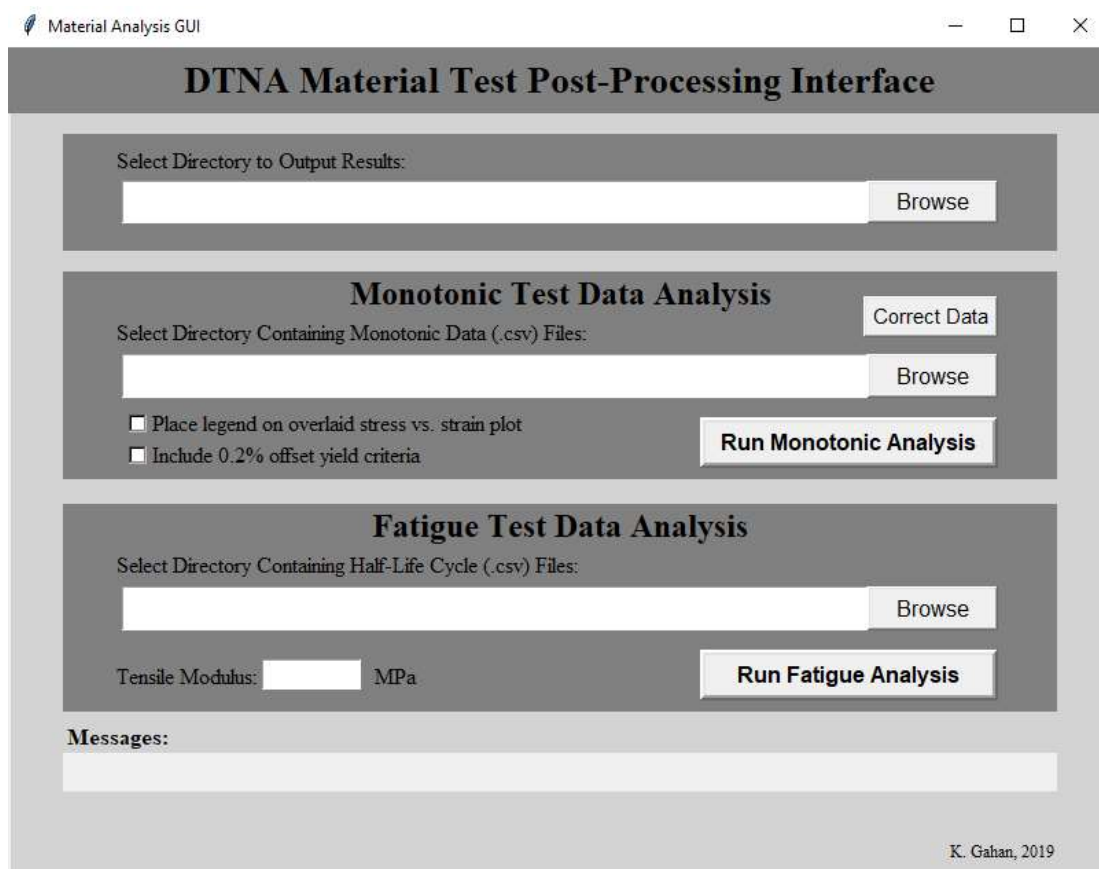


Figure 17: Test Data Post-Processing GUI

This GUI is designed with ease-of-use in mind for future users. To run the monotonic analysis function, the user must create a directory folder that contains only the monotonic data files for the material that is being analyzed. If all of the data is formatted correctly (according to provided instructions), the user can select the location of the monotonic data using the “Browse” button attached to the input location field, as well as the location where they would like the results to be placed using the “Browse” button attached to the “Select Directory to Output Results” field. Some additional settings such as creating a plot legend or including the 0.2% offset yield criteria can also be toggled on or off. When the “Run Monotonic Analysis” button is selected, the progress of each analysis task will be printed to a terminal window as the process is completed. When it is finished, there will be a new folder titled “Monotonic_Results” in the selected save-location. This new folder will contain two items, as shown below:

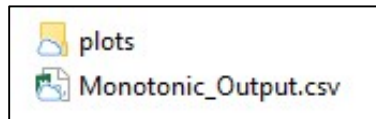


Figure 18: “Monotonic_Results” Folder Contents

The .csv file called “Monotonic_Output.csv” contains the tabulated material parameters determined from each test, as well as the averaged values of the parameters. The “plots” folder contains a stress-strain curve for every test, as well as an overlaid plot where the stress vs. strain curve for every test is plotted on one figure. An example of an individual stress-strain curve and the output .csv file are displayed in Figure 19. An example of the overlaid stress-strain plot is Figure 21.

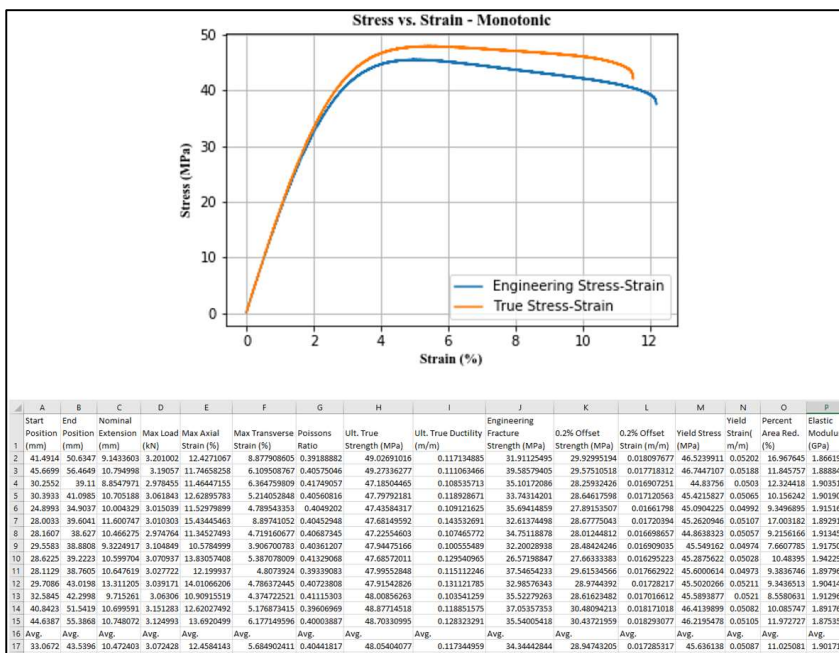


Figure 19: GUI Monotonic analysis output: Stress-strain curve (top) and material parameters (bottom).

The fatigue analysis function works similar to the monotonic analysis, where the locations of the input data and the desired output location are selected by the user in their respective input fields using the attached “Browse” buttons. In this case, the input directory must contain the “tracking”.csv data file for every fatigue test that was performed, edited such that only the data from the half-life cycle is included within each file. Before running the fatigue analysis, the user must also input the monotonic tensile elastic modulus (MPa) that was determined by the monotonic analysis function. If the data is formatted correctly (according to provided instructions) and the elastic modulus has been input to its respective input field, the “Run Fatigue Analysis” button can be selected. As the analysis process is completed, the progress of each analysis task will be printed to a terminal window. When it is finished, there will be a new folder titled “Fatigue_Results” in the selected save-location.

Within the “Fatigue_Results” folder, there will be three items: “HysteresisData_Out.csv”, “Fatigue_Results.log”, and a folder called “plots”. The .csv file “HysteresisData_Output.csv” contains a table with several columns pertaining to the half-life cycle values for the elastic and plastic strain amplitudes, true stress amplitude, true stress range, true strain amplitude, average strain amplitude and cycles to failure, where every row represents a separate fatigue test. This provides the data on which the GUI performs curve-fitting operations to create the material parameters. The log file “Fatigue_Results.log” contains the strain-life, cyclic stress-strain and stress-life parameters that were determined from the test data (shown in Figure 20). The “plots” folder contains plots that display the strain-life and stress-life fatigue results conveniently for reporting purposes. These plots include plastic strain vs. reversals, true stress vs. reversals, strain amplitude vs. reversals, log-log of plastic, elastic and total strain vs. reversals, and stress range vs. reversals.

```

-----
Strain-Life (R = -1)
Fatigue Ductility Coefficient (Ef'):
Fatigue Ductility Exponent (c):
Fatigue Strength Coefficient (Sf'):
Fatigue Strength Exponent (b):
Plastic Standard Error (SEp):
Elastic Standard Error (SEe):
-----
Cyclic Strength Coefficient (K'):
Cyclic Strain Hardening Exponent (n'):
Cyclic Standard Error (SEc):
-----
Stress-Life (R = -1)
Stress Range Intercept (SRI1):
Stress-Life Slope 1 (b1):
Stress-Life Standard Error (SEs):
-----
Number of Data Points:

```

Figure 20: Example Fatigue Parameters Output from the GUI.

The GUI also features a “messages” display at the bottom of the window. This will show updates that tell the user what analysis is running, if the process failed, and if the process completed successfully. This immediately allows the user to be aware if there is an issue with the data, and will save time if any debugging is necessary. It is hoped that this automated material test data analysis process will save a significant amount of time for DTNA test engineers.

Chapter 4

4 Results for DTNA Material Database

In this chapter, the results from monotonic and fatigue testing of pDCPD and 40% GF-PP are presented. Following the procedures outlined in chapter 3, this testing was completed in an effort to obtain the desired material properties for the DTNA material database. In some cases, a comparison will be included between the material parameters determined from this testing and the pre-existing data that was available within the database and any differences will be discussed. All of the results presented here are calculated using the post-processing GUI presented in section 3.5.

4.1 Monotonic Results

The results from monotonic testing – for pDCPD, 40% GF-PP in-flow, and 40% GF-PP cross-flow – are presented in this section. The main deliverables of this testing are a plot of stress vs. strain for every test, and material properties such as tensile modulus, Poisson's ratio, ultimate tensile strength, failure elongation, and yield point. As stated in section 3.3, the monotonic test method deforms the material at a rate of 5 millimeters per minute until a failure occurs.

4.1.1 pDCPD Monotonic Results

There were 14 monotonic tests completed for pDCPD, and the values determined from the tests are presented in Table 2 below. It is important to note that both the 0.2% offset criteria and the plastics yield criteria (maximum stress-strain point) are included in these results for the reasons discussed in section 3.4.1.

Table 2: PDCPD Monotonic Test Results and Properties

Max Load (kN)	Max Axial Strain (%)	Max Transverse Strain (%)	Poissons Ratio	Ult. True Strength (MPa)	Ult. True Ductility (m/m)	Engineering Fracture Strength (MPa)	0.2% Offset Strength (MPa)	0.2% Offset Strain (m/m)	Yield Stress (MPa)	Yield Strain (m/m)	Percent Area Red. (%)	Elastic Modulus (GPa)
3.201	12.427	8.878	0.392	49.027	0.117	31.911	29.93	0.018	46.524	0.052	16.968	1.866
3.191	11.747	6.11	0.406	49.273	0.111	39.586	29.575	0.018	46.745	0.052	11.846	1.889
2.978	11.464	6.365	0.417	47.185	0.109	35.102	28.259	0.017	44.838	0.05	12.324	1.904
3.062	12.629	5.214	0.406	47.798	0.119	33.743	28.646	0.017	45.422	0.051	10.156	1.902
3.015	11.53	4.79	0.405	47.436	0.109	35.694	27.892	0.017	45.09	0.05	9.35	1.915
3.01	15.434	8.897	0.405	47.681	0.144	32.614	28.678	0.017	45.262	0.051	17.003	1.893
2.975	11.345	4.719	0.407	47.226	0.107	34.751	28.012	0.017	44.864	0.051	9.216	1.913
3.105	10.578	3.907	0.404	47.945	0.101	32.2	28.484	0.017	45.549	0.05	7.661	1.918
3.071	13.831	5.387	0.413	47.686	0.13	26.572	27.663	0.016	45.288	0.05	10.484	1.942
3.028	12.2	4.807	0.393	47.996	0.115	37.547	29.615	0.018	45.6	0.05	9.384	1.898
3.039	14.011	4.786	0.407	47.915	0.131	32.986	28.974	0.017	45.502	0.052	9.344	1.904
3.063	10.909	4.375	0.411	48.009	0.104	35.523	28.616	0.017	45.589	0.052	8.558	1.913
3.151	12.62	5.177	0.396	48.877	0.119	37.054	30.481	0.018	46.414	0.051	10.086	1.892
3.125	13.692	6.177	0.4	48.703	0.128	35.54	30.437	0.018	46.22	0.051	11.973	1.875
Avg.	Avg.	Avg.	Avg.	Avg.	Avg.	Avg.	Avg.	Avg.	Avg.	Avg.	Avg.	Avg.
3.072	12.458	5.685	0.404	48.054	0.117	34.344	28.947	0.017	45.636	0.051	11.025	1.902

These tests are also displayed on the overlaid engineering stress vs. engineering strain plot in Figure 21 below. The individual stress vs. strain plots for every test are included in Appendix D – including both an “engineering” curve and a “true” curve, calculated using equations (5) and (6) for every test. As seen in the overlaid plot below, each test experienced an almost-identical elastic deformation, providing an average tensile modulus value of 1.902 GPa with a standard deviation of 0.018 GPa. The deformation curve then flattens near 45-47 MPa (the yield point as defined for plastic materials), and begins to strain-soften until failure occurs at an average axial strain of 12.458%, with a standard deviation of 1.3218%.

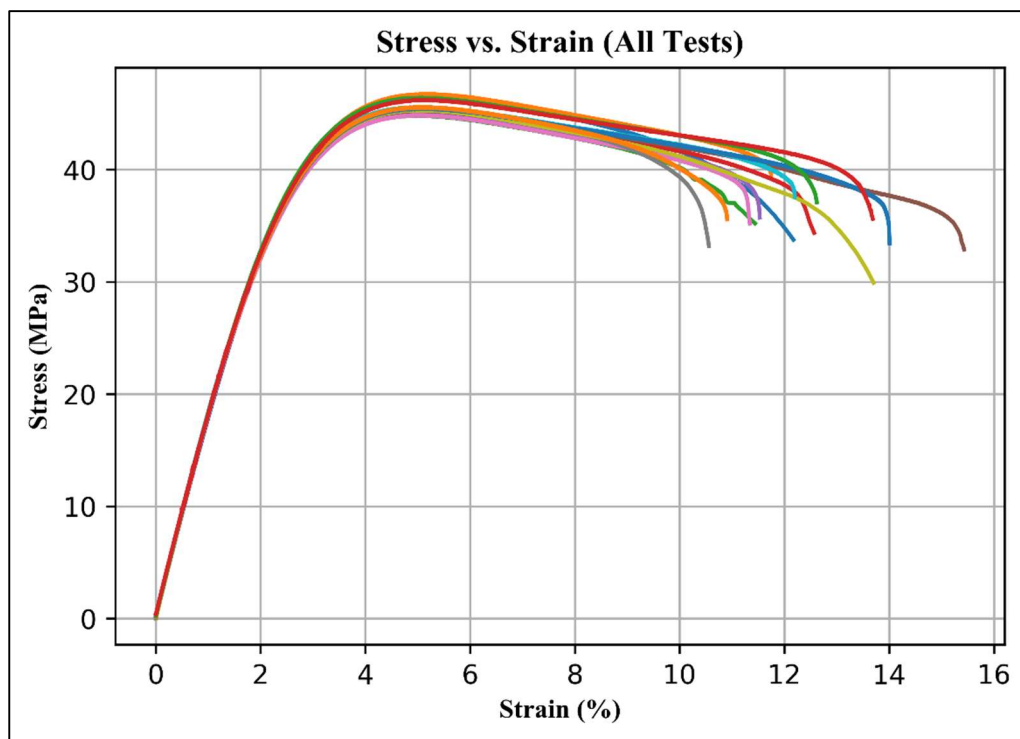


Figure 21: pDCPD Monotonic Engineering Stress vs. Strain (overlaid)

Some of these properties will be compared to the pre-existing monotonic data for pDCPD from the DTNA database before this testing was completed because some interesting differences do exist – this comparison can be seen in section 6.2. The value

of 12.458% average axial strain at failure is used to plan the strain-amplitude input values for the various strain-controlled fatigue tests that will subsequently be conducted. As presented in section 3.3.2 and Table 1, the strain amplitude inputs are determined by scaling the average monotonic strain at failure using multipliers ranging between 0.7 and 0.05. The results of this operation are shown in Table 3, providing the necessary input information for the fatigue testing of pDCPD.

Table 3: pDCPD Strain Amplitude Input Values

Axial Strain at Failure (Monotonic) = 12.627 %	
Multiplier (Relative to Failure Strain)	Strain Amplitude (%)
0.7	8.839
0.6	7.576
0.5	6.314
0.4	5.051
0.3	3.788
0.25	3.157
0.2	2.525
0.15	1.894
0.12	1.515
0.1	1.263
0.09	1.136
0.075	0.947
0.05	0.631

4.1.2 40% GF-PP Monotonic Results (In-Flow)

Seven monotonic tests were completed using 40% GF-PP samples cut in the in-flow orientation. The material values determined from the tests are presented in Table 4 below. In this case, due to the characteristics of the material, only the 0.2% offset yield criteria is included and the maximum point is called “Failure Stress” and “Failure Strain”. This will be expanded upon below.

Table 4: 40% GF-PP (In-Flow) Monotonic Test Results and Properties

Max Load (kN)	Max Axial Strain (%)	Max Transverse Strain (%)	Poissons Ratio	Ult. True Strength (MPa)	Ult. True Ductility (m/m)	Engineering Fracture Strength (MPa)	0.2% Offset Strength (MPa)	0.2% Offset Strain (m/m)	Failure Stress (MPa)	Failure Strain (m/m)	Percent Area Red. (%)	Elastic Modulus (GPa)
2.533	2.664	0.864	0.339	67.542	0.026	65.305	46.119	0.009	65.862	0.025	1.721	6.205
3.392	2.484	1.106	0.451	88.767	0.025	80.919	61.209	0.009	86.671	0.024	2.200	8.426
3.125	2.492	1.138	0.439	82.156	0.025	75.372	56.410	0.009	80.204	0.024	2.262	7.758
2.926	2.625	1.124	0.420	78.810	0.026	73.970	52.620	0.009	76.883	0.025	2.235	7.209
2.409	2.625	0.918	0.359	64.908	0.026	62.082	44.054	0.009	63.308	0.025	1.828	6.136
2.695	2.842	1.151	0.418	71.110	0.028	68.081	47.393	0.009	69.252	0.027	2.289	6.770
2.498	2.816	0.882	0.360	65.684	0.028	61.324	44.319	0.009	64.020	0.026	1.756	6.067
Avg.	Avg.	Avg.	Avg.	Avg.	Avg.	Avg.	Avg.	Avg.	Avg.	Avg.	Avg.	Avg.
2.797	2.650	1.026	0.398	74.140	0.026	69.579	50.303	0.009	72.314	0.025	2.042	6.939

These tests are all displayed on the overlaid engineering stress vs. engineering strain plot in Figure 22. The individual stress vs. strain plots for every test are included in Appendix D –including both an “engineering” curve and a “true” curve that is calculated using equations (5) and (6) for each test.

The initial deformation for all of these samples is very similar, with major deviations occurring outside of the small elastic region. The average value for the tensile modulus (6.939 GPa) was determined with a standard deviation of 0.789 GPa. The axial strain at failure, however, was quite consistent with an average value of 2.657% and a standard deviation of 0.129%.

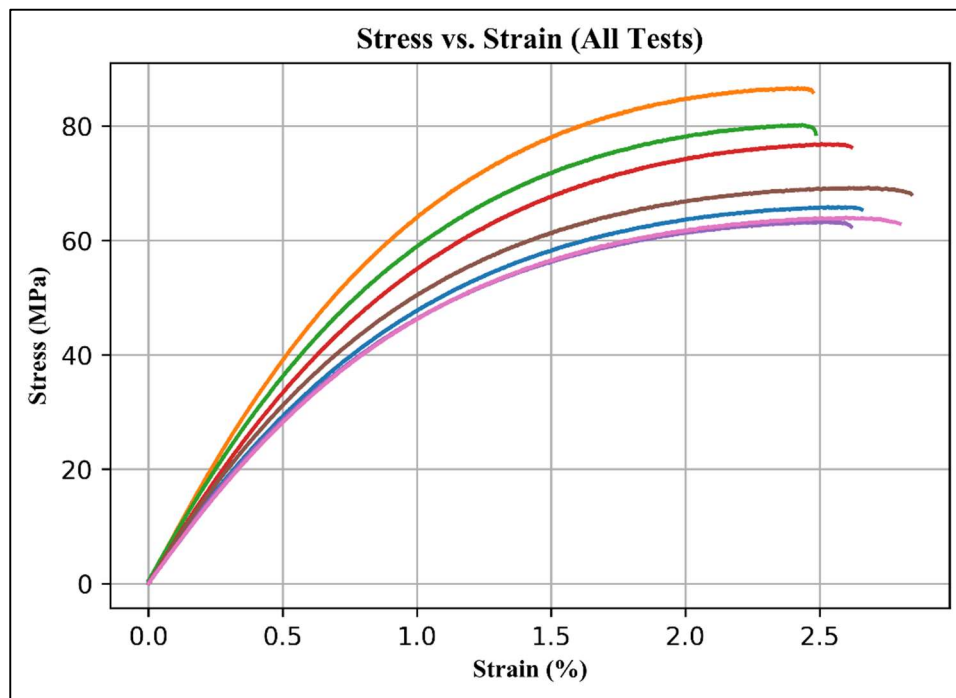


Figure 22: 40% GF-PP (In-Flow) Monotonic Engineering Stress vs. Strain (overlaid)

It should be noted that the 40% GF-PP in-flow samples showed much stiffer characteristics when compared to the monotonic results for pDCPD. All of the in-flow samples failed before a maximum stress vs. strain point was reached (no strain

softening occurred) and therefore the 0.2% offset yield point method should be used as the yield criteria for this material in this orientation, rather than the maximum stress-strain yield point that is defined for plastic materials. Lastly, the average axial strain at failure is again used to calculate the strain-amplitude input values for subsequent strain-controlled fatigue testing – shown in Table 5 below.

Table 5: 40% GF-PP In-Flow Strain Amplitude Input Values

Axial Strain at Failure (Monotonic) = 2.657 %	
Multiplier (Relative to Failure Strain)	Strain Amplitude (%)
0.7	1.8602
0.6	1.5944
0.5	1.3287
0.4	1.0630
0.3	0.7972
0.27	0.7175
0.25	0.6643
0.2	0.5315
0.17	0.4518
0.15	0.3986
0.12	0.3189
0.1	0.2657
0.09	0.2392
0.075	0.1993
0.05	0.1329

4.1.3 40% GF-PP Monotonic Results (Cross-Flow)

There were also seven monotonic tests completed for 40% GF-PP in the cross-flow orientation, and the results of these tests are presented in Table 6 and Figure 23. Again, due to the characteristics of this material, only the 0.2% offset yield criteria is included and the maximum point is called “Failure Stress” and “Failure Strain”. The material experiences failure before a “maximum” point has been reached, and therefore the 0.2% offset criteria should be considered as the yield point.

Table 6: 40% GF-PP (Cross-Flow) Monotonic Test Results and Properties

Max Load (kN)	Max Axial Strain (%)	Max Transverse Strain (%)	Poissons Ratio	Ult. True Strength (MPa)	Ult. True Ductility (m/m)	Engineering Fracture Strength (MPa)	0.2% Offset Strength (MPa)	0.2% Offset Strain (m/m)	Failure Stress (MPa)	Failure Strain (m/m)	Percent Area Red. (%)	Elastic Modulus (GPa)
1.76642	1.91702	0.4262686	0.22603	46.09338	0.018989	44.9824482	33.1533	0.00932	45.2343	0.01899	0.85072	4.54389
1.5534	1.40306	0.3165551	0.22468	40.35968	0.013933	39.7193003	33.4398	0.00965	39.8039	0.01397	0.632108	4.38586
1.57859	1.46575	0.3353837	0.22659	41.34229	0.014551	39.817744	33.6413	0.00956	40.7535	0.01445	0.669643	4.47418
1.66505	1.60888	0.3637466	0.22336	42.75449	0.015961	36.3309605	32.6952	0.00943	42.0831	0.01596	0.72617	4.41578
1.49085	1.42295	0.3386757	0.23061	40.73465	0.014129	40.0492819	33.1095	0.00953	40.1648	0.01419	0.676204	4.40875
1.63856	1.47784	0.3427042	0.21969	41.35406	0.01467	40.6050516	32.9029	0.00954	40.7534	0.01474	0.684234	4.38458
1.73246	1.86438	0.4317383	0.24702	47.89692	0.018472	46.6779279	34.8083	0.00925	47.0266	0.01851	0.861613	4.81452
Avg.	Avg.	Avg.	Avg.	Avg.	Avg.	Avg.	Avg.	Avg.	Avg.	Avg.	Avg.	Avg.
1.63219	1.59427	0.3650103	0.22828	42.93364	0.015815	41.1689592	33.3929	0.00947	42.2599	0.01583	0.72867	4.48965

The overlaid engineering stress vs. strain plots for the monotonic tests completed on the 40% GF-PP cross-flow material samples are shown in Figure 23. The individual stress vs. strain plots for every test (both engineering and true stress/strain) are included in Appendix D.

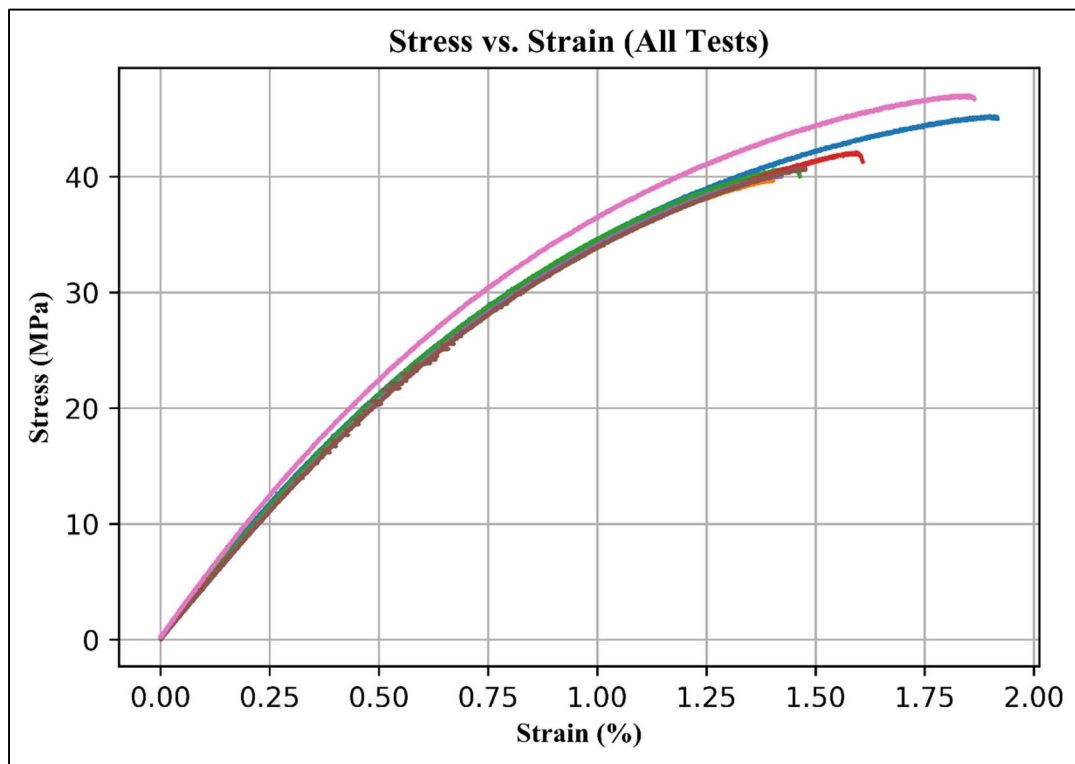


Figure 23: 40% GF-PP (Cross-Flow) Monotonic Engineering Stress vs. Strain (overlaid)

The cross-flow samples (reinforcement-fiber orientation is perpendicular to the axis of loading) provide a smaller ultimate strength than the in-flow samples – failing at 42.3 MPa, with a standard deviation of 2.57 MPa. They elongated to an axial strain of 1.59%, with a standard deviation of 0.197%, and the average tensile modulus (4.48 GPa) was determined with a standard deviation of 0.142 GPa. Visually and numerically, the cross-flow data set is more consistent than in-flow (smaller differences between each test).

Again, the average value for axial strain at failure is used to determine the various strain-amplitude levels to be used as inputs for subsequent strain-controlled fatigue testing. These strain amplitude values are shown in Table 7 below.

Table 7: 40% GF-PP Cross-Flow Strain Amplitude Input Values

Axial Strain at Failure (Monotonic) = 1.594 %	
Multiplier (Relative to Failure Strain)	Strain Amplitude (%)
0.7	1.1160
0.6	0.9566
0.5	0.7971
0.4	0.6377
0.3	0.4783
0.27	0.4305
0.25	0.3986
0.2	0.3189
0.17	0.2710
0.15	0.2391
0.12	0.1913
0.1	0.1594
0.09	0.1435
0.075	0.1196
0.05	0.0797

4.1.4 40% GF-PP Monotonic Results – comparison

As expected, the cross-flow samples (reinforcement-fiber orientation is perpendicular to the axis of loading) provide a smaller ultimate strength than the in-flow samples – cross-flow failed around 43 MPa, whereas in-flow failed around 74 MPa. The cross-flow samples, however, showed less elongation than in-flow, failing at an average axial strain of 1.59% rather than the 2.65% seen for in-flow. When the cross-flow oriented samples are tested, there is a much larger load placed on the polypropylene matrix without the addition of glass-fiber reinforcement in the direction of the loading. For this reason, it makes sense to see less elongation and less strength

from this orientation of the material because the matrix alone cannot withstand as much load as the glass fibers. The two monotonic results are compared in Table 8.

Table 8: 40% GF-PP In-Flow and Cross-Flow Monotonic Comparison

Property	In-Flow	Cross-Flow
Tensile Modulus (MPa)	6938.7	4489.6
0.2% offset yield (MPa)	50.3	33.4
Ultimate True Strength (MPa)	74.1	42.9
Axial Strain @ Fail	2.65%	1.59%
Poisson's Ratio	0.397	0.228

4.2 Strain-Controlled Fatigue Results

The results of the strain-controlled fatigue testing – for pDCPD, 40% GF-PP in-flow, and 40% GF-PP cross-flow – are presented in this section. The deliverables of this testing include the cyclic stress-strain, strain-life and stress-life fatigue parameters, as derived in section 3.4.2, along with the various S-N and ϵ -N plots that can be created with those material parameters.

4.2.1 pDCPD Strain-Controlled Fatigue Results

The strain-controlled fatigue test results for pDCPD are presented in Table 9 below. These tests are given a test ID using the following convention: C-D-X-Y, where C stands for “cyclic test”, D stands for “pDCPD”, X is a placeholder for the strain multiplier value, and Y is a placeholder for the test number (in order) at that specific strain multiplier level. The test ID's presented below may not start at 1, as some initial tests are not included due to incorrect testing parameters (a sine wave was used rather than a triangular-shaped wave).

Table 9: pDCPD Strain-Controlled Fatigue Tests

Test ID	Strain Multiplier Level	Target Strain Amp. (%)	Frequency (Hz)	Sample ID	Actual Average Strain Amp. (%)	Cycles to Sample Failure
C-D-12-8	0.12	1.5152	3	26-2	1.51453	4040
C-D-12-9	0.12	1.5152	3	30-1	1.51043	22550
C-D-06-1	0.06	0.7576	3	24-4	0.75584	908000
C-D-12-10	0.12	1.5152	3	29-2	1.51485	12480
C-D-15-7	0.15	1.8941	3	27-4	1.89184	826
C-D-15-8	0.15	1.8941	3	26-4	1.89392	419
C-D-15-9	0.15	1.8941	3	30-2	1.88710	610
C-D-10-10	0.1	1.2627	5	29-2	1.24913	67100
C-D-075-5	0.075	0.9470	5	24-3	0.94280	372770
C-D-06-3	0.06	0.7576	5	24-2	0.75563	1131010
C-D-05-2	0.05	0.6314	10	27-1	0.62887	200000 ®
C-D-09-5	0.09	1.1364	5	23-4	1.13531	122510
C-D-10-11	0.1	1.2627	5	28-3	1.25948	58640
C-D-075-8	0.075	0.9470	5	26-1	0.94541	423560
C-D-075-9	0.075	0.9470	5	25-3	0.94414	383900
C-D-05-3	0.05	0.6314	5	25-1	0.63080	200000 ®
C-D-09-6	0.09	1.1364	3	29-3	1.13598	46440
C-D-09-7	0.09	1.1364	3	31-1	1.13593	38110
C-D-075-10	0.075	0.9470	3	31-2	0.94671	123350
C-D-06-4	0.06	0.7576	3	32-1	0.75717	863900
C-D-10-12	0.1	1.2627	3	36-1	1.25705	19600
C-D-10-13	0.1	1.2627	3	31-4	1.26186	18500
C-D-10-14	0.1	1.2627	3	33-2	1.26198	19950
C-D-10-15	0.1	1.2627	5	38-3	1.23626	5360
C-D-10-16	0.1	1.2627	5	32-2	1.26147	11700
C-D-12-11	0.12	1.5152	3	34-2	1.44706	1360
C-D-12-12	0.12	1.5152	1	37-3	1.51397	4940
C-D-05-4	0.05	0.6314	10	35-2	0.62938	1875680
C-D-15-12	0.15	1.8941	1	35-3	1.89276	337
C-D-20-4	0.2	2.5254	1	36-3	2.52423	151
C-D-25-1	0.25	3.1568	1	34-3	3.13349	17
C-D-06-5	0.06	0.7576	10	33-4	0.75431	796020
C-D-06-6	0.06	0.7576	10	32-3	0.75552	1061580
C-D-20-5	0.2	2.5254	1	32-4	2.52470	207
C-D-20-6	0.2	2.5254	1	33-1	2.52472	115

Table 9: pDCPD Strain-Controlled Fatigue Tests (continued)

Test ID	Strain Multiplier Level	Target Strain Amp. (%)	Frequency (Hz)	Sample ID	Actual Average Strain Amp. (%)	Cycles to Sample Failure
C-D-25-2	0.25	3.1568	1	36-2	3.15387	45
C-D-30-4	0.3	3.7881	1	37-1	3.76294	9
C-D-30-5	0.3	3.7881	1	38-1	3.76400	6
C-D-30-6	0.3	3.7881	1	37-2	3.76370	10
C-D-40-1	0.4	5.0508	1	33-3	5.02786	2
C-D-075-11	0.075	0.9470	10	35-4	0.94512	131250
C-D-075-12	0.075	0.9470	10	36-4	0.94340	216840
C-D-40-2	0.4	5.0508	1	37-4	5.23543	2
C-D-06-7	0.06	0.7576	5	38-4	0.75640	588210
C-D-50-3	0.5	6.3135	1	39-1	6.35714	1
C-D-50-4	0.5	6.3135	1	39-4	6.36175	1
C-D-06-8	0.06	0.7576	10	41-3	0.75418	594390
C-D-05-5	0.05	0.6314	10	41-4	0.62656	1812840
Note: ® = “Runout Test” (no failure)						

The half-life cycle data from this set of tests was processed using the custom GUI presented in section 3.5 to produce the fatigue parameters and data plots for pDCPD. These parameters are shown in Figure 24 below – a screenshot of the “Fatigue_Results.log” file that is output from the post-processing GUI.

Strain-Life (R = -1)	
Fatigue Ductility Coefficient (Ef')	0.03166
Fatigue Ductility Exponent (c):	-0.3067
Fatigue Strength Coefficient (Sf')	68.7307 MPa
Fatigue Strength Exponent (b):	-0.11226
Plastic Standard Error (SEp):	0.0773
Elastic Standard Error (SEe):	0.0617

Cyclic Strength Coefficient (K')	243.2202 MPa (calculated)
Cyclic Strain Hardening Exponent (n')	0.366 (calculated)
Cyclic Standard Error (SEc):	0.0348

Stress-Life (R = -1)	
Stress Range Intercept (SRI1):	127.171 MPa
Stress-Life Slope 1 (b1):	-0.11226
Stress-Life Standard Error (SEs):	0.0617

Number of Data Points: 47	

Figure 24: pDCPD Fatigue Parameters (strain-controlled results)

The low standard errors (all < 0.1) attest to how well the curve-fitting operation worked for this data set. This is immediately visible in the plots of plastic strain amplitude vs. reversals to failure (Figure 25) and elastic strain amplitude vs. reversals-to-failure (Figure 26) – the relationships from which the strain-life fatigue properties are derived. As shown, both data sets follow the expected trend of a downward-sloping linear line when plotted using log-log axes. A plot of total strain amplitude vs. reversals-to-failure (Figure 27) also displays an exceptional curve-fit with minimal scatter in the data. The quality of this data set can be attributed, in part, to the number of data points (47 fatigue tests is a large amount due to the significant time that fatigue testing requires). It should be noted that the red data points displayed in the following figures represent “runout” tests, where no failure occurred and the test was stopped at 2 million cycles (4 million reversals).

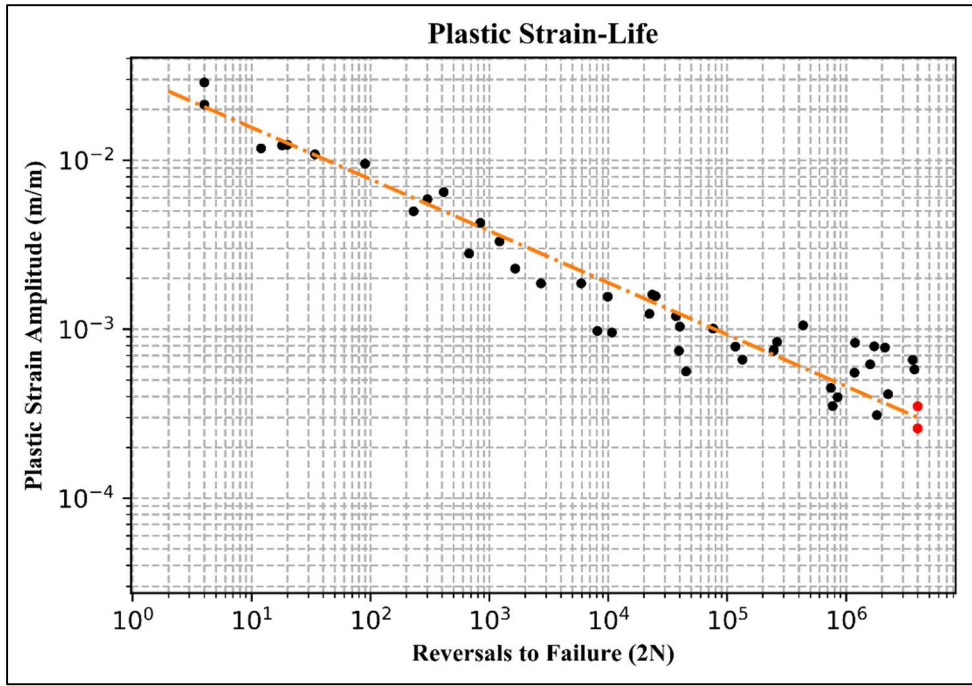


Figure 25: pDCPD Plastic Strain-Life

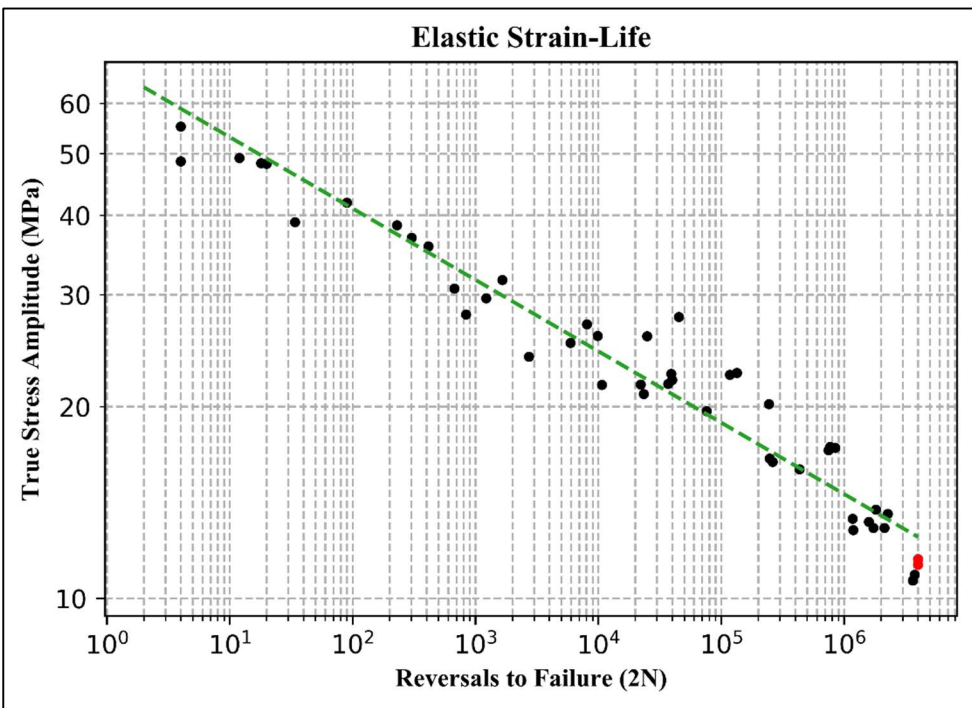


Figure 26: pDCPD Elastic Strain-Life

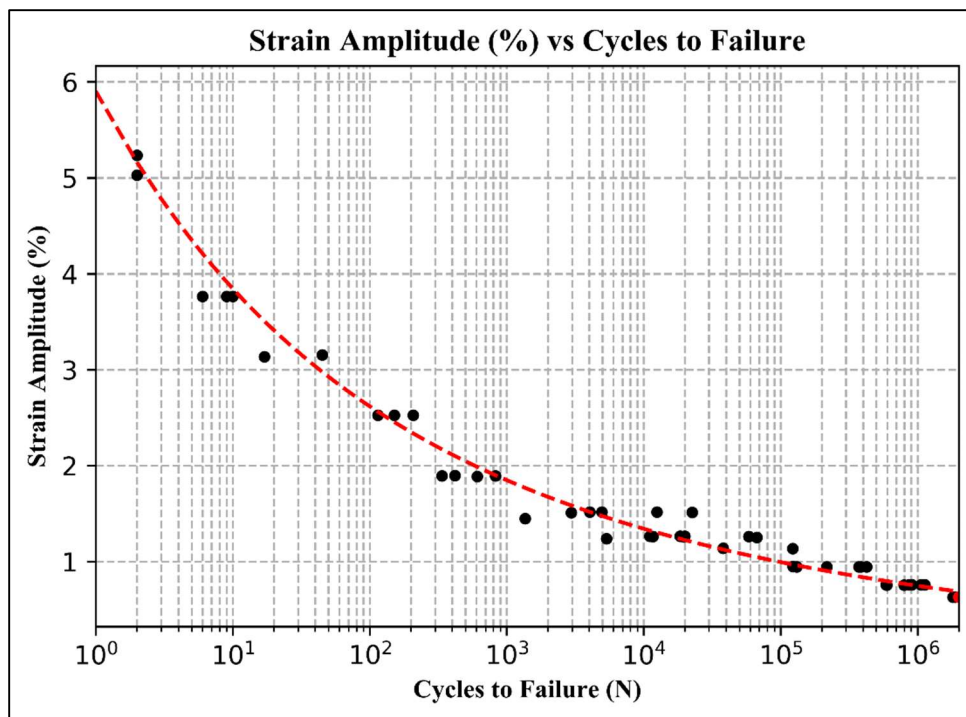


Figure 27: pDCPD Total Strain Amplitude vs. Reversals

The curve-fits displayed in these plots are created in conjunction with the calculation of the material's fatigue parameters using the post-processing GUI – the values of those parameters are what define the shape of the curves. This visualization of the results allows a judgement to be made regarding the accuracy of the material parameters that were determined. In the case of this data set for pDCPD, the results are determined to be accurate judging by the visible quality of the curve-fitting.

The total strain-life relationship is presented in Figure 28 – a log-log plot of strain amplitude vs. reversals to failure that includes the elastic strain-life, plastic strain-life and total strain-life lines plotted simultaneously. As previously stated, the true stress amplitude vs. reversals to failure relationship is converted to the elastic strain-life relationship by dividing the true stress amplitude by the tensile modulus. It should be noted that the elastic and plastic lines do not intersect, and therefore there is no

transition point as defined in literature regarding strain-life fatigue theory (see section 3.4.2). The plastic strain-life curve does still influence the behavior of the material, however, as the total strain-life line increases away from the elastic strain-life line in the low-cycle region because the plastic strain-life has its largest influence in that region. Therefore, the presence of the plastic relationship is still beneficial to defining pDCPD's low-cycle fatigue behavior. A more in-depth discussion about the application of these strain-life results to a polymer like pDCPD will take place in Chapter 6: Discussion.

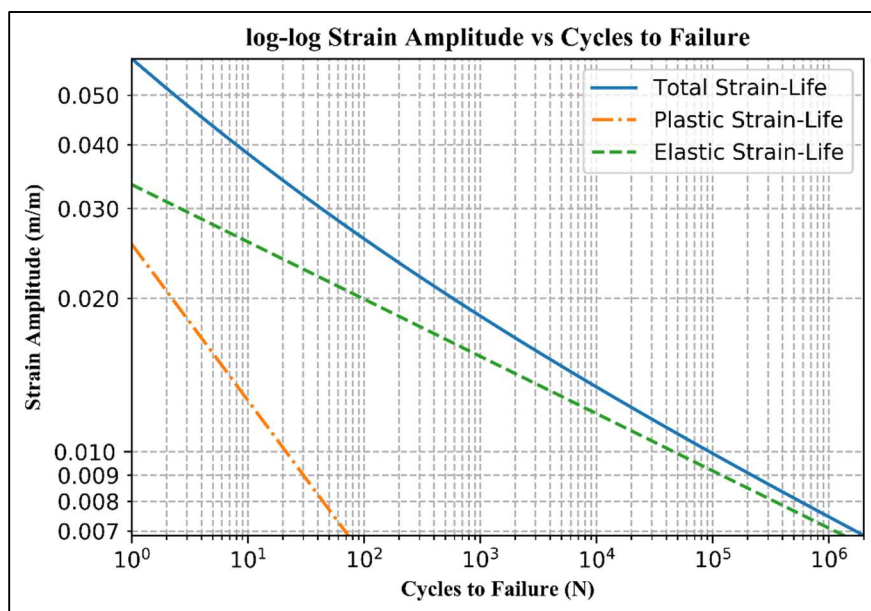


Figure 28: log-log Strain-Life with Elastic and Plastic lines

In addition to the strain-life relationship, the results also include the cyclic stress-strain curve (Figure 29) and the strain-controlled stress-life curve (Figure 30). The cyclic stress-strain curve, determined by considering the maximum stress-strain point during the half-life cycle of every test, is what defines the relationship between stress and strain in a stable cyclic state.

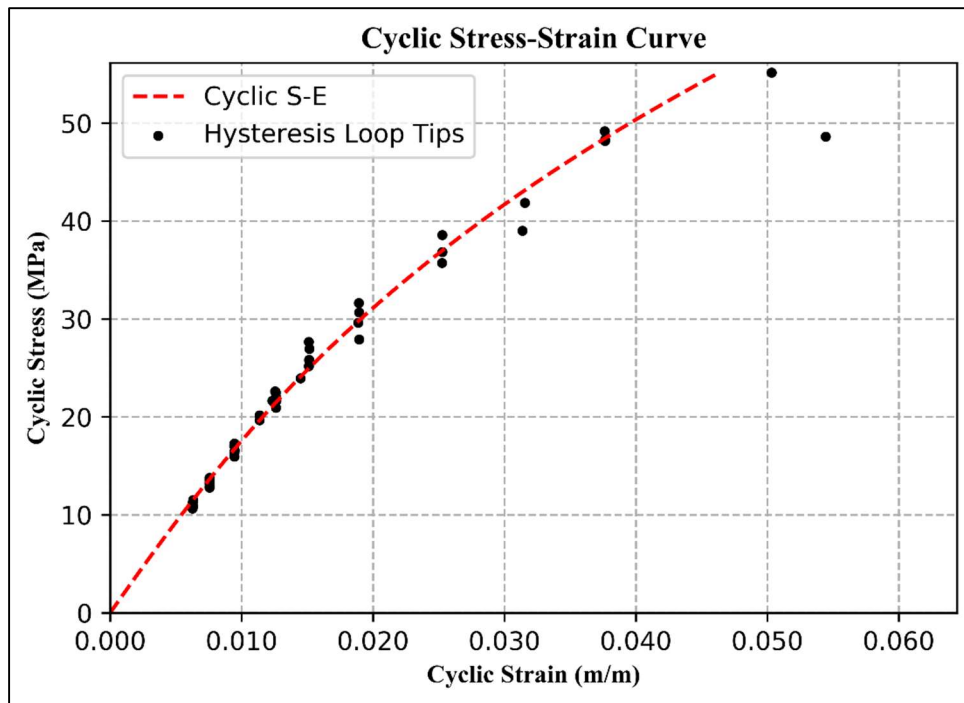


Figure 29: pDCPD Cyclic Stress-Strain Curve

The strain-controlled stress-life (Figure 30) is simply the stress-life relationship that is determined from strain-controlled testing. Obtaining this relationship is possible because load data is collected regardless of whether the test is controlled by the strain or the load, as explained in section 3.4.3. This relationship will later be compared to the more conventional load-controlled stress-life relationship determined from load-controlled testing of pDCPD. The comparison is made in section 5.2.

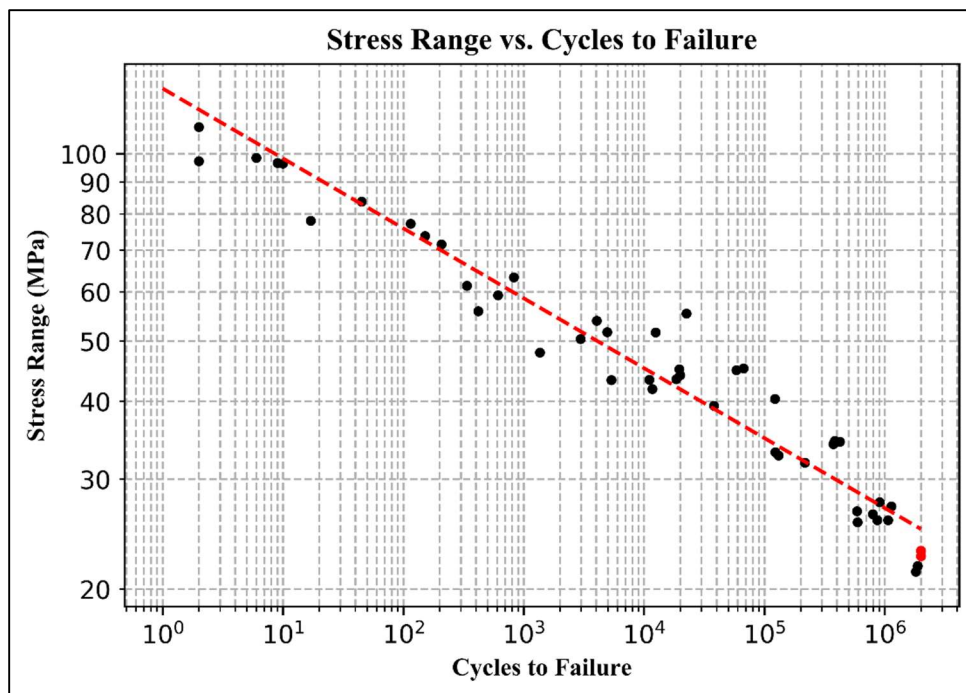


Figure 30: pDCPD Strain-Controlled Stress-Life

4.2.2 40% GF-PP Strain-Controlled Fatigue Results (In-Flow)

The strain-controlled fatigue tests that were completed for 40% GF-PP in the “in-flow” orientation are presented in Table 10 below. These tests are given a test ID using the following convention: C-IF-X-Y, where C stands for “cyclic test”, IF stands for “in-flow-oriented polypropylene”, X is a placeholder for the strain multiplier, and Y is a placeholder for the test number (in order) at that specific strain multiplier level. The test ID’s presented below may not start at 1 as some tests are not included due to a load frame error causing some tests to not be fully reversed – applying a larger stress in the tensile direction than in the compressive direction. When this error did occur, the test sample and any data collected from the test was discarded and not used for analysis.

Table 10: 40% GF-PP (In-Flow) Strain-Controlled Fatigue Tests

Test ID	Strain Multiplier Level	Target Strain Amp. (%)	Frequency (Hz)	Sample ID	Actual Average Strain Amp. (%)	Cycles to Sample Failure
C-IF-40-2	0.4	1.0629	1	I9-1	1.06234	174
C-IF-40-3	0.4	1.0629	1	I12-5	1.06239	689
C-IF-10-1	0.1	0.2657	10	I3-5	0.26181	2000000 ®
C-IF-12-1	0.12	0.31888	10	I5-2	0.31064	2000000 ®
C-IF-15-1	0.15	0.398609	10	I5-3	0.39577	2000000 ®
C-IF-20-2	0.2	0.53148	3	I4-7	0.53046	182870
C-IF-20-3	0.2	0.53148	3	I4-5	0.53091	149110
C-IF-20-4	0.2	0.53148	3	I4-4	0.53095	192450
C-IF-15-2	0.15	0.398609	5	I4-2	0.39751	1044570
C-IF-17-1	0.17	0.45175	5	I2-4	0.45027	461640
C-IF-17-2	0.17	0.45175	5	I4-1	0.45185	1248000
C-IF-17-3	0.17	0.45175	10	I5-4	0.44863	1481300
C-IF-25-1	0.25	0.66435	1	I1-2	0.66374	22130
C-IF-25-2	0.25	0.66435	3	I2-5	0.66364	16120
C-IF-25-5	0.25	0.66435	1	I3-2	0.66384	32940
C-IF-40-4	0.4	1.0629	1	I3-4	1.05849	880
C-IF-40-5	0.4	1.0629	3	I6-4	1.04730	278
C-IF-50-1	0.5	1.3286	1	I6-6	1.32748	122
C-IF-60-1	0.6	1.5944	1	I7-4	1.61472	12
C-IF-60-2	0.6	1.5944	1	I1-5	1.58968	51
C-IF-70-1	0.7	1.8601	1	I9-6	1.83864	13
C-IF-70-2	0.7	1.8601	1	I6-7	1.83548	12
C-IF-80-1	0.8	2.1259	1	I10-3	2.10127	8
C-IF-80-2	0.8	2.1259	1	I3-6	2.11412	1
C-IF-12-2	0.12	0.3188	10	I11-2	0.31391	2000000 ®
C-IF-27-1	0.27	0.7175	5	I5-6	0.70633	1240
C-IF-27-2	0.27	0.7175	5	I1-6	0.71175	3180
C-IF-80-3	0.8	2.1259	1	I2-6	2.09505	3
C-IF-80-4	0.8	2.1259	1	I7-5	2.09452	1
C-IF-80-6	0.8	2.1259	1	I8-4	2.10362	8
C-IF-70-3	0.7	1.8601	1	I9-7	1.82788	2
C-IF-70-5	0.7	1.8601	1	I15-5	1.91418	2
C-IF-50-2	0.5	1.3286	1	I12-4	1.32656	67
Note: ® = “Runout Test” (no failure)						

The half-life cycle data that was collected from the fatigue tests was analyzed using the custom post-processing GUI presented in section 3.5. The output of the GUI, displaying all of the cyclic stress-strain, strain-life and stress-life fatigue parameters is shown below in Figure 31.

Strain-Life (R = -1)	
Fatigue Ductility Coefficient (Ef')	0.01406
Fatigue Ductility Exponent (c)	-0.20897
Fatigue Strength Coefficient (Sf')	95.0732 MPa
Fatigue Strength Exponent (b)	-0.10071
Plastic Standard Error (SEp)	0.1156
Elastic Standard Error (SEe)	0.0858

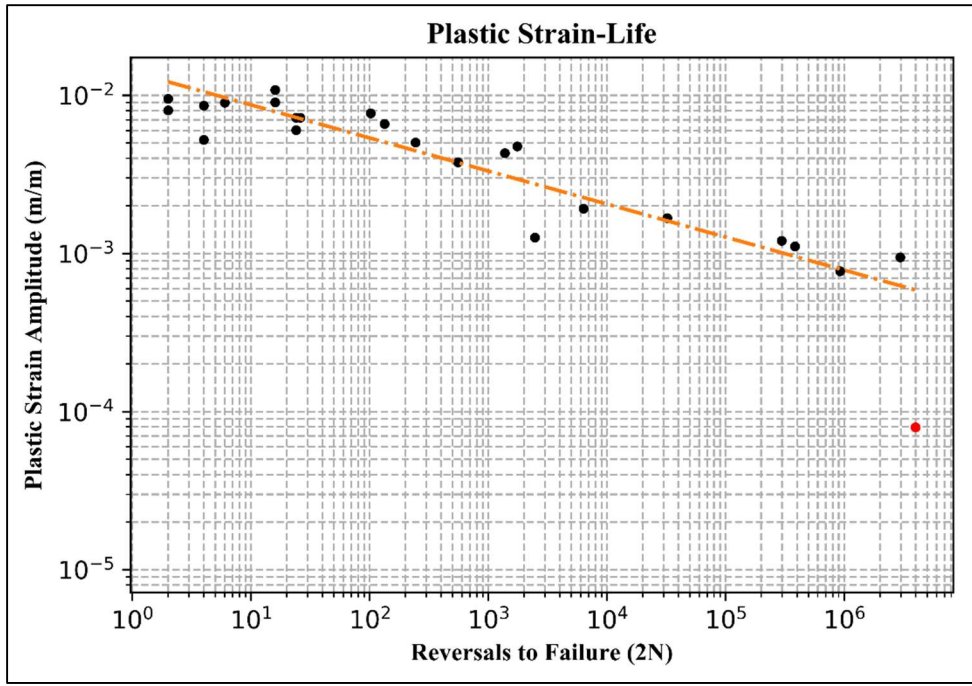
Cyclic Strength Coefficient (K')	742.3951 MPa (calculated)
Cyclic Strain Hardening Exponent (n')	0.4819 (calculated)
Cyclic Standard Error (SEc)	0.0286

Stress-Life (R = -1)	
Stress Range Intercept (SRI1)	174.9442 MPa
Stress-Life Slope 1 (b1)	-0.09934
Stress-Life Standard Error (SEs)	0.089

Number of Data Points: 29	

Figure 31: 40% GF-PP in-Flow Fatigue Parameters (strain-controlled results)

The curve fitting that was used to determine these parameters is displayed in the following plots of plastic strain-life, elastic strain-life, total strain-life and stress-life (Figure 32 through Figure 37). This data set had slightly more scatter than the data collected for pDCPD, with all standard errors less than 0.1 except for the plastic standard error (SEp) of 0.1156. Regardless, this dataset is still acceptable as an accurate representation of the material's behavior in the in-flow orientation. It should also be noted that the data points plotted in red color still represent runout tests in which the sample did not fail before the test was stopped at 2 million cycles (4 million reversals). These points are displayed, but they are not included in curve-fitting operations and therefore do not affect the fatigue parameter results.



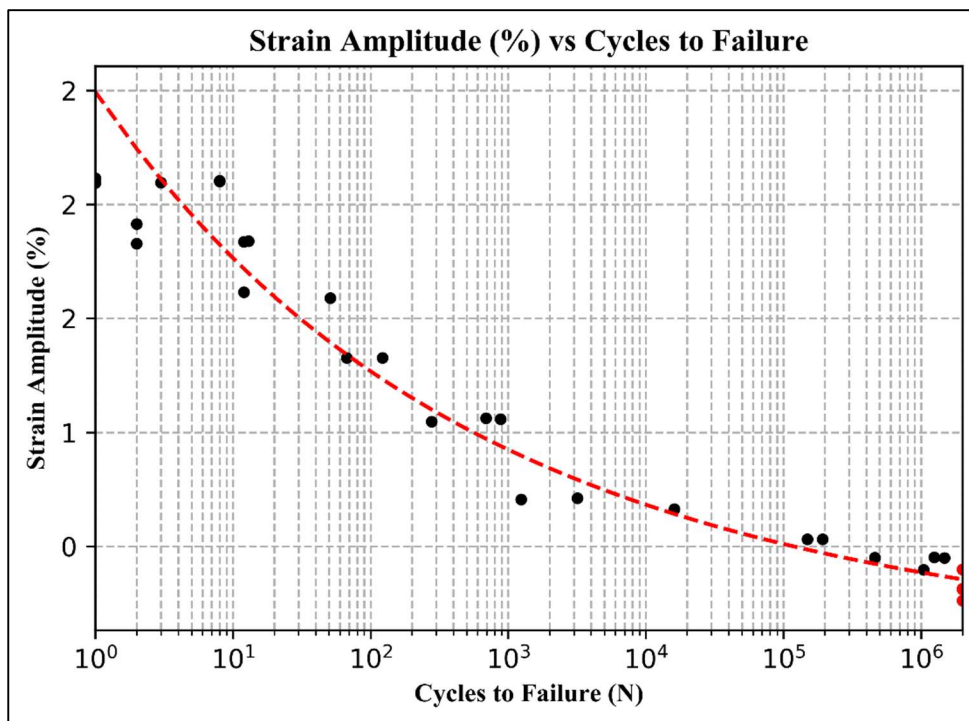


Figure 34: 40% GF-PP in-Flow Total Strain Amplitude vs. Reversals

The strain-amplitude vs. reversals to failure plot above shows that the sample is able to withstand a strain-amplitude of roughly 2.5% for exactly one reversal – approaching the monotonic failure strain of 2.65%. This makes sense for a material such as 40% GF-PP in the in-flow orientation that does not reach a true “yield” point as defined for plastic materials (there is no maximum on the monotonic stress-strain curve before failure). This differs from the case of pDCPD, where the yield strain is less than half of the monotonic failure strain. The faster cyclic motion of a low-cycle fatigue test induces a fast strain rate, which could cause the material to fail before reaching its monotonic failure strain. In summary, the results suggest that ductile materials such as pDCPD – that experience significant plastic deformation after the yield point – tend to fail at a strain that is much lower than the monotonic failure strain when subjected to a low-cycle fatigue load case. In contrast, more brittle materials like

40% GF-PP will reach strains closer to the monotonic failure strain when subjected to a low-cycle fatigue load case.

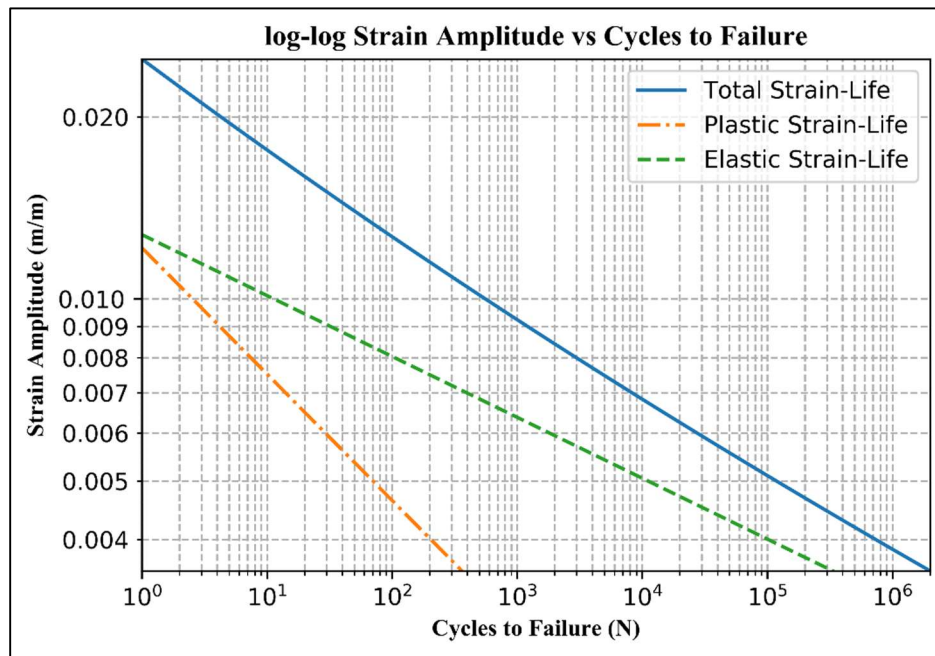


Figure 35: 40% GF-PP in-Flow log-log Strain-Life with Elastic and Plastic Lines

Similar to pDCPD, there is no intersection between the elastic strain-life line and the plastic strain-life line and therefore the material does not have a *transition point*. Consequently, when the material is deformed cyclically, the plastic strain remains very small (compared to the elastic strain) even in the low-cycle region. This does not mean that the plastic strain is insignificant, however, as the total strain life curve increases away from the elastic strain-life within the low-cycle region. This is a visual representation of the effect of the plastic strain, though its value may be small in this type of material. This idea will be expanded upon in section 6.1.

The cyclic stress-strain curve is shown below in Figure 36.

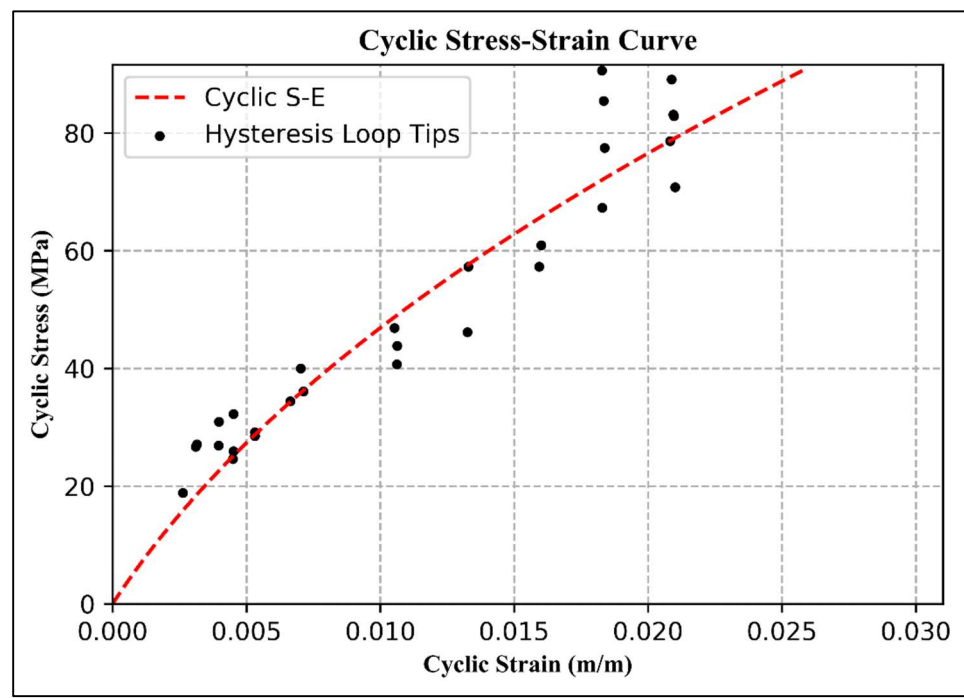


Figure 36: 40% GF-PP in-Flow Cyclic Stress-Strain Curve

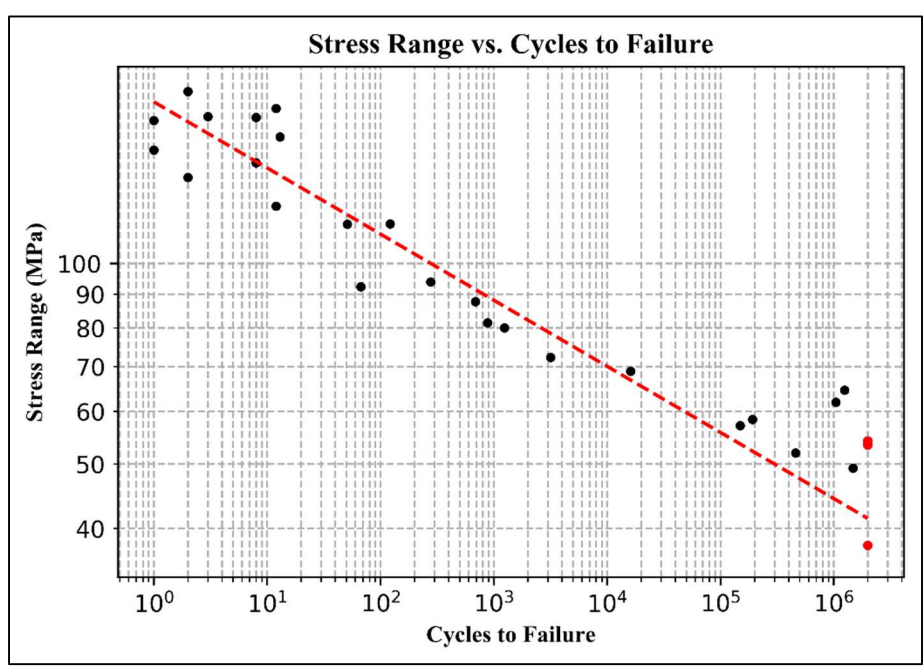


Figure 37: 40% GF-PP in-Flow Strain-Controlled Stress-Life

The strain-controlled stress-life relationship is shown in Figure 37 above. This is simply the stress-life relationship that is determined from the strain-controlled fatigue testing. Obtaining this relationship is possible because load data is collected regardless of whether the test is controlled by the strain or the load, as explained in section 3.4.3. This relationship is defined in terms of the stress range (maximum stress – minimum stress) vs. the cycles (rather than reversals) to failure. There will not be a stress-life comparison between strain-controlled and load-controlled testing for this material due to time constraints. As previously stated, this comparison will be made for pDCPD to validate the methodology of using strain-controlled testing to get the stress-life material parameters.

4.2.3 40% GF-PP Strain-Controlled Fatigue Results (Cross-Flow)

The strain-controlled fatigue tests that were completed for 40% GF-PP in the “cross-flow” orientation are presented in Table 11 below. These tests are given a test ID using the following convention: C-CF-X-Y, where C stands for “cyclic test”, CF stands for “cross-flow-oriented polypropylene”, X is a placeholder for the strain multiplier, and Y is a placeholder for the test number (in order) at that specific strain multiplier level. The test ID’s presented below may not start at 1 as some tests are not included due to a load frame error causing some tests to not be fully reversed – applying a larger stress in the tensile direction than in the compressive direction. When this error did occur, the test sample and any data collected from the test was discarded and not used for analysis.

Table 11: 40% GF-PP (Cross-Flow) Strain-Controlled Fatigue Tests

Test ID	Strain Multiplier Level	Target Strain Amp. (%)	Frequency (Hz)	Sample ID	Actual Average Strain Amp. (%)	Cycles to Sample Failure
C-CF-15-1	0.15	0.23914	5	C1-2	0.23808	2000000 ®
C-CF-50-1	0.5	0.7971	3	C7-3	0.79604	413
C-CF-50-2	0.5	0.7971	3	C3-2	0.79540	191
C-CF-50-3	0.5	0.7971	1	C9-2	0.79616	267
C-CF-60-1	0.5	0.9565	3	C6-1	0.95101	58
C-CF-27-1	0.27	0.43045	5	C2-5	0.42923	465880
C-CF-27-2	0.27	0.43045	5	C5-1	0.42830	300090
C-CF-27-3	0.27	0.43045	5	C2-4	0.42838	91650
C-CF-20-1	0.2	0.31885	5	C1-3	0.31780	2000000 ®
C-CF-30-1	0.3	0.47828	3	C2-1	0.47730	1232950
C-CF-30-2	0.3	0.47828	5	C5-2	0.47716	230980
C-CF-30-4	0.3	0.47828	5	C1-4	0.47622	221150
C-CF-30-5	0.3	0.47828	5	C2-2	0.47627	252330
C-CF-35-1	0.35	0.55799	5	C3-1	0.55515	220030
C-CF-35-2	0.35	0.55799	5	C10-2	0.55667	182800
C-CF-15-1	0.15	0.23914	10	C10-5	0.23485	2000000 ®
C-CF-40-2	0.4	0.6377	3	C5-4	0.63650	8610
C-CF-40-3	0.4	0.6377	3	C10-1	0.63694	12380
C-CF-50-6	0.5	0.7971	1	C13-3	0.99644	1
C-CF-70-1	0.7	1.1159	1	C4-3	1.10657	2
C-CF-40-4	0.4	0.6377	3	C4-2	0.63653	16120
Note: ® = “Runout Test” (no failure)						

The half-life cycle data that was collected from these fatigue tests was used to determine the fatigue parameters with the custom post-processing GUI presented in section 3.5. The output of this analysis – including both the strain-life and stress-life fatigue parameters – is shown below in Figure 38.

Strain-Life (R = -1)	
Fatigue Ductility Coefficient (Ef')	0.00411
Fatigue Ductility Exponent (c)	-0.1946
Fatigue Strength Coefficient (Sf')	43.3734 MPa
Fatigue Strength Exponent (b)	-0.05505
Plastic Standard Error (SEp)	0.1336
Elastic Standard Error (SEe)	0.1103

Cyclic Strength Coefficient (K')	205.1895 MPa (calculated)
Cyclic Strain Hardening Exponent (n')	0.2829 (calculated)
Cyclic Standard Error (SEc)	0.0304

Stress-Life (R = -1)	
Stress Range Intercept (SRI1)	83.4993 MPa
Stress-Life Slope 1 (b1)	-0.05505
Stress-Life Standard Error (SEs)	0.1103

Number of Data Points: 21	

Figure 38: 40% GF-PP cross-Flow Fatigue Parameters (strain-controlled results)

The larger standard errors for this data set (all > 0.1 except for the cyclic standard error SEc) attest to the slightly increased scatter within the data, as well as the smaller amount of data points that were collected for this material. The expected trends are still present, however, and the following plots (Figure 39 through Figure 41) provide visual evidence that the parameters determined from the curve fitting accurately describe the fatigue behavior of the material. The data points plotted in red color represent runout tests in which the sample did not fail before the test was stopped at 2 million cycles (4 million reversals). These points are displayed, but they are not included in curve-fitting operations and therefore do not affect the fatigue parameter results. It should also be noted that the plastic strain-life plot (Figure 39) does not show these red dots – this is because the value of the plastic strain for the runout tests was negligibly small and was therefore not included within the limits of that figure.

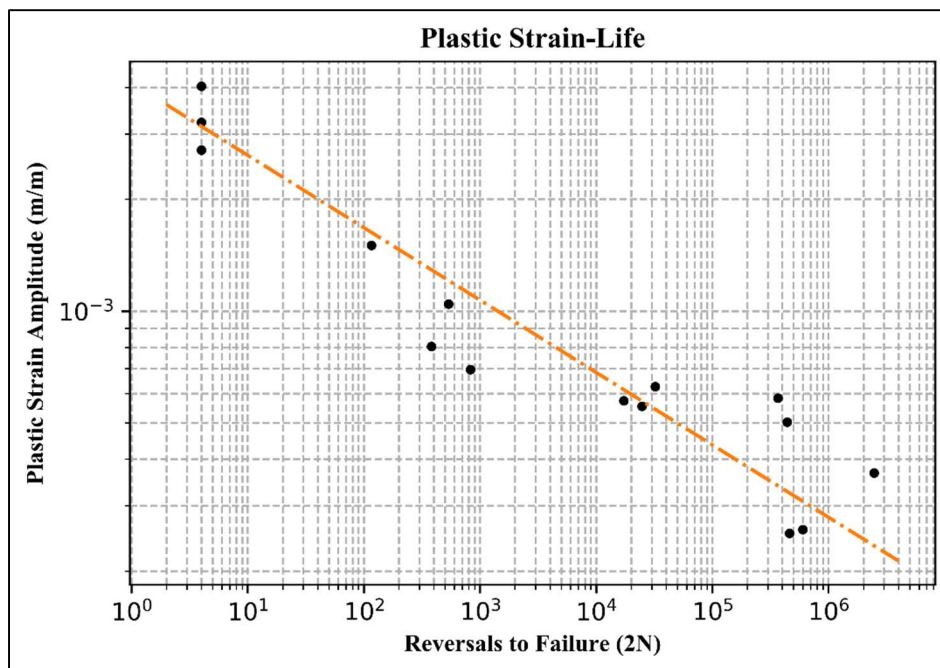


Figure 39: 40% GF-PP cross-Flow Plastic Strain-Life

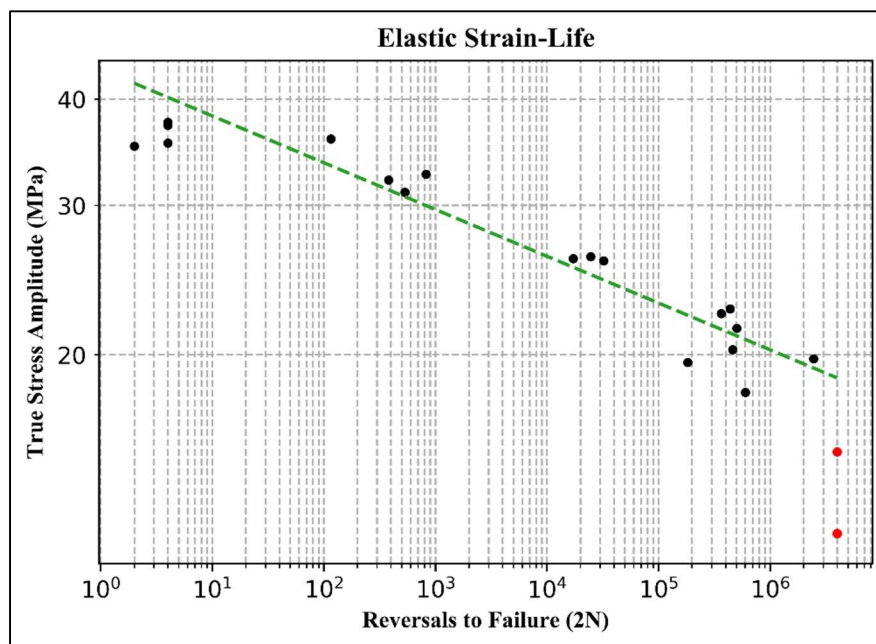


Figure 40: 40% GF-PP cross-Flow Elastic Strain-Life

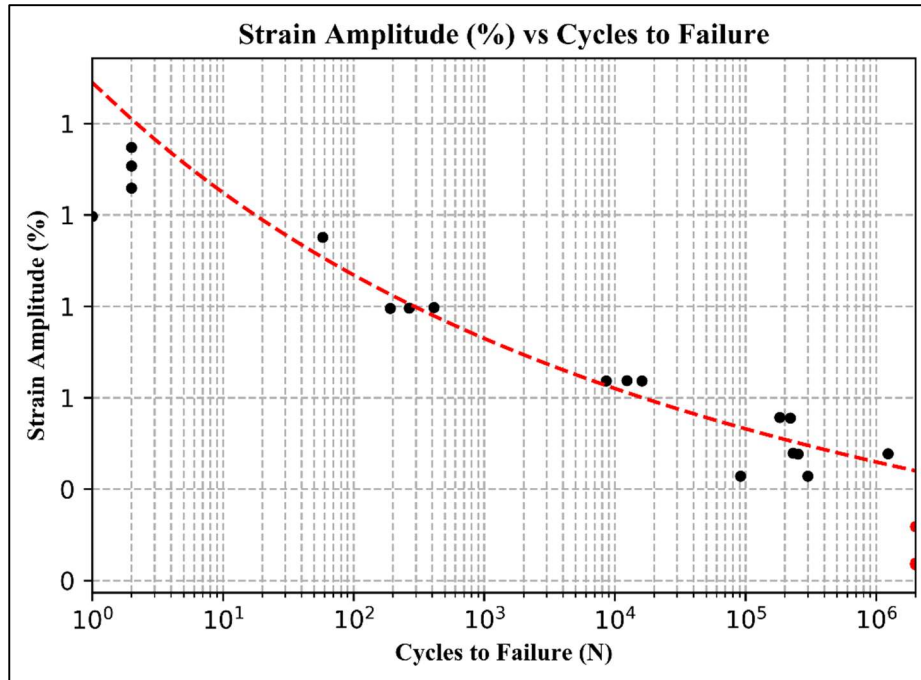


Figure 41: 40% GF-PP cross-Flow Total Strain Amplitude vs. Reversals

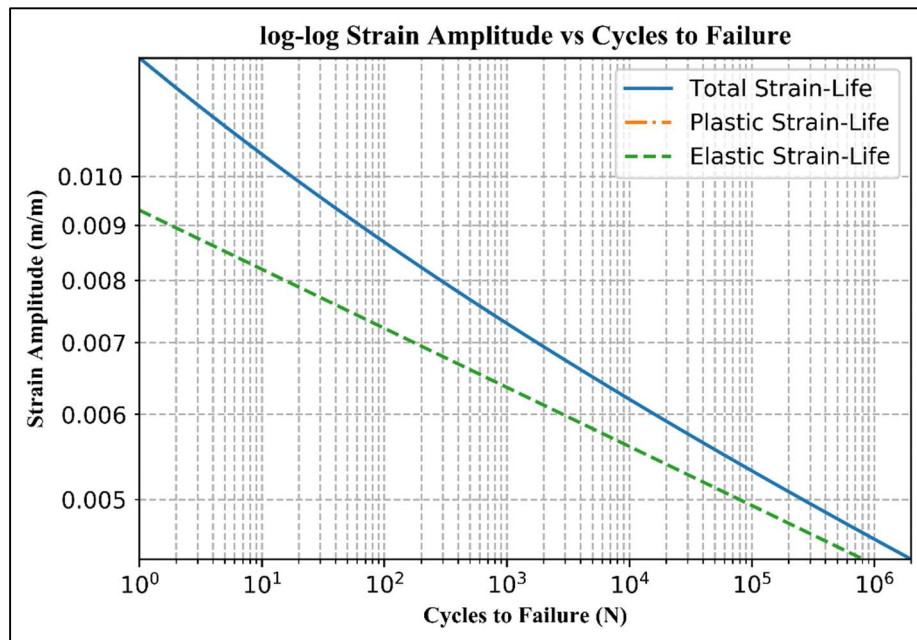


Figure 42: 40% GF-PP cross-Flow log-log Strain-Life with Elastic and Plastic Lines

In the cross-flow orientation, the plastic strain-life line is not visible within the bounds of the total strain-life log-log plot (Figure 42 above) because the plastic strain

is small when the material is loaded cyclically. The plastic strain is not visually negligible, however, as the total strain-life curve increases away from the elastic strain-life line in the low-cycle region. This indicates that the plastic strain contributes to the shape of the strain-life relationship, though it may not be significant. The cyclic stress-strain curve is also shown below.

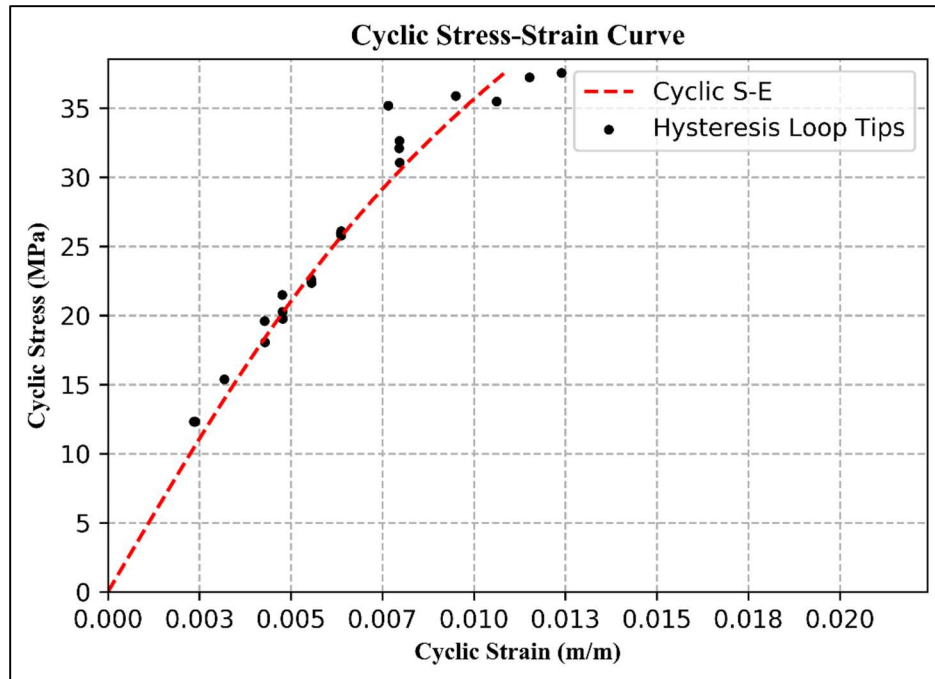


Figure 43: 40% GF-PP cross-Flow Cyclic Stress-Strain Curve

The strain-controlled stress-life relationship is shown in Figure 44. This is simply the stress-life relationship that is determined from the strain-controlled fatigue testing of 40% GF-PP cross-flow. Obtaining this relationship is possible because load data is collected regardless of whether the test is controlled by the strain or the load, as explained in section 3.4.3. This relationship is defined in terms of the stress range (maximum stress – minimum stress) vs. the cycles (rather than reversals) to failure.

There will not be a stress-life comparison between strain-controlled and load-controlled testing for this material.

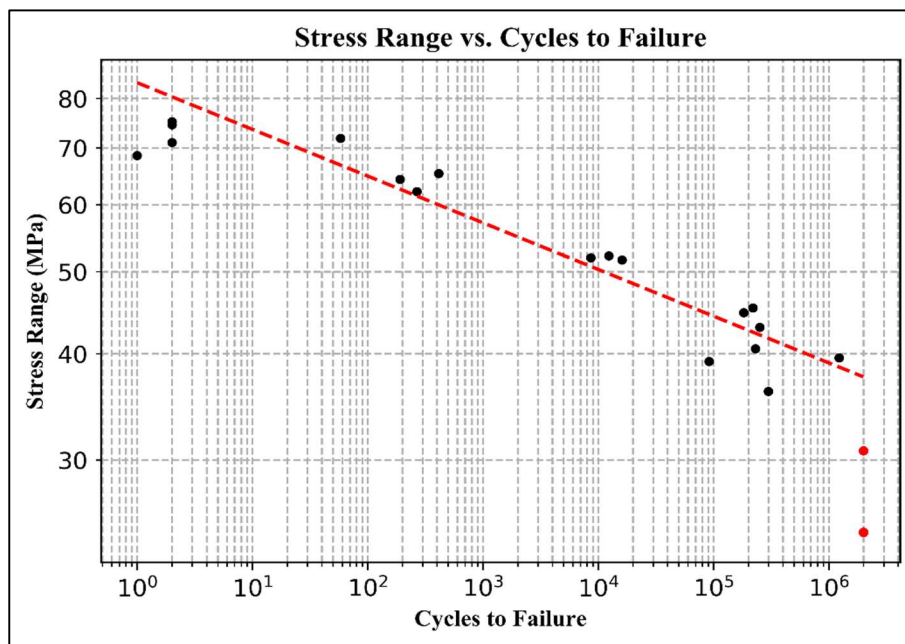


Figure 44: 40% GF-PP (cross-flow) Strain-Controlled Stress-Life

4.2.4 40% GF-PP Strain Controlled Fatigue Results – Comparison

This section provides a side-by-side comparison of the fatigue results for 40% GF-PP in the two glass-fiber reinforcement orientations that were tested. As expected, the cross-flow orientation provided overall weaker behavior for both monotonic and cyclic loading. This is because, for coupons cut in this orientation, the majority of the reinforcement fibers are oriented perpendicular to the direction of loading. The polypropylene matrix is then subjected to the majority of the load without significant assistance from the much stronger glass fibers that have a better resistance to both cyclic and monotonic loading conditions.

All of the properties for both orientations of 40% GF-PP are listed in Table 12, showing that the cross-flow orientation is consistently weaker.

Table 12: 40% GF-PP Strain-Controlled Fatigue Results Comparison

	Material Parameter	In-Flow	Cross-Flow
Monotonic	Tensile modulus (MPa)	6938.7	4489.6
	Poisson's Ratio	50.3	33.4
	Tensile @ Yield (Mpa)	74.1	42.9
	Tensile @ Break (Mpa)	2.65%	1.59%
	Elongation @ Break (%)	0.397	0.228
Stress-Life	b1 (S-N Slope)	-0.0993	-0.055
	SRI1 (S-N intercept) (MPa)	174.94	83.49
Strain-Life	Sf' (Elastic E-N Intercept) (Mpa)	95.07	43.37
	b (Elastic E-N Slope)	-0.1007	-0.055
	Ef' (Plastic E-N Intercept)	0.014	0.004
	c (Plastic E-N Slope)	-0.2089	-0.1946
	n' Cyclic strain hardening exponent	0.482	0.2829
	K' Cyclic strength coefficient (MPa)	742.39	205.19
	SE (Standard errors)?	all <0.1 except SEp=0.11	all >0.1

The in-flow orientation reached a larger strain than the cross-flow orientation (2.65% and 1.59%, respectively) though this may not mean that the in-flow orientation is more ductile than cross-flow. At such small strain values (as compared with some metals or ductile plastics similar pDCPD) there is very little plastic deformation occurring. This is further proven by the shape of the tensile stress-strain curve for both orientations of 40% GF-PP – there is no easily definable yield point. Therefore, the increased strain in the in-flow orientation is attributed to the increased strength rather than a perceived increase in ductility.

Figure 45 and Figure 46 below give a visual representation of the differences between the stress-life and strain-life fatigue behavior for the two orientations of 40% GF-PP that were tested.

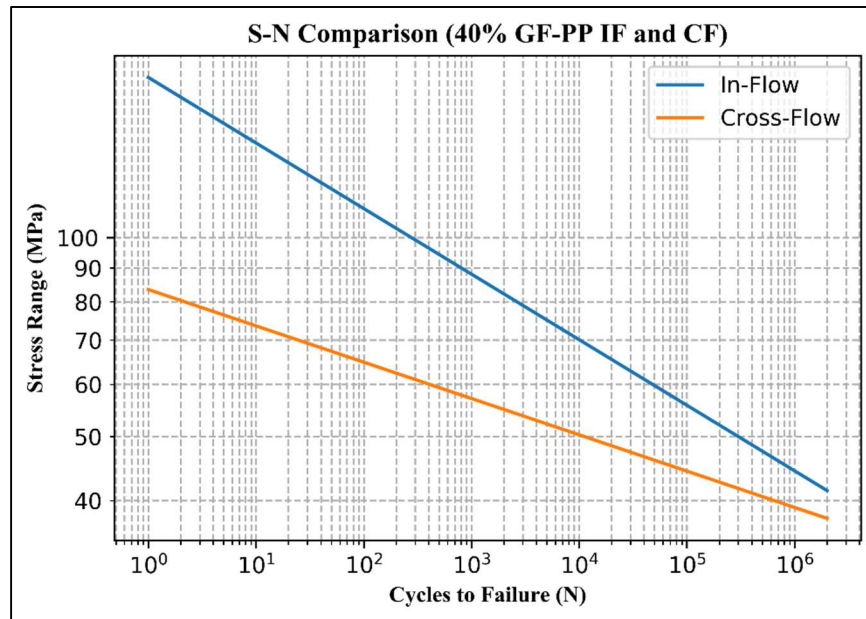


Figure 45: 40% GF-PP Stress-Life Comparison (in-flow and cross-flow)

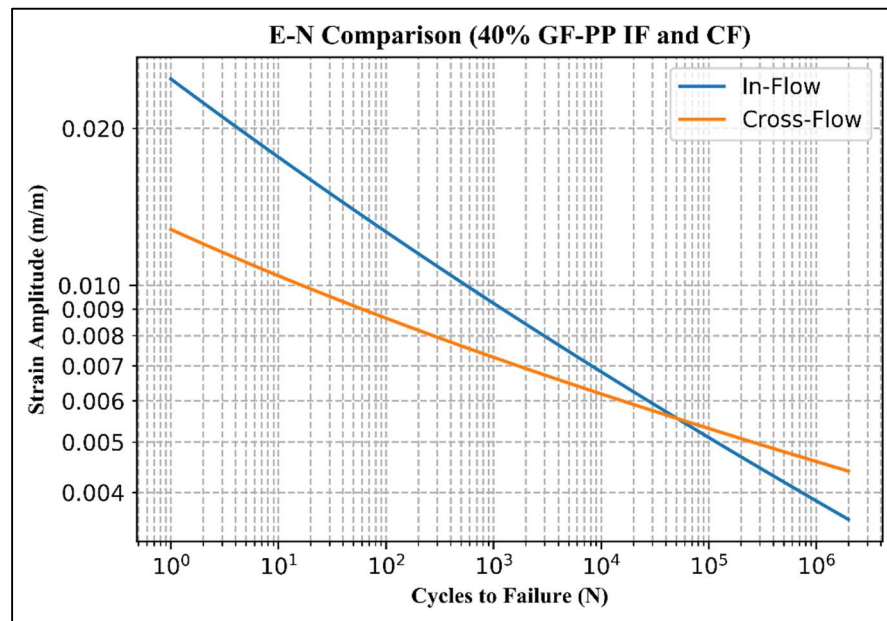


Figure 46: 40% GF-PP Strain-Life Comparison (in-flow and cross-flow)

As shown in the above plots, the cross-flow orientation has a lower stress-life curve with a shallower slope than the in-flow orientation. The strain-life curves show a similar relationship, with the cross-flow curve lower and shallower than the in-flow curve. Interestingly, the strain-life curves intersect at around 50,000 cycles, and the cross-flow curve is higher than in-flow beyond that point. This could point to some advantages for the cross-flow oriented material in the high-cycle region (greater than 50,000 cycles).

Chapter 5

5 Additional Considerations

The main deliverable of this body of work is the addition of accurate monotonic and fatigue data for multiple materials in the DTNA material database used by the structural analysis team. The specific results of the testing procedures that were completed to collect this data are presented in the previous chapter. During the process of completing this testing, however, multiple areas of interest arose in which further research could answer some interesting questions. These topics include the strain-softening behavior that was observed in the monotonic tensile testing of pDCPD, as well as the differences in pDCPD stress-life parameters if the testing is completed in load-control mode rather than strain-control. These topics are expanded upon in the following sections.

5.1 pDCPD Strain-Softening Behavior

It was briefly noted in section 4.1.1 that pDCPD experiences a condition called strain-softening during its monotonic deformation. This simply describes the situation in which an increased elongation in the material (increase in strain) results in a decreased stress within the material – less load needs to be applied to continue the elongation. Figure 47 shows an annotated version of the overlaid stress-strain plot for pDCPD. As shown, the deformation begins with an elastic region in which the relationship between stress and strain is linear (a straight line). The stress vs. strain

curve then flattens to reach a yield (maximum) point, before the strain-softening begins and lasts until the failure point.

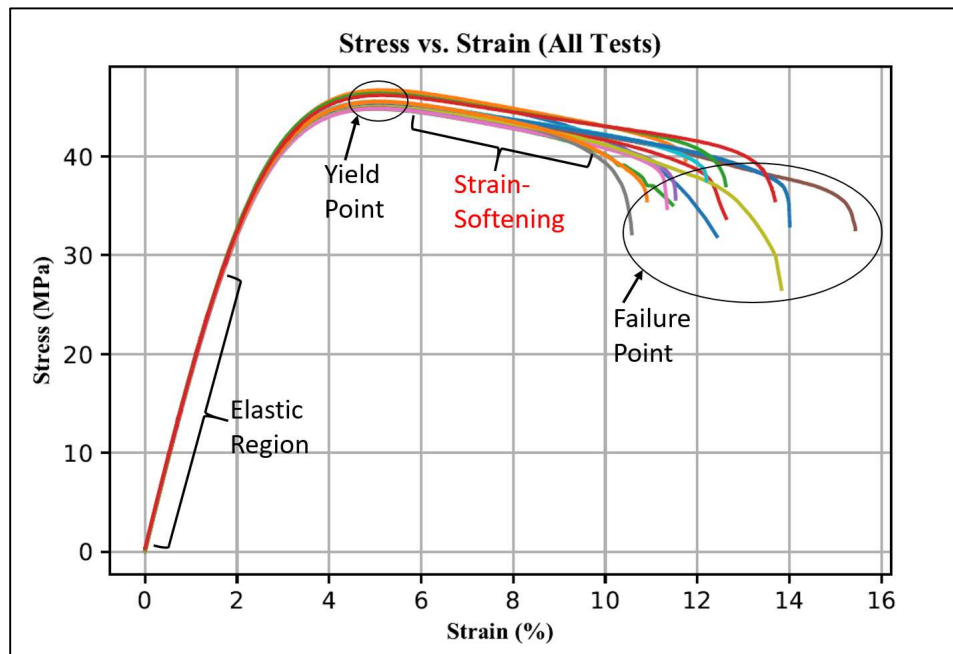


Figure 47: pDCPD Monotonic Tests (annotated)

The reasons behind this behavior are quite interesting, and it relates to the characteristics of polymeric materials. In order to discuss this, the atomic-level effects of the monotonic deformation of a metal will be explained and then compared to the behavior of plastics like pDCPD under the same loading conditions.

5.1.1 Plastic Deformation in Metals – a brief summary

When discussing the monotonic deformation of a metal (steel, for example), it is important to consider the material's microstructure on an atomic level and how it responds to the applied loading. There are three main microstructure shapes (shown in Figure 48), each of which represent one instance (called a "unit cell") of the pattern that continuously occurs throughout the crystal structure: face-centered-cubic (FCC), body-centered-cubic (BCC), and hexagonal close-packed (HCP) [5].

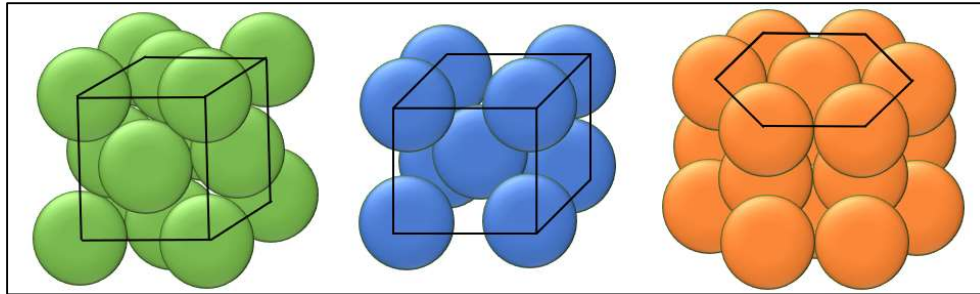


Figure 48: Crystal Structure of Metals – FCC (left), BCC (center) and HCP (right)
(adapted from [5])

Not pictured in Figure 48 is the “simple cubic” shape that also exists, consisting of eight atoms, each centered on a corner of a cubic unit cell. The microstructure pattern of any given metallic material depends, in part, on the chemical makeup of that material – which atoms are present and the sizes of each type of atom.

In reality, these crystal structures are not perfect, and many defects tend to exist within the above-mentioned patterns that can aid or inhibit the material’s deformation when a load is applied. These defects can be either the result of an extra atom or “impurity” present as an interstitial within the crystal structure, the total replacement of an atom with one of a different element (called a “substitutional”) or the misalignment, addition, or removal of an entire plane of atoms within the structure, called a dislocation. A commonly studied type of dislocation is the edge dislocation, shown in Figure 49 below, where the edge of an extra half-plane of atoms causes slight warpage of the location of the surrounding atoms. The extra half-plane is present in the top half of the pictured crystal structure, but is not present in the bottom half. This can be seen by counting the number of atoms in the top and bottom row – there are 4 on the bottom, and 5 on the top.

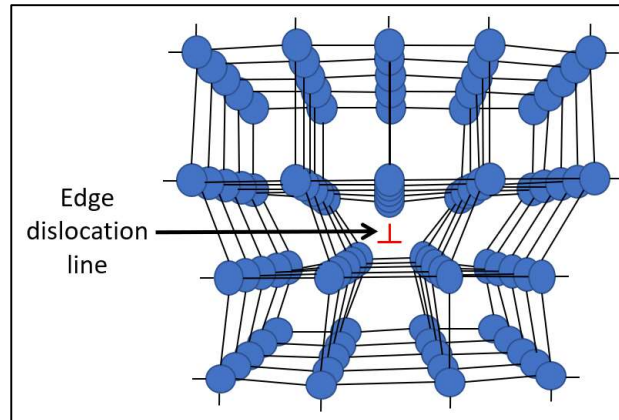


Figure 49: Edge Dislocation (adapted from [5])

When an external load is applied to metal that contains edge dislocations, it induces shear stresses along the planes of atoms that can be aligned at arbitrary angles with respect to the axis of loading. This condition is illustrated in Figure 50 below, where the shear stress τ' is induced on plane p' in response to the applied normal stress σ . The plane p' is aligned at angle θ from the plane p , which is normal to σ .

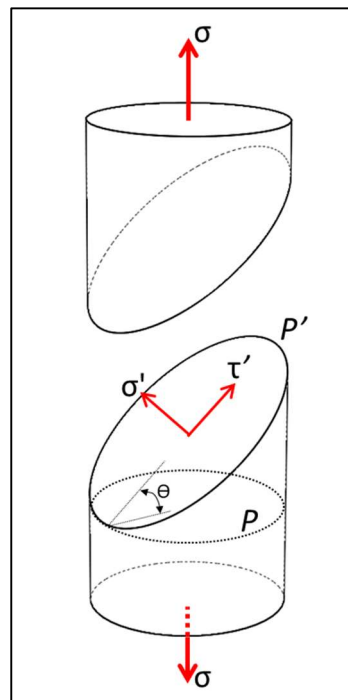


Figure 50: Shear Stress τ' Induced on Crystallographic Plane p' from Applied Normal Stress σ (adapted from [5]).

When the induced shear stress gets large enough, it can cause plastic deformation (permanent atomic movement) within the material by means of dislocation motion, illustrated below in Figure 51. For an edge dislocation, this process involves breaking the covalent bond next to the dislocation, and re-forming that bond with the atom that was previously directly on top of the dislocation, moving the location of the defect over by one atomic position. This process occurs rapidly and continuously, allowing the dislocation to move along the plane of atoms beneath it, called a “slip plane”.

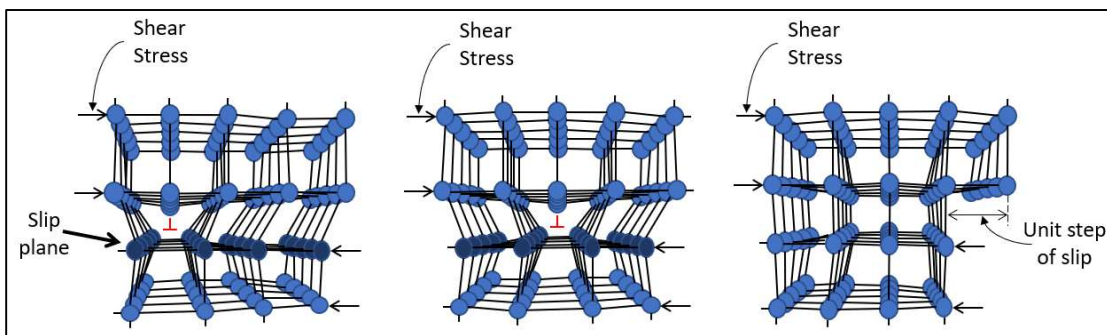


Figure 51: Edge Dislocation Motion on Slip Plane (adapted from [5]).

Millions of these dislocations can exist and move simultaneously within a material, not including the various other types of defects that can have other methods of movement when a load is applied. This motion of defects – breaking and re-forming covalent bonds – is what results in the material’s plastic deformation after the yield point. Figure 52 shows the common shape of the stress-strain curve for a steel sample. As shown, there is a steep and narrow region of elastic deformation, representing the stretching of atomic bonds before any plastic deformation occurs. When the applied stress is sufficiently large, the metal yields, and plastic deformation in the form of the dislocation motion described above (along with many other deformation mechanisms) begins to occur.

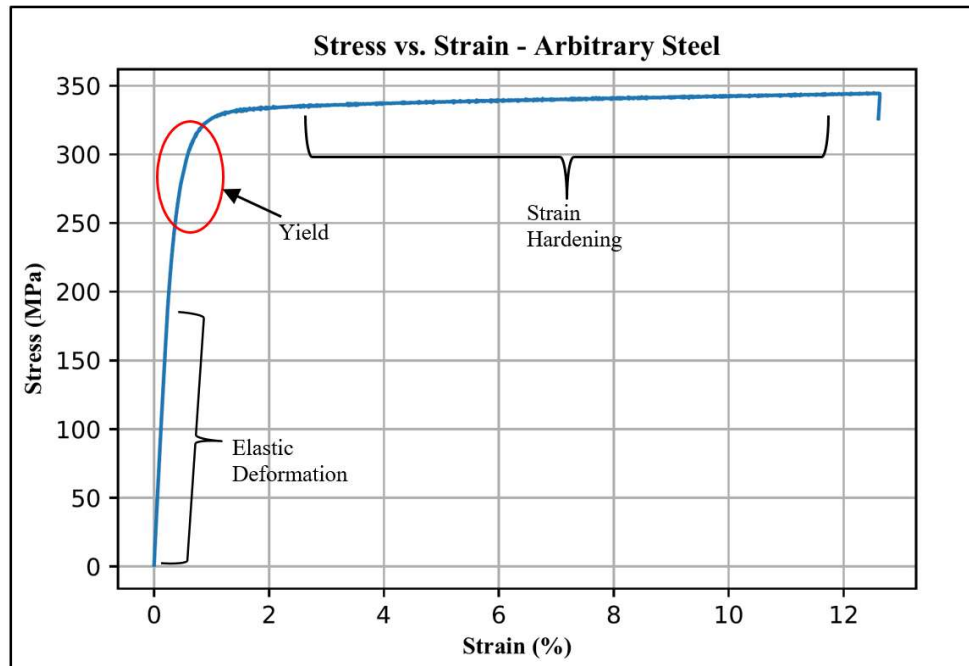


Figure 52: Stress-Strain Curve for an Arbitrary Steel Type

During the plastic deformation of a crystalline material like steel, a condition called strain hardening arises (labeled in Figure 52) in which the stress required to continue elongation is continuously increasing as the strain increases. This is visible as the upward-trend seen in the post-yield section of the stress-strain curve above. The cause of this condition is the interactions that occur between defects as they move throughout the crystal structure. The movement of one dislocation may interfere with the path of another, or multiple dislocations might become stuck on an impurity in the crystal structure, causing a condition called “dislocation pile-up”. These interactions between defects that inhibit dislocation motion will work together to make the material harder to deform with every increase in strain – hence the name “strain hardening”.

5.1.2 Atomic Structure of Polymers

Polymers have a much different atomic structure than metals, and therefore display different behavior when deformed monotonically. While the structure of a

metal is a pattern of individual atoms connected with covalent bonds in a crystal, polymers are made up of entire molecules (monomers) bonded in long chains that interact with one-another either indirectly through weak attractive Van der Waals forces, or directly through covalent cross-linking. There are four main types of polymer structures, involving various combinations of bonding types: linear, branched, cross-linked, and network polymers (not discussed here) [41]. The linear, branched and cross-linked polymer structure types are shown in Figure 53 below, where every orange dot represents a monomer.

Linear and branched polymers are similar in the fact that they consist of polymer chains that are held together not through covalent bonding, but by weak attractive Van der Waals forces that occur between molecules. Branched polymers, however, may have several “branches” of bonded monomers protruding from the main polymer chains. While the chains are not directly connected in either linear or branched polymers, the branched formation should show larger resistance to external loads due to the increased attractive Van der Waals forces induced by the branches interacting with other polymer chains and branches.

In a cross-linked polymer, the main polymer chains will also have branches of connected monomers protruding. These branches, however, are called “cross-links” because they directly connect the main polymer chains together using covalent bonding.

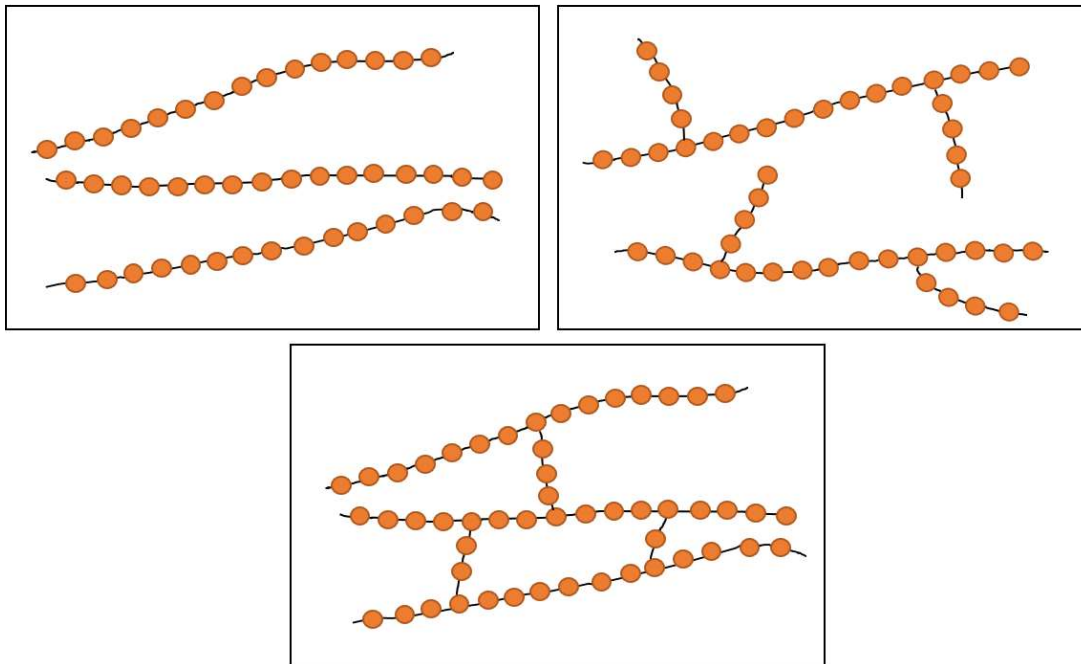


Figure 53: Polymer Structures: Linear (top left), branched (top right), and cross-linked (bottom). (adapted from [5])

It is important to note that Polymers do not always identify with just one of these definitions. For example, a predominantly linear polymer may have some cross-linking. The materials are classified based on the predominant structures that are present [5].

5.1.3 Polymerization and Molding Process for pDCPD

pDCPD is a heavily cross-linked polymer made up of dicyclopentadiene molecules. This is why the full name for pDCPD is polydicyclopentadiene – the connection of these dicyclopentadiene monomers is what makes up the polymeric material. The material is manufactured via a process called reaction injection molding (RIM), in which a polymer material is molded into a part as the polymerization reaction takes place simultaneously. To accomplish this, two liquid resins are initially kept separated, each containing the monomer and other mixtures to facilitate the polymerization reaction. The resins are then mixed in a pre-determined ratio, with

several parameters closely monitored such as temperature, pressure, flow turbulence and flow rate as the material flows into the part mold. The chemical reaction then finishes and the liquid resin hardens into the desired material [42].

Regarding the molding process for DCPD (illustrated in Figure 54), the two resins both consist of the DCPD monomer, one mixed with an activating agent (the “activator”) and the other mixed with a reaction catalyst. They are mixed in a 1:1 ratio in a chamber called a “mix head” directly before entering the mold, where the ring-opening metathesis polymerization (ROMP) reacting begins. Within 4 to 6 minutes, the material will finish its polymerization and harden in the desired shape inside the mold [43,44]. After this process, the material has become the rigid, thermoset, heavily cross-linked polymer called polydicyclopentadiene (pDCPD) with excellent impact resistance, and desirable strength properties [43].

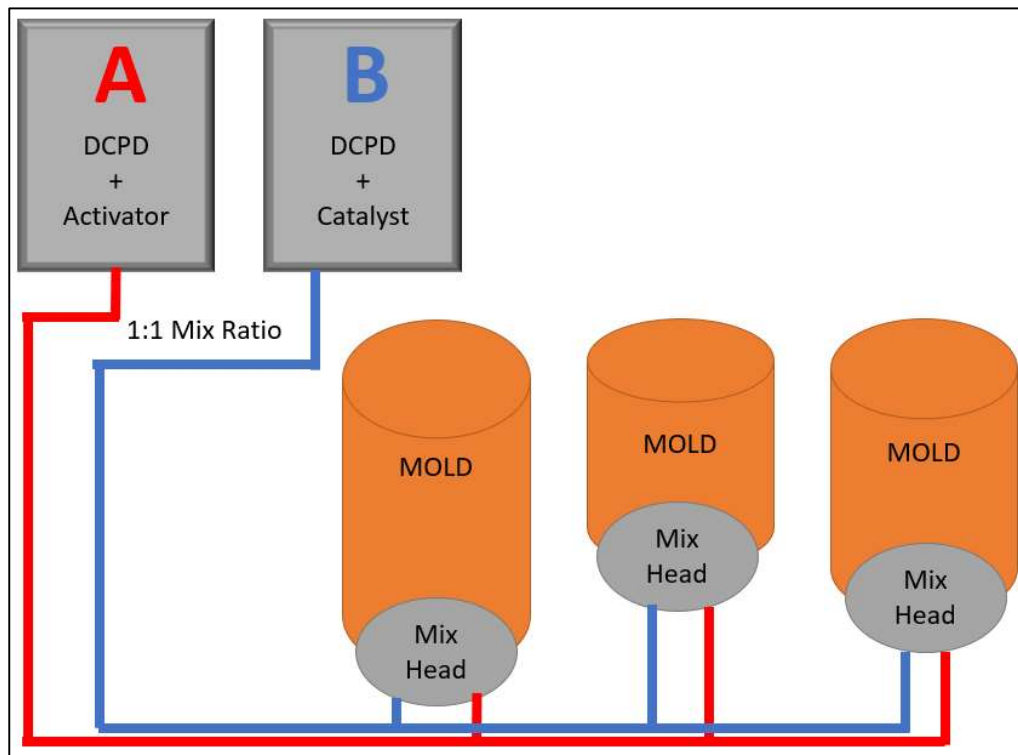


Figure 54: pDCPD Reaction Injection Molding Process (adapted from [44])

5.1.4 Plastic Deformation of Polymers

The way by which a polymer will experience plastic deformation is dependent upon the internal structure of the material, and differs greatly from the behavior of metals described above. Linear and branched polymers (typically called thermoplastics) are affected greatly by the Van der Waals interactions between polymer chains. When the applied load becomes large enough, yielding will occur and cause plastic deformation consisting of the polymer chains overcoming the weak Van der Waals forces and sliding relative to one-another. The chain branches in a branched polymer increase the effects of the Van der Waals interactions, therefore making the material harder to deform. Eventually, the deformation will cause the chains to become tangled and stuck, no longer able to move in a cooperative fashion – this causes strain hardening behavior. This increasingly places the load directly onto the covalent bonding within the chains, which will eventually break as the material fails [41]. For these materials, an increased strain rate will cause more brittle behavior as the chains have less time to move cooperatively and therefore become stuck more easily.

For a cross-linked thermoset polymer like pDCPD, the Van der Waals forces have a very little effect on the deformation, and the covalent bonds within the cross-linking govern the deformation and yielding [41]. As a cross-linked polymer yields – as labeled in the stress-strain curve for DCPD in Figure 47 – the covalent bonds are stretched beyond the elastic limit, and the cross-links between polymer chains begin to break. This condition is what causes the strain softening that is labeled in Figure 47, where the stress that is required to continue deforming the material continuously

decreases as the strain increases after the yield point. This is due to the breaking of cross-links, providing a continuously decreasing resistance to the applied load.

For the pDCPD material that was tested in this study, the strain softening condition lasted until the failure point as the lack of cross-linking applied too much load to the individually bonded polymer chains, causing them to break. As aging affects take place within the material, its characteristics can change to show some strain hardening behavior after the strain softening is finished, proving a stress-strain curve shape similar to that shown in Figure 55. This would be caused by the polymer chains beginning to behave like a linear polymer after a sufficient number of cross-links have been broken.

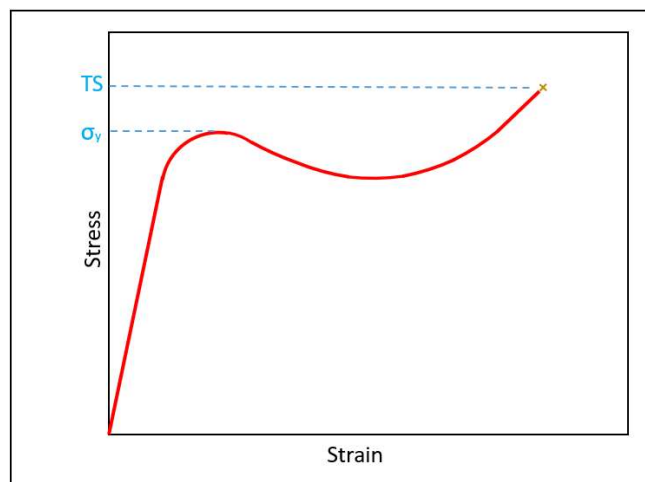


Figure 55: Strain Softening Followed by Strain Hardening (adapted from [5])

5.1.5 Summary

The strain-softening behavior seen in the monotonic deformation of pDCPD became apparent when trying to solve for the monotonic strain hardening coefficient (n) that is referred to in ASTM D638 and SAE J1099, the standard testing procedures that are being referenced [2, 9]. After several iterations in the analysis, it was concluded that this parameter could not be accurately determined for pDCPD and was therefore

not a valid parameter for a material that displays this strain softening behavior after yielding. In this discussion, it was determined that the cause of this behavior is the breaking of the cross-links that are a necessary factor in the material's structure after the polymerization during the RIM process. When pDCPD is used for a truck part, it will be designed to operate within the material's elastic region. Therefore, this post-yield behavior of the polymer should not affect the part's performance or safety.

5.2 Comparison of Strain-Controlled and Load-Controlled Testing

In existing literature regarding the fatigue behavior of materials – especially plastic materials – the stress-life relationship is derived from a data set of load-controlled (or stress-controlled) fatigue tests. In this type of testing, the cyclic waveform that is applied to the material is controlled by the load (or stress), with a set amplitude in terms of newtons (load) or Pascals (stress). This differs from the strain-controlled version of fatigue testing that was presented in chapter 4 of this document, in which the cyclic waveform is controlled by the strain amplitude, or the amount of deformation that is applied to the sample during every cycle.

Military Handbook-5H (MIL-HDBK-5H) states that, if a fully reversed strain-controlled waveform is used for a cyclic test and there are no errors in the data, the induced stress waveform will also be fully reversed [45]. Building off this idea, the goal of this section is to prove that it is possible to obtain accurate stress-life fatigue results from strain-controlled testing despite this not being standard practice. This would save significant time and money for material test programs, having only to complete monotonic testing and one set of strain-controlled tests in order to fully and accurately define the material's mechanical behavior with both stress-life and strain-

life fatigue results, rather than needing monotonic, strain-controlled fatigue, as well as load-controlled fatigue testing. To support this proof, a load-controlled fatigue data set was collected for pDCPD for the purpose of making a side-by-side comparison between the stress-life results obtained from strain-controlled testing and the results from the load-controlled testing presented here. The results and comparisons are presented in the following sub-sections.

5.2.1 pDCPD Load-Controlled Fatigue Results

The load-controlled fatigue tests are completed following the method described in section 3.3.3 of this document. First, the load-amplitude input values were determined from pDCPD's monotonic maximum (yield) load of 3072 N. Similar to the strain-controlled testing methods, "load multiplier" values are used to scale this maximum load, creating load-amplitude inputs for load-controlled fatigue tests. This process is shown below in Table 13.

Table 13: pDCPD Load-Amplitude Input Values

Maximum Tensile Load = 3072.428 N	
Multiplier (Relative to Maximum Load)	Load Amplitude (kN)
0.6	1.8434
0.5	1.5362
0.45	1.3825
0.4	1.2289
0.35	1.0753
0.3	0.9217
0.27	0.8295
0.25	0.7681
0.2	0.6144
0.15	0.4608
0.12	0.3686
0.1	0.3072
0.09	0.2765

The details of the load-controlled fatigue tests using pDCPD samples are shown below in Table 14. This set of data contains less tests than the previous data that was presented (for the DTNA database) because the purpose of these load-controlled tests is only to get a visualization of the general trends of the stress-life curve. The data presented here provides enough information to make an accurate comparison between load-controlled and strain-controlled testing methods without potentially wasting testing time that could be necessary for testing other materials.

Table 14: pDCPD Load-Controlled Fatigue Tests

Test ID	Load Multiplier Level	Target Load Amp. (kN)	Frequency (Hz)	Sample ID	Actual Average Load Amp. (kN)	Cycles to Sample Failure
30-1	0.3	0.9217	3	40-1	0.8830	485000
30-2	0.3	0.9217	5	48-2	0.8698	272000
40-1	0.4	1.2289	3	45-4	1.1871	33800
40-2	0.4	1.2289	3	47-4	1.1994	46500
40-3	0.4	1.2289	3	44-1	1.1956	84500
27-1	0.27	0.82955	10	47-1	0.7595	1338000
27-2	0.27	0.82955	10	42-4	0.7594	1692000
45-1	0.45	1.3826	3	44-3	1.3691	13200
45-2	0.45	1.3826	3	50-2	1.367	10500
45-3	0.45	1.3826	5	47-2	1.3812	19000
50-1	0.5	1.5362	1	50-3	1.5312	2300
50-2	0.5	1.5362	1	45-3	1.5298	2100
50-3	0.5	1.5362	1	44-2	1.5309	3600
20-1	0.2	0.6145	10	43-1	0.5487	2000000 ®
60-1	0.6	1.8435	1	46-2	1.8394	690
60-2	0.6	1.8435	1	43-4	1.8358	640
Note: ® = “Runout Test” (no failure)						

The half-life cycle data from these tests was collected and analyzed using a modified version of the analysis GUI presented in section 3.5, programmed to handle

load-controlled data and produce stress-life fatigue results. The results of this analysis are shown below in Figure 56 and Figure 57.

Load-Controlled Stress-Life (R = -1)	
Stress Range Intercept (SRI1):	119.8176 MPa
Stress-Life Slope 1 (b1):	-0.11852
Stress-Life Standard Error (SEs):	0.0651

Figure 56: pDCPD Load-Controlled Stress-Life Parameters

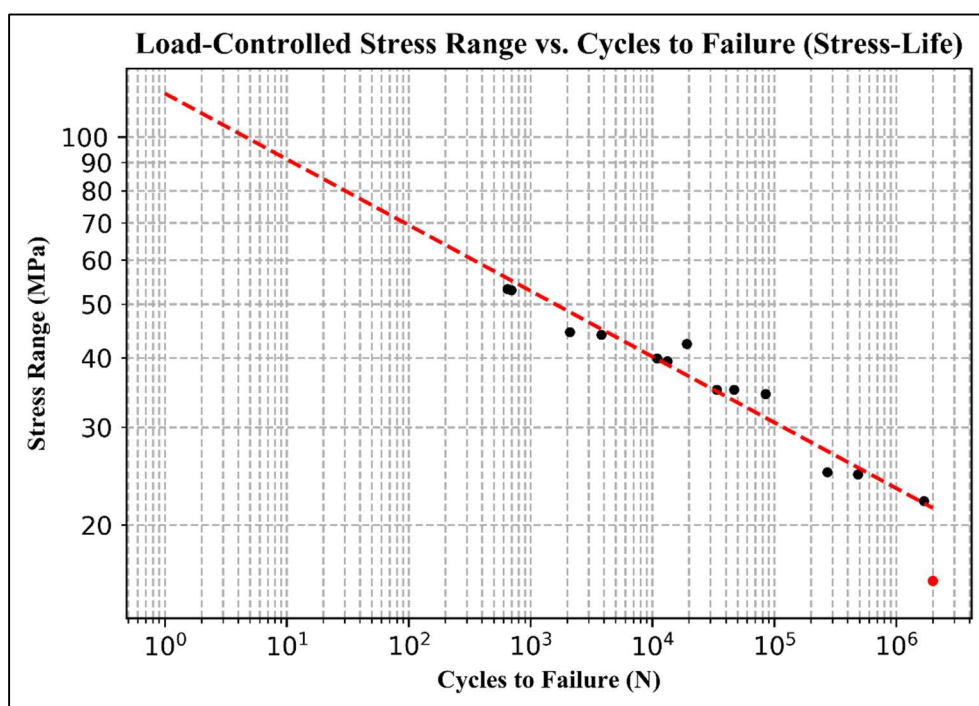


Figure 57: pDCPD Load-Controlled Stress-Life

It should be noted again that the red data point is a runout test where the sample did not fail before the test was stopped at 2 million cycles. This point was not included in the curve-fitting operations to create the fatigue parameters. If the runout test was allowed to run until failure, it is likely that it would fit onto the stress-life trend line that is displayed. In addition, the low standard error (0.0651) attests to the validity and accuracy of the curve-fitting results.

5.2.2 pDCPD Strain-control and Load-control Stress-life Comparison

The stress-life fatigue results determined from the load-controlled testing are compared in Table 14 and Figure 58 with those obtained from strain-controlled testing. The stress-life parameters are similar, with a 5.954% difference in the stress range intercept (SRI1), and a 5.373% difference in the stress-life exponent (b1). The strain-controlled SRI1 is larger than the load-controlled value, whereas the load-controlled stress-life exponent b1 is larger than that of the strain-controlled testing.

Table 15: pDCPD Load-control vs. Strain-control Stress-Life Comparison

Stress-Life Parameter	Load-Control	Strain-Control	% difference
Stress Range Intercept SRI1 (MPa)	119.818	127.171	5.954%
Stress-Life Slope b1	-0.11852	-0.11226	5.373%
Stress-Life Standard Error	0.0651	0.0617	N/A
Number of Data Points	16	47	N/A

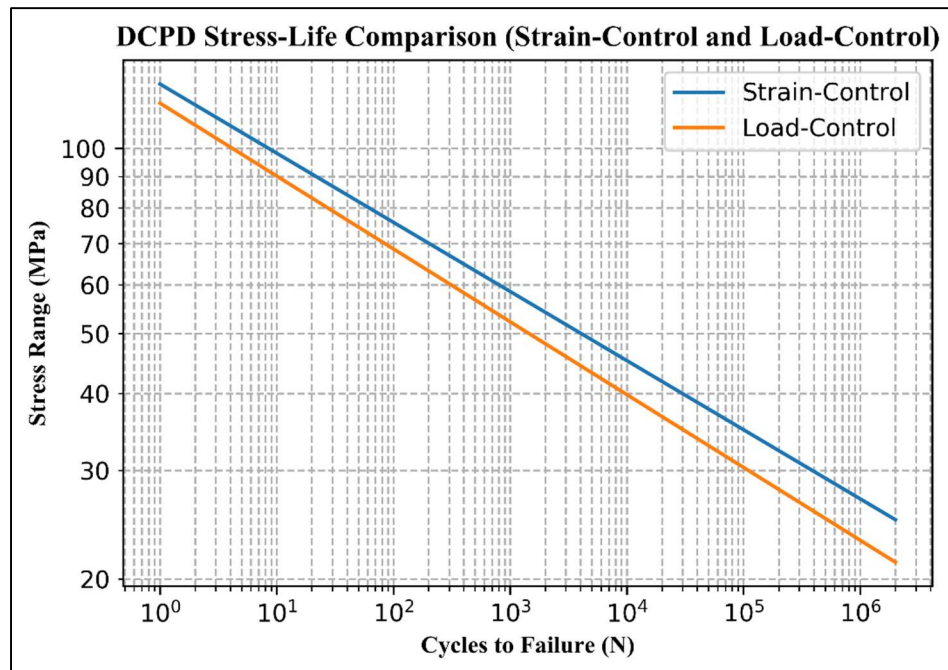


Figure 58: pDCPD Stress-Life Comparison (Load-Control and Strain-Control)

In Figure 58, the stress-life curve from both load-control and strain-control is plotted for a visualization of the differences between the two. The slopes of the curves are very similar, and there is only a slight deviation in the value of stress range (MPa) throughout the low, mid, and high-cycle fatigue regions – mainly due to the 5.954% change between the stress-range intercept values. In order to rule out any variability between the stress-life fatigue parameters as determined from load-control and strain control test scenarios, a decision would need to be made if the approximate 5% difference between the parameters is statistically significant in the context of the work to which the data is being applied. In the case of dynamic analysis of heavy-duty truck parts, this difference may not cause errors in results and therefore test engineers could continue to perform only strain-controlled testing. For detailed research and development work, however, this difference could be quite significant and engineers would have to be very mindful of which test method is used to create material data.

With these findings, it cannot be stated with complete certainty that the method of fatigue testing that is used has no effect on the fatigue parameters that are determined from the test data. Future work could focus on making this same comparison using many other materials. One could determine a universal scale factor that, when applied to the strain-controlled stress-life parameters, makes an accurate conversion to match what the load-controlled values would be. Further research could also determine that any differences in fatigue parameters can be attributed to normal statistical scatter that is common when studying fatigue.

Chapter 6

6 Discussion

This chapter includes a brief discussion about the results obtained for the DTNA material database, and the application of the theory and analysis that was used to obtain the data will be analyzed. In addition, the IMAGE simulation results for a truck hood assembly containing pDCPD and 40% GF-PP will be presented from both before and after the data obtained from this testing was added to the material database. This will give a representation of the direct impact of this work.

6.1 Applying the Strain-Life Fatigue Method to Plastics

In most existing literature regarding the fatigue of plastic materials, a stress-controlled or load-controlled testing method is used and the stress-life fatigue definition is applied. The strain-life fatigue method is either not included at all, or is discussed briefly but not applied in the results.

For the application of this work, it is desirable to define both the strain-life fatigue behavior in conjunction with stress-life. With this data, a strain gauge can be placed on a truck part as the vehicle is driven, and the data can be correlated with simulations containing accurate strain-based fatigue parameters to understand the loading that was induced onto the part. Furthermore, the strain-life method fully defines both the high-cycle and low-cycle fatigue regions, and is therefore desirable over stress-life, despite the increased difficulty in testing methods. However, the lack of available

literature in support of applying the strain-life method to plastics invites some skepticism about the validity of this approach.

6.1.1 Overlap of the Strain-Life and Stress-Life Derivations

In section 3.4.2, the mathematical relationships that derive the strain-life fatigue approach are discussed in detail. Within that explanation, it is shown that the elastic strain – the parameter from which the elastic-strain-life is derived – is solved for by simply dividing the true stress amplitude by the material's elastic modulus, because the true stress and elastic strain are proportional within the region of elastic deformation (Hooke's Law). The elastic strain-life is then defined as the elastic strain plotted over the cycles-to-failure. The stress-life relationship for the same material is defined in section 3.4.3 as the true stress (range) plotted over the cycles to failure.

When considering these two derivations, it becomes apparent that, if the appropriate conversions are made to account for differences between amplitude and range, the elastic strain-life and the stress-life represent the same set of data points. The elastic strain-life just happens to convert the data from true stress into strain using the above-mentioned relationship from Hooke's Law. This overlap in the derivation of the stress-life and the elastic portion of the strain-life definitions provides some promising evidence of the validity of strain-life for plastics. The question remains, however, if the additional trouble of accounting for plastic strain along with the elastic strain is necessary for such materials.

6.1.2 Plastic-Elastic Strain-Life Intersection Point

While similarities exist between the stress-life and elastic strain-life relationships, the total strain-life also incorporates the plastic strain in conjunction with

the elastic strain. Specifically, the total strain-life relationship is simply the sum of the elastic strain-life and the plastic strain-life, all of which are plotted together against the cycles to failure on log-log axes to create the visualization of the strain-life as it is commonly presented. On this plot, the elastic strain-life and plastic strain-life are both downward sloping linear lines – the plastic line steeper than the elastic – and the total strain-life is a concave-up, non-linear line that should closely follow the elastic and plastic lines. The strain-life results obtained from this work differ, however, from the strain-life that is presented in the literature regarding the topic (in SAE J1099, for example). In this literature, which is written in terms of metals, the plastic strain-life line is larger than the elastic line throughout the low-cycle region, and therefore the plastic strain controls the low-cycle fatigue behavior [9]. Consequently, there is an intersection point – called the “fatigue transition point” – where the elastic and plastic lines meet in the mid-high cycle region (called out on the left side of Figure 59 below). Beyond that intersection point, the elastic line is larger than the plastic line and therefore controls the high-cycle fatigue behavior.

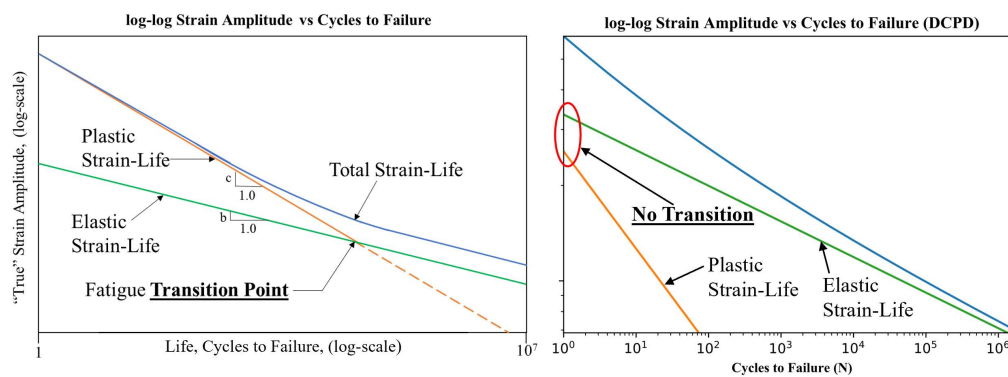


Figure 59: Strain-Life Transition Point – Expected (left) vs. Results (right)

The results from this work, as seen on the right side of Figure 59, do not align with the trends described in the literature that was mentioned. As circled in red, the

elastic line is larger than the plastic line at $N=1$ cycle, and therefore there is not a plastic-elastic intersection. This can be explained by reviewing the atomic-level topics discussed in section 5.1.

Referring to section 5.1.1, when a metal is plastically deformed, there is motion that takes place on an atomic level including the movement of defects within the crystal structure such as dislocations. When the value of plastic strain is significantly higher than the elastic strain, as shown in the low-cycle region on the left-side plot of Figure 59, it means that there is significant atomic movement (plastic deformation), and the material is deformed beyond its yield point during every cycle. In the case of pDCPD, the total strain amplitude at $N=1$ cycle is around 0.067 m/m, or 6.7%, which barely exceeds the material's yield strain of 5.1%. This means that, for any strain amplitude that is large enough to cause plastic deformation, the material will fail before even 10 cycles are completed. The behavior of the material is then more closely controlled by the elastic strain for the majority of the material's fatigue life.

6.1.3 Summary

The differences between the strain-life presented in literature and the strain-life determined from these results does not disprove the mathematical validity of applying the strain-based fatigue approach to plastic materials, but it can be concluded that the extra effort of performing strain-controlled testing may not always be necessary due to the plastic strain not playing a large role in determining fatigue behavior. In such cases, stress-life fatigue can be a "good enough" definition.

Regardless, any inconsistency between literature and the presented results can be attributed to the various atomic-level effects that differ between metals and plastics

– most importantly the fact that the yield point for a metal often occurs at a much lower strain than that of a plastic, and therefore the plastic deformation plays a much larger role in a cyclic fatigue loading scenario. The strain-life fatigue approach fully defines the behavior of a material because it considers both elastic and plastic effects, defining not only the high-cycle fatigue region, but also the low-cycle region where the stress-life method lacks in accuracy. This fully defines important low-cycle behavior that is not captured if the stress-life method is used alone. However, if no *transition point* is present within the strain-life plot (as called out in Figure 59), it could point to the fact that the plastic strain is not significant enough to warrant implementing strain-life material parameters. This is a judgement that will need to be made based on the presence of the fatigue *transition point*.

6.2 Comparisons to Pre-Existing Material Data

The material data for pDCPD that was determined from this work differs from the pre-existing data that was given to DTNA by the material supplier. Some of these differences may be due to misinterpretations of the testing conditions that were used to obtain the supplier's data. Specifically, the pre-existing fatigue data was produced from non-fully reversed tension-tension ($R = 0.1$) fatigue testing that was completed in load-control mode (rather than strain-control as used in this work). The analysis processes at DTNA assumes that all fatigue data is produced from fully reversed ($R = -1$) testing which, as previously mentioned, means that the sample is placed into both tension and compression by the same strain or load (stress) during every cycle. Because of this, the pre-existing data was not fully applicable to the analysis that it was being used for due

to the assumptions that are made within the analysis process. This could produce either inaccurate or misrepresented results.

The new data is presented side-by-side with the pre-existing values in Table 16 below. As shown, the monotonic values are similar, though the tensile modulus that was previously used is around 300 MPa lower than the value determined from this testing, and the tensile stress at break is significantly changed. The pre-existing fatigue data did not include strain-life parameters because the testing was completed in load-control. The data determined from this work was completed in strain-control, and therefore both stress-life and strain-life fatigue parameters are included to fully define the material. The new data also includes standard error values to help quantify the scatter in the testing results.

Table 16: Comparison of pDCPD Properties – old vs. new

	Material Parameter	Pre-Existing Values	New Values (From Testing)
Monotonic	Tensile modulus (MPa)	1600	1901
	Poisson's Ratio	0.39	0.40
	Tensile @ Yield (Mpa)	40	45.6
	Tensile @ Break (Mpa)	83	48.1
	Elongation @ Break (%)	4.7	12.45
Stress-Life	b1 (S-N Slope)	-0.097	-0.1123
	SRI1 (S-N intercept) (MPa)	165.76	127.171
Strain-Life	Sf' (Elastic E-N Intercept) (Mpa)	N/A	68.731
	b (Elastic E-N Slope)	N/A	-0.1123
	Ef' (Plastic E-N Intercept)	N/A	0.0317
	c (Plastic E-N Slope)	N/A	-0.3067
	n' Cyclic strain hardening exponent	N/A	0.366
	K' Cyclic strength coefficient (MPa)	N/A	243.22
S.E.	Standard Errors (SN, EN _c , EN _p , EN _c)	N/A	all < 0.1

Further comparisons are made by plotting the stress-life determined from both the pre-existing data and the new data on the same plot, as shown in Figure 60 below. The pre-existing data from the supplier creates a stress-life curve that is noticeably

larger than the new stress-life curve determined from this work, and the slopes of the two curves are similar (-0.09 and -0.1). Consequently, any simulation that uses the new data for a stress-life analysis will identify more failures or points of interest that may not have been identified using the old data.

From this, some concerns arise regarding the validity of any simulation results that used the old data. Due to the above-mentioned assumptions regarding the fully reversed waveform that must be used for any fatigue data in within the DTNA analysis process, the new data (called “DTNA S-N” in Figure 60) is more applicable and should be trusted over the old data. Simulation results using both sets of data (new and old) are presented and compared in section 6.3.

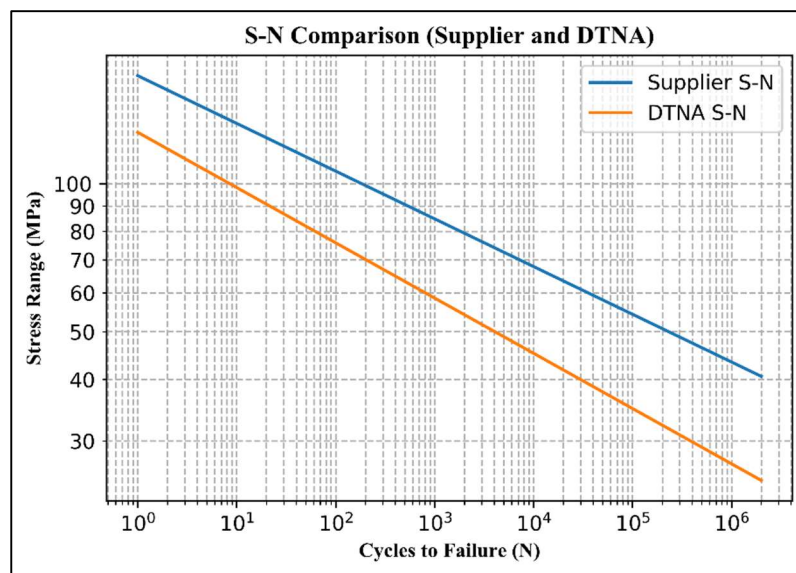


Figure 60: New Data vs. Old Data Stress-Life Comparison

6.2.1 Corrections Applied to Stress-Life Data

It should be noted that, in order to apply stress-life data to an analysis simulation successfully, a few corrections must be applied to the data. The two stress-life fatigue parameters that are determined from fatigue testing, the stress range intercept and slope

(SRI1 and b1), represent the shape of stress amplitude (or range) vs. cycles to failure curve. In some cases, however, the stress range intercept – which defines the value of the stress that can be applied to the material for exactly one cycle – is determined to be larger than the material's monotonic ultimate tensile strength (UTS). This condition is obviously impossible, being that the material cannot withstand any stress greater than the ultimate tensile strength, so a simple correction is applied. In the region of 1-1000 cycles, the slope of the curve is adjusted such that the intercept of the stress amplitude (or range) axis is equal to the material's ultimate tensile strength [40]. In the case of pDCPD, the SRI1 is determined to be 127.17 MPa. If this is converted to the stress amplitude (half of the range), it is equal to 63.6 MPa which is greater than the UTS of 45.6 MPa. Therefore, the correction is applied as shown in Figure 61 below.

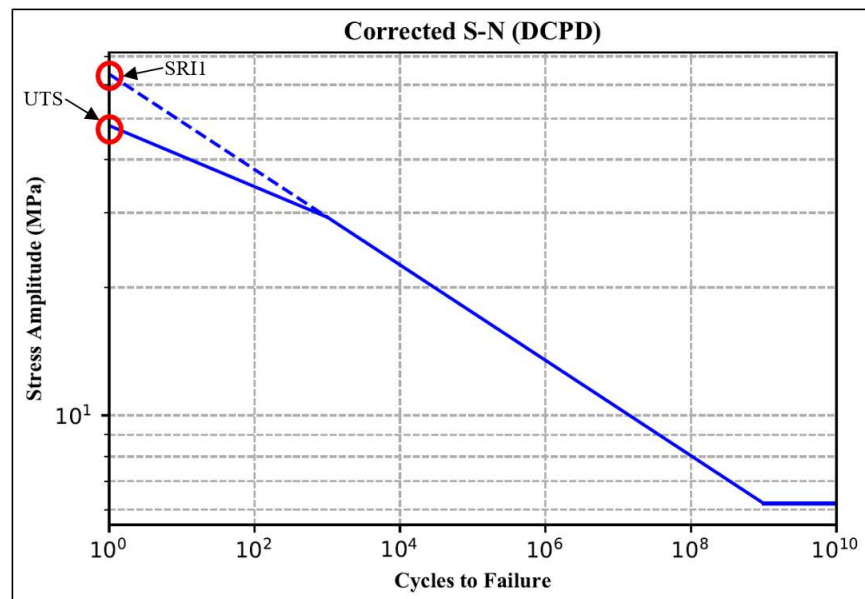


Figure 61: Stress-Life Curve with Corrections Applied

From 10^3 cycles to 10^9 cycles, the curve is defined as expected, using the SRI1 and b1 parameters determined from testing. At 10^9 the slope of the curve is set to 0, as consistent with other plastics in the DTNA material database. This is the material's

infinite fatigue life point or “fatigue cutoff” [40]. The stress-life data, as it appears in Figure 61, can then be applied to simulations.

6.3 Updated Simulation Results

In this section, some simulation results will be presented and compared in an effort to provide a visualization of the direct impact of the material data collected through this work. The images are taken from both the FE analysis portion of the IMAGE process (described in the introduction section) as well as the processed results. The model in question is a truck hood assembly containing a significant amount of pDCPD and some 40% GF-PP parts, though the focus will be on an individual pDCPD part (shown in Figure 62 below). Results for this part will be presented from both before and after the data from this thesis was applied to the DTNA analysis database, using both strain-life and stress-life fatigue analysis wherever both datasets are available.

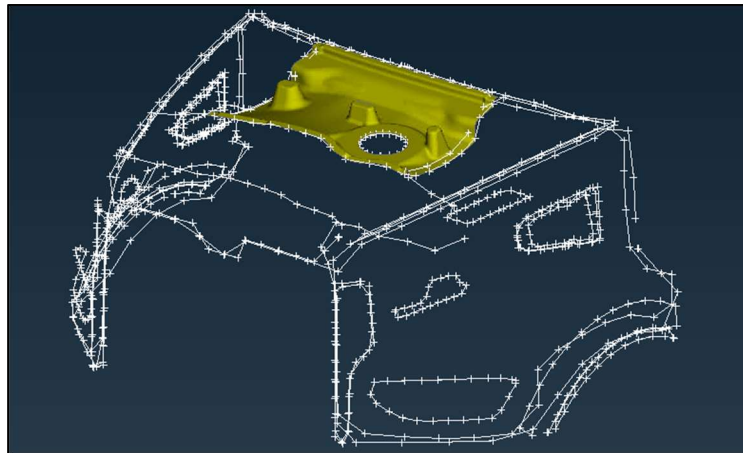


Figure 62: Truck Hood with pDCPD Part Shown

It should also be noted that the results show “hot spots” in terms of damage, calculated using Miner’s rule [20]. With this method, the individual damages accumulated by loading events during the trucks assigned duty cycle are summed together to obtain the final damage value for each finite-element (from the FEA model)

on the part. Damage values larger than 1.0 indicate a crack or failure, and the color of the damage callout changes between green, yellow and red as the value approaches and exceeds 1.0.

6.3.1 IMAGE Results Using Old Data

Figure 63 below shows the IMAGE results for this part using the old pDCPD data that, as previously discussed, only includes a stress-life fatigue definition.

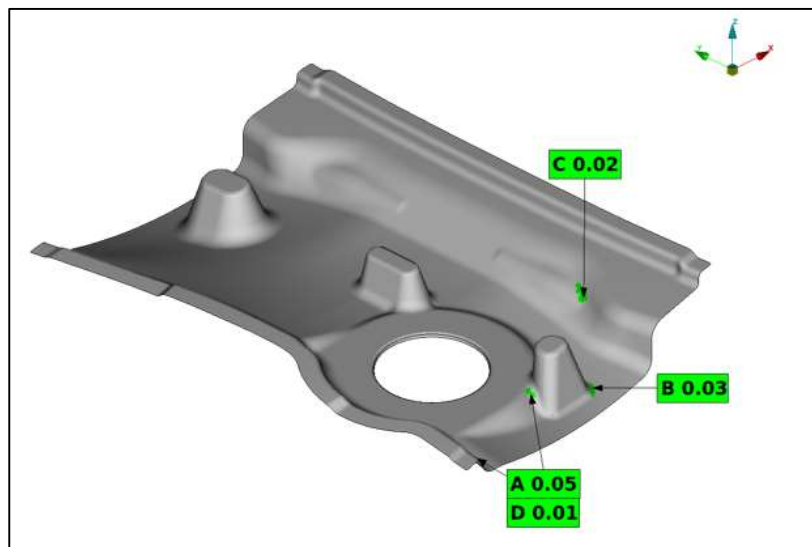


Figure 63: IMAGE Results using Old pDCPD Stress-Life Properties

As shown, there are four total callouts, each remaining within the “green” (< 0.1) region of damage – the largest of the four is a damage value of 0.05. From these results, little or no redesign would be necessary, and very little focus would be placed on this part being that there is not significant damage shown in the simulation results.

6.3.2 IMAGE Results Using New Data – Stress-Life

In Figure 64, IMAGE results for the same part are shown using the new data – from the work presented in this thesis – for pDCPD, still using the stress-life fatigue definition for analysis. As expected, the results show much larger damage values, indicating a failure (> 1.0) in four of the five total callout points. The largest damage

value is 1.30, indicated in an area that showed a value of 0.02 using the old data. This comparison shows how large of an impact the material data input can have on the results of digital analysis simulations.

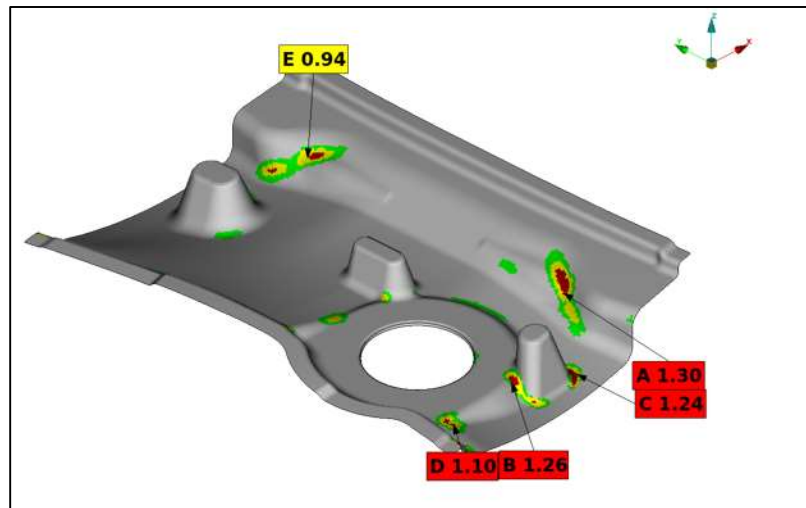


Figure 64: IMAGE Results Using New pDCPD Stress-Life Properties

It is also visible from Figure 64 that damage is shown in areas where no damage was previously detected or called out (see Figure 63). This is the case for callout points “D” (1.10) and “E” (0.94).

6.3.3 IMAGE Results Using New Data – Strain-Life

The data from this thesis includes both stress-life and strain-life definitions, whereas the old pDCPD data only defined stress-life. Therefore, no comparison can be made in this section. However, the IMAGE results obtained from using the new strain-life definition are still included in Figure 65 below.

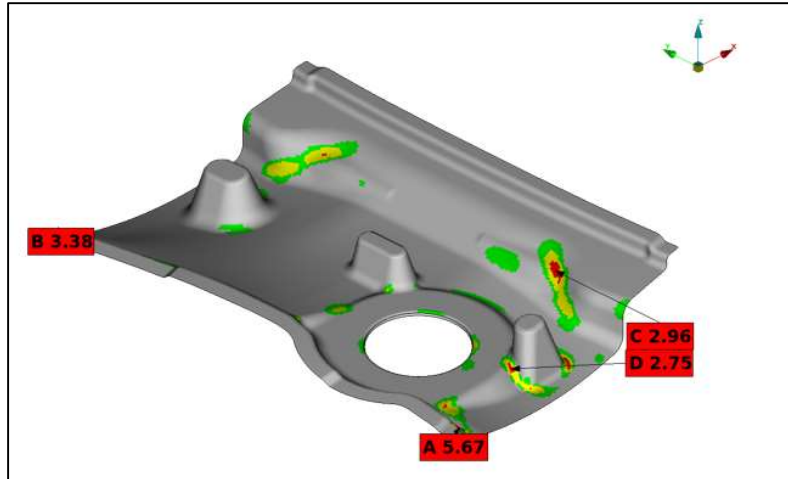


Figure 65: IMAGE Results Using New pDCPD Strain-Life Properties

As seen in the figure above, the location of damage accumulated using the strain-life definition is similar to the location of damage using the stress-lifer analysis (see Figure 64). The damage value, however, is much larger using strain-life. For example, point A in Figure 64 (where damage = 1.30) and point C in Figure 65 (where damage = 2.96) are in the same location.

Chapter 7

7 Conclusion

The purpose of the work presented in this thesis was to identify the most common plastic and composite materials that are used in new truck designs at Daimler Trucks North America, and derive methods to collect the relevant monotonic and fatigue data for these materials to be applied in digital simulation tools and used by all DTNA engineering teams. This work also expands to other topics including an investigation of the interesting strain-softening behavior experienced by some polymer materials, and a comparison between the stress-life parameters that are determined from strain-controlled and load-controlled testing. The materials selected for the purposes of this work are polydicyclopentadiene (pDCPD), 40% wt. glass-fiber-reinforced polypropylene (40% GF-PP), and vinyl-ester sheet molding compound (SMC), although SMC was not presented here. The testing and analysis methods that were used, derived using a combination of pre-existing standard testing procedures, were presented in chapter 3, and the results obtained using those methods were included in chapter 4 (for pDCPD and 40% GF-PP). Chapter 5 discussed the additional topics mentioned above, and chapter 6 presented a discussion about the culmination of all findings.

The material testing and data analysis methods described in this document were sufficient for collecting all necessary monotonic and fatigue test data for the selected materials. The material parameters determined from the data (monotonic, strain-life

fatigue and stress-life fatigue) were then correctly integrated into the database used by the Structural & Dynamic Analysis team at DTNA. It should be noted that the curve-fitting operations used to obtain the power-function (fatigue) parameters did not make use of external curve-fit tools. Instead, the fitting occurred manually within the analysis GUI (section 3.5), loosely following ASTM E739. This proved to be quite accurate, with the largest standard error values only slightly exceeding 0.10, and visually very few outlier data points exist when the curve-fit is plotted on top of the raw data.

The impact of this data in the DTNA analysis simulations was immediately apparent, especially in the case of pDCPD. For this material, the pre-existing data was obtained from the material supplier with little knowledge of testing methods or conditions, and it differed greatly from the testing results presented here. For example, the elastic modulus was previously thought to be 1600 MPa, whereas this testing found that it was closer to 1900 MPa. Furthermore, the pre-existing stress-life data was from non-fully reversed testing and was therefore not applicable to the analysis processes in which it was being used. The application of this new data produced more accurate results, and determined a larger number of issues within the truck parts that it was applied to (see section 6.3). This can result in monetary and time-related savings during future design processes as failure points will be identified and fixed much sooner.

In addition to obtaining this useful data for analysis simulations, other topics of study led to some interesting discoveries. First, it was found that the strain-softening behavior experienced by pDCPD when deformed monotonically is caused by the atomic-level structure of cross-linked polymer materials. The breaking of polymer chain cross-linking and lack of post-yield atomic interactions (as seen in metals during

dislocation motion, etc.), means that any increase in strain after the material reached its yield point (plastic deformation) will result in a decreased stress required to continue deformation. Second, a comparison was made between the stress-life parameters determined for pDCPD from both strain-controlled and load-controlled testing. It was found that the results were quite similar, with only an approximate 5-6% difference between the strain-controlled and load-controlled stress-life fatigue parameters. Depending on the application of the data, this difference could be considered negligible and one could continue to get both stress-life and strain-life from one set of strain-controlled testing, saving significant lead-time for data collection. Lastly, a discussion was presented regarding the application of the strain-life fatigue definition for plastic materials. It was found that, while this method is typically only applied to metals, it remains mathematically valid for plastic materials. However, the strain-life method should only be applied to these materials if proper fixturing or sample geometry is used to assure no buckling occurs under compressive load, and judgement is made regarding the significance of accounting for plastic strain based on the presence of a *fatigue transition point* on the strain-life plot. If there is no transition point, it is often the case that the elastic strain controls the fatigue behavior throughout the entire fatigue-life of the material, and the stress-life definition alone can account for this.

Unfortunately, there remains a significant lack of fatigue-related research or publicly accessible data for polymers or composite materials. Therefore, it was the goal of this work to provide an overview of feasible test methods, as well as some initial considerations that can be followed when beginning a project involving durability life estimations of plastic parts. Further work should use the testing methods presented here

to build a robust database for all plastic materials to be accessed publicly by engineering teams. This work presents a foundation from which other topics can build regarding environmental and strain-rate effects during testing, test specimen design and improvement, and the development of tools for selecting the correct plastic material *before* a part is designed, rather than after. In conclusion, it is hoped by the author that the information derived from this thesis will be used for significant time to come as the study and analysis of plastic materials is continuously advanced and developed.

Bibliography

- [1] Dowling, N. E., Siva Prasad, K., and Narayanasamy, R., 2013, *Mechanical Behavior of Materials: Engineering Methods for Deformation, Fracture, and Fatigue*, Pearson, Boston, Mass.
- [2] ASTM, 2014, *D638-14 Standard Test Method for Tensile Properties of Plastics*, ASTM International, West Conshohocken, PA.
- [3] Yung-Li Lee, Jwo Pan, Richard Hathaway, M. B., 2004, *Fatigue Testing and Analysis: Theory and Practice*, Elsevier Science & Technology.
- [4] Huang, L., Lai, H. S., and Liu, K. L., 2018, “A Novel Method to Predict the Low-Cycle Fatigue Life,” *J. Fail. Anal. Prev.*, **18**(6), pp. 1484–1489.
- [5] Callister, W. D., and Rethwisch, D. G., 2014, *Materials Science and Engineering: An Introduction, 9th Edition*, Wiley, Hoboken, NJ.
- [6] Hu, X. L., Liu, Y. J., Khan, M. K., and Wang, Q. Y., 2017, “High-Cycle Fatigue Properties and Damage Mechanism of Q345B Structural Steel,” *Strength Mater.*, **49**(1), pp. 67–74.
- [7] Gu, Z., and Ma, X., 2018, “A Feasible Method for the Estimation of the Interval Bounds Based on Limited Strain-Life Fatigue Data,” *Int. J. Fatigue*, **116**(May), pp. 172–179.
- [8] ASTM, 1998, *E606/E606M-12 Standard Practice for Strain-Controlled Fatigue Testing*, West Conshohocken, PA.
- [9] SAE International, 2002, “SAE J1099 Technical Report on Low Cycle Fatigue Properties Ferrous and Non-Ferrous Materials,” pp. 1–2.
- [10] ASTM, 2015, “E739-10 Standard Practice for Statistical Analysis of Linear or Linearized Stress-Life (S-N) and Strain-Life (ϵ -N) Fatigue Data,” *Stat. Anal. Fatigue Data*, pp. 129-129–9.
- [11] Park, J. H., and Song, J. H., 2003, “New Estimation Method of Fatigue Properties of Aluminum Alloys,” *J. Eng. Mater. Technol. Trans. ASME*, **125**(2), pp. 208–214.
- [12] Schütz, W., 1996, “A History of Fatigue,” *Eng. Fract. Mech.*, **54**(2), pp. 263–300.
- [13] Braithwaite, F., 1854, “On the Fatigue and Consequent Fracture of Metals,” *Institutuon Civ. Eng. Minutes Proc.*, **XIII**, pp. 463–467.
- [14] Johnson, B., “The London Beer Flood of 1814” [Online]. Available: <https://www.historic-uk.com/HistoryUK/HistoryofBritain/The-London-Beer-Flood-of-1814/>.

- [15] Rankine, W. J., 1843, "On the Breakage of the Journals of Railway Axles," *J. Franklin Inst.*, **36**(3), pp. 178–180.
- [16] Zenner, H., and Hinkelmann, K., 2019, "August Wöhler – Founder of Fatigue Strength Research : On the 200th Anniversary of August Wöhler's Birth," *Steel Constr.*, **12**(2), pp. 156–162.
- [17] Zerbst, U., Mädler, K., and Hintze, H., 2005, "Fracture Mechanics in Railway Applications - An Overview," *Eng. Fract. Mech.*, **72**(2), pp. 163–194.
- [18] Basquin, O. H., 1910, "The Exponential Law of Endurance Tests," *Proc. Annu. Meet. American Soc. Test. Mater.*, **10**, pp. 625–630.
- [19] Cadwell, S.M., Merrill, R.A., Sloman, C.M., Yost, F. L., 1940, "Dynamic Fatigue Life of Rubber," *Rubber Chem. Technol.*, **13**(2), pp. 304--315.
- [20] Miner, M., 1945, "Cumulative Damage in Fatigue," *J. Appl. Mech.*, **12**(3), pp. 159–164.
- [21] Coffin, L. F., 1954, "A Study of the Effects of Cyclic Thermal Stresses on a Ductile Metal," *Trans. Am. Soc. Test. Mater.*, **76**, pp. 931–950.
- [22] Manson, S. S., 1953, "Behaviour of Materials under Conditions of Thermal Stress," *Heat Transf. Symp. Univ. Michigan Eng. Res. Inst.*, pp. 9–75.
- [23] Agrawal, R.; Uddanwadiker, R.; Padole, P., 2014, "Low Cycle Fatigue Life Prediction," *Int. J. Emerg. Eng. Res. Technol.*, **2**(4), pp. 5–15.
- [24] S. H. BAEK, S. S. CHO, W. S. J., 2008, "FATIGUE LIFE PREDICTION BASED ON THE RAINFLOW CYCLE COUNTING METHOD FOR THE END BEAM OF A FREIGHT CAR BOGIE," *Int. J. Automot. Technol.*, **9**(1), pp. 95–101.
- [25] Winkler, A., 2010, "Concerning the Fatigue of Semi-Crystalline Engineering Polymers Part 1 : A Contemporary Overview of Technical Concerning the Fatigue of Semi-Crystalline Engineering." (November).
- [26] Opp, D. A., Skinner, D. W., and Wiktorek, R. J., 1969, "A Model for Polymer Fatigue," *Polym. Eng. Sci.*, **9**(2), pp. 121–130.
- [27] Hertzberg, R. W., Manson, J. A., and Skibo, M., 1975, "Frequency Sensitivity of Fatigue Processes in Polymeric Solids," *Polym. Eng. Sci.*, **15**(4), pp. 252–260.
- [28] Lesser, A. J., 1995, "Changes in Mechanical Behavior during Fatigue of Semicrystalline Thermoplastics," *J. Appl. Polym. Sci.*, **58**(5), pp. 869–879.
- [29] Mortazavian, S., and Fatemi, A., 2015, "Tensile and Fatigue Behaviors of Polymers for Automotive Applications," *Materwiss. Werksttech.*, **46**(2), pp. 204–213.

- [30] Reifsnider, K. L., 1991, "Chapter 7: Fatigue Behavior of Short Fiber Composite Materials," *Fatigue of Composite Materials, Volume 4*, pp. 232–338.
- [31] Olsson, N. E. J., Lundström, T. S., and Olofsson, K., 2009, "Design of Experiment Study of Compression Moulding of SMC," *Plast. Rubber Compos.*, **38**(9–10), pp. 426–431.
- [32] Pan, B. L., Zhang, C. F., Zhao, J., Zhang, Y. Q., and Zhang, Y. Z., 2012, "Mechanical Properties of Polydicyclopentadiene/Graphite Nanosheet Composites Prepared by Reaction Injection Moulding," *Plast. Rubber Compos.*, **41**(8), pp. 319–325.
- [33] Mallick, P. K., 1981, "Fatigue Characteristics of High Glass Content Sheet Molding Compound (SMC) Materials," *Polym. Compos.*, **2**(1), pp. 18–21.
- [34] Fleckenstein, J., Jaschek, K., Büter, A., and Stoess, N., 2011, "Fatigue Design Optimization of Safety Components Made of SMC," *Procedia Eng.*, **10**, pp. 390–396.
- [35] Sonsino, C. M., 2007, "Course of SN-Curves Especially in the High-Cycle Fatigue Regime with Regard to Component Design and Safety," *Int. J. Fatigue*, **29**(12), pp. 2246–2258.
- [36] Malo, T., Adam, L., Assaker, R., Matsumoto, T., and Giacomini, R., 2013, "Multi-Scale Modeling of High Cycle Fatigue of Chopped and Continuous Fiber Composites," *Soc. Plast. Eng. - 13th Annu. Automot. Compos. Conf. Exhib. ACCE 2013*, **2**, pp. 1070–1080.
- [37] Bi, Z. M., and Mueller, D. W., 2016, "Finite Element Analysis for Diagnosis of Fatigue Failure of Composite Materials in Product Development," *Int. J. Adv. Manuf. Technol.*, **87**(5–8), pp. 2245–2257.
- [38] Gahan, K. W. F., and Parmigiani, J. P., 2019, "Monotonic and Fatigue Testing of Polymer and Composite Materials Used in Heavy Duty Trucks," *IMECE2019-11680*, ASME, Salt Lake City, UT, pp. 1–10.
- [39] MTS Systems Corporation, 2006, "MTS 810 & 858 Material Testing Systems," pp. 4–9.
- [40] HBMPresencia, 2018, "NCode Practical Fatigue Theory Guide."
- [41] Anderson, T. ., 2005, *Fracture Mechanics, Fundamentals and Applications*, Taylor and Francis Group, Boca Raton, FL.
- [42] Tucker, C. L., and Suh, N. P., 1980, "Mixing for Reaction Injection Molding. I. Impingement Mixing of Liquids," *Polym. Eng. Sci.*, **20**, pp. 875–886.
- [43] "Metton Material & Process Benefits," Mett. LMR® [Online]. Available: <https://www.metton.com/about-metton-lmr/benefits>.

- [44] ParamountMFG, “The Molding Process” [Online]. Available: <http://www.paramontmfg.com/>.
- [45] US Department of Defense, 1998, *MIL-HDBK-5H: Metallic Materials and Elements for Aerospace Vehicle Structures*.

APPENDICES

Appendix A: Project Cost Breakdown

Spending				
Item/Service	Provider	Quantity	Cost	Total
PDCPD Waterjet Cut	Viper NW	1	\$716.36	\$716.36
Axial/Transverse Extensometers	Epsilon Tech	1	\$3,971.00	\$3,971.00
Bolts for anti-spin/buckle fixture	McMaster	4	\$3.50	\$14.00
Nuts for anti-spin/buckle fixture	McMaster	1	\$6.25	\$6.25
System Verification/Calibration	DMTE	1	\$2,468	\$2,468
Hydraulic Maintenance	IPS	1	\$1,470	\$1,470
MTS Wedge Grips	MTS	1	\$1,614	\$1,614
PDCPD Waterjet Cut 2	Viper NW	1	\$432.00	\$432.00
PDCPD Waterjet Cut 3	King Machine	1	\$284.00	\$284.00
40% GF-PP Waterjet Cut (IF&CF)	King Machine	1	\$918.00	\$918.00
TOTAL				\$11,893.61

Budget	
Item	Total
Materials and Supplies Budget	\$15,000
Spending	(\$11,893.61)
REMAINING BUDGET	\$3,106.39

Appendix B: Monotonic Testing Procedure/Checklist

1. Pick a random material coupon and a blank test card.
2. Begin Filling out test card information (coupon number, date, name, etc.)
3. Measure coupon gauge width, average, and record on test card.
4. Measure coupon gauge thickness, average, and record on test card.
5. In Console, set the transverse extensometer gauge length to the measured coupon gauge width (mm).
6. Load the sample into the bottom grips, close grips.
7. Adjust position to align with the top grips.
8. In Console, turn Specimen Protect to ON.
9. Close top grips, then turn specimen protect to OFF.
10. In Console, balance the load cell.
11. Install Axial Extensometer – PULL THE PIN OUT.
12. Install Transverse Extensometer near the top grip of the Axial Extensometer – PULL THE PIN OUT.
13. CHECK THAT BOTH PINS ARE PULLED.
14. In Console, balance the axial extensometer.
15. In Console, balance the transverse extensometer.
16. Open the wavematrix test method, change file name to be accurate.
17. In the test method tab go to “transducers” and change the transverse extensometer gauge length to the gauge width of the coupon.
18. Record room temperature on test card.
19. Start Test.
20. When fracture occurs, press the STOP button in wavematrix.
21. Carefully un-install extensometers, put pins back in place.
22. In wavematrix, press the FINISH button, save test file.

Appendix C: Fatigue Testing Procedure/Checklist

1. If the hydraulic pump is off, press the green button on the power box (to the left of the MTS load frame, against the wall and on the floor).
 - You should hear the pump turn on
2. Make sure the Instron controller is turned on (located beneath the computer desk – white plastic box)
 - There is a power switch on the upper end of the back side. DO NOT TURN IT OFF.
3. Unlock the computer and open “Instron Console” from the desktop. Wait for the console to appear.
4. Turn the load frame to low power by pressing the “I” button on the hand controller.
 - Will sound like the pump is cycling in a rhythmic fashion.
5. Turn the load frame to high power by pressing the “II” button on the hand controller.
 - The sound of the pump should stabilize.
6. Jog the actuator up and down by pressing the “^” and “v” buttons on the hand controller to conform that the system is in position control
7. Open “Instron Wavematrix” from the computer desktop.
8. To Begin a test, grab a test card and write the following information:
 - Name, Test Date, Test #
 - Room temperature (read thermometer)
 - Sample # (written on each material coupon)
 - Material Type
 - Width and thickness of gauge section (average of 5 measurements with calipers)
 - Test Strain level
 - Test frequency
9. In Wavematrix, click the “Test” button.
10. Input the test folder name, and the location to save the data files to.
 - Data folder name example: “Cyc_Coupon25-1_5-02-2019_05_3_PDCPD”
 - Change the coupon #, date, strain amp. category, test #, and material name. Use PDCPD for PDCPD, “GI” for glass-filled

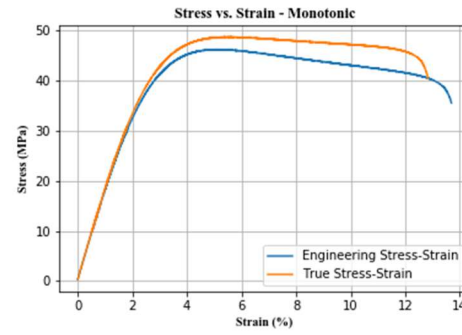
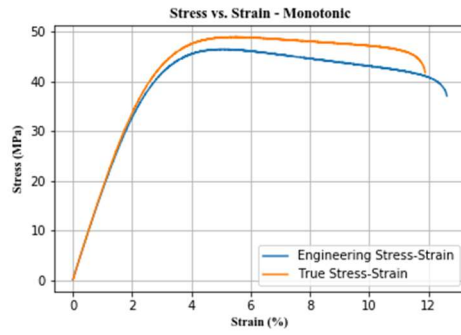
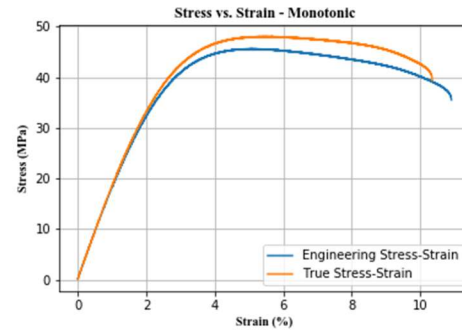
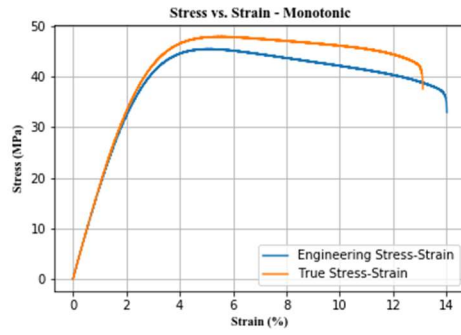
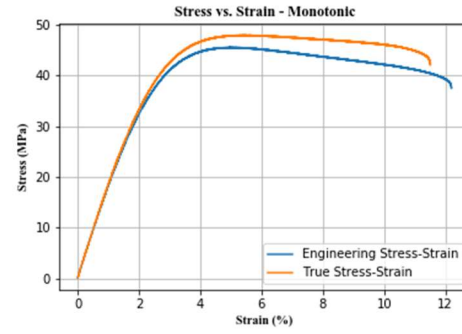
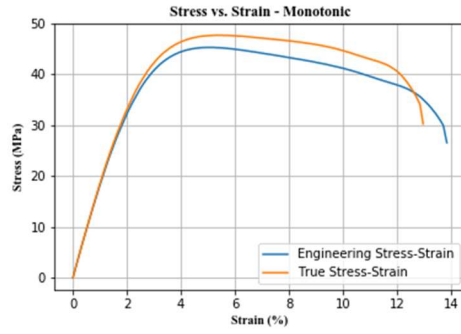
polypropylene in-flow, or “GC” for glass-filled polypropylene cross-flow.

- Save location: (C:)/users/public/public documents/Instron/WaveMatrix/Gahan-DTNA Fatigue Program ... Then choose the correct folder based on material type and strain amplitude category
11. Click Next.
 12. Select Test method – “Gahan_DTNA_Cyclic”
 13. Click Next... You should now see the test control window.
 14. Click on the “Method” tab at the top of the screen. Then click on the box under “Step 2” – this box should have a wave-shaped blue line in it.
 15. Input the Amplitude (%) and Frequency (Hz). Do not change any other input parameters.
 - Note: Even in the amplitude and frequency are the same as the previous test, re-input the parameters every time.
 -
 16. Record these values in the “Notes:” section of the test card in the following form:
 - “_____ % Amplitude @ _____ Hz”
 17. Go back to the “Test” Tab on the top of the screen.
 18. In the Console window, disarm all limits with the following steps:
 - Enter the console window. You should see four boxes at the top labeled “Position”, “Load”, “Axial Strain”, and “Transverse Strain”.
 - Click on the button in the “Position” box that has two arrows – one up and one down.
 - The window should say “8800 (0,1) : Position – Limits”. At the bottom of the window, click the “Disarm all limits in this test group” button.
 19. Align the specimen in the bottom grip, assuring that the top and bottom grip sections of the specimen are pressed firm against the alignment fixtures connected to the grips (L-shaped pieces of metal). Make sure the specimen is aligned correctly in the anti-buckling fixture. If it is PDCPD, make sure the rough-side of the sample faces out.
 20. Close the bottom grip.
 21. Use the hand remote (“^” and “v” buttons) to jog the specimen into place with respect to the top grip.

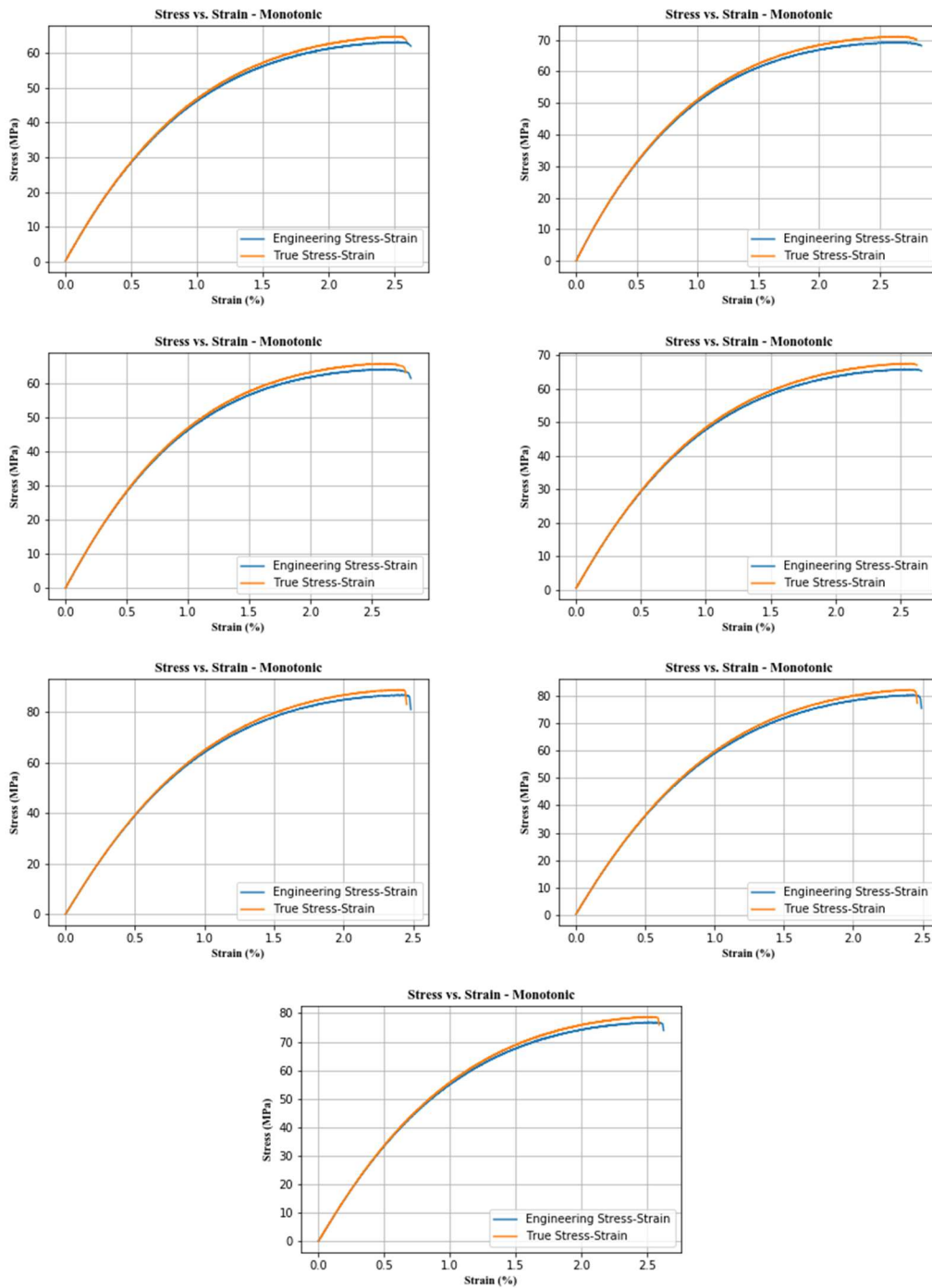
22. Close the top grip. This will cause a slight negative load (0.1 – 0.2 kN) that can be viewed in the “Load: Filtered” readout at the top of the screen.
23. Use the “fine adjustment” jog wheel on the hand remote to slowly move the actuator down until the “Load: Filtered” channel shows a positive load between 0.0 and 0.005 kN – this will take some practice: make very very small adjustments’
24. With the specimen loaded into the machine, clamp the axial extensometer onto the sample within the gauge-length. Be sure it is aligned with the length-axis of the specimen, not at an angle.
25. Use the tweezers to fit rubber bands around the specimen, securing the extensometer.
26. REMOVE EXTENSOMETER PIN.
27. With the extensometer attached, re-open the console window on the computer.
28. In the “Axial Strain” box at the top of the console window, click on the button that depicts a strain gauge next to a ruler.
29. In the window that comes up, click “Calibration” and then click “Balance”. This should cause the “Axial Strain” readout at the top of the screen to change to read 0.0000%.
30. ARM all limits with the following steps:
 - In the console window, look for the four boxes at the top labeled “Position”, “Load”, “Axial Strain”, and “Transverse Strain”.
 - Click on the button in the “Position” box that has two arrows – one up and one down.
 - The window should say “8800 (0,1) : Position – Limits”. At the bottom of the window, click the “Arm all limits in this test group” button.
 - The up and down arrows in all four boxes should turn green.
31. Close the console window. Check once more that the correct strain amplitude (%) and frequency (Hz) are input into the Wavematrix methods tab.
32. In the Wavematrix “Test” tab, click the “Start” button on the right-side of the screen.
33. This will prompt a window confirming the file saving location. Press “OK” and the test will begin.

POST TEST:

34. The test method is set up such that the machine will stop when it detects that the specimen has cracked.
35. CAUTION: DO NOT TOUCH THE EXTENSOMETER. The system will still be in Strain-control, and any movement in the extensometer will cause dangerously fast movement of the actuator.
36. Put the system back in Position-control by opening the console window and following these steps:
 - In the click on the left-side button in the “Position” box that depicts an actuator.
 - Click the “Transfer” and then click “Immediately”.
 - The system is now in position control.
37. Record the cycles-to-failure in the “Notes:” section of the test card in the following form:
 - “Test Fail @_____Cycles”.
38. Click the “End” button on the right side of the screen.
39. Click the “Finish” button on the bottom right side of the screen.
40. It will ask about replacing the test-method file. Click “OK”. This will take you back to the screen from step #10.
41. Disarm all limits following step #18.
42. Safely remove the extensometer. Release the bottom grip and move it out of the way using the hand controller. Then release the top grip and remove the sample.
43. If the sample has separated into 2 parts, duct-tape them together with the sample # visible.



40% GF-PP Monotonic (In-Flow) Stress vs. Strain



40% GF-PP Monotonic (Cross-Flow) Stress vs. Strain

